UNIVERSITY OF READING

Department of Mathematics and Statistics

Low order models of storm track variability

Author:
Melanie Kobras

Supervisors:
Maarten H. P. Ambaum
Valerio Lucarini

A thesis submitted in fulfillment of the requirements for the degree of Doctor of Philosophy

April 2023

Declaration

I confirm that this is my own work and the use of all material from other sources has been properly and fully acknowledged.

Melanie Kobras

Abstract

The storm tracks in the mid-latitudes are a key component of the general circulation by transporting heat, momentum, and moisture from the equator towards the poles. However, the non-linear dynamics related to the interaction between mean flow and eddies are not yet fully understood. The aim of this thesis is to broaden this understanding by developing models based on minimal necessary ingredients that can capture some of the observed properties of the mid-latitudes.

The derived models are based on Phillips' quasi-geostrophic two-level model, the simplest model that can capture barotropic as well as baroclinic processes together with diabatic heating and surface friction. Both models are comprised of a set of ordinary differential equations, describing the interaction of the zonal flow with the eddies, and are analysed by means of classical dynamical systems theory.

The first model, based on a highly simplified flow geometry, exhibits two physically realisable steady states, one purely zonal flow and one where, additionally, finite eddy motions are present. As the diabatic heating increases, the zonal solution loses stability and the eddy solution becomes attracting. After this transition, the zonal components of the solution are independent of the baroclinic forcing, a mechanism called eddy saturation.

The second model, based on a zonal flow with variable latitudinal maximum and tilted eddies, enabling a positive momentum flux contrary to the first model, exhibits three states. In addition to a purely zonal state, the system features a barotropic eddy regime with poleward momentum flux, but zero poleward heat flux for lower diabatic heating. Increasing the forcing pushes the system into a baroclinic eddy regime with finite poleward heat flux. In both regimes, the zonal flow maximum is pushed polewards, whereas the growth rate of the flow speed is weakened in the baroclinic eddy regime, exhibiting incomplete eddy saturation.

Acknowledgements

First, I want to thank my supervisors Maarten, for guiding me through the process of getting to know the Earth's atmosphere, and for continuously reminding me of the physical nature of the problem that I sometimes lost due to my background in maths, and Valerio, for adding his viewpoint to the project but also for supporting my personal development, and for the always uplifting conversations.

I am particularly grateful to my family — I couldn't wish for a better one — for encouraging me along my path, no matter how far away I've decided to go next. My special gratitude goes to my parents, to whom the whole academic world is a mystery but who nevertheless trusted me in all my decisions and supported me in every possible way.

I also wish to acknowledge the help and encouragement of my best friends. Thank you to Anna, who is there since the beginning of my academic journey, for being an inspiring role model and making these evening and weekend working hours more enjoyable. Thank you to Dipl. Jur. Vivien Morawiak LLM, for everything and nothing really. And thank you to Tobias for your brilliant agile and productivity coaching, without which I would have never been able to finish this thesis, and for never becoming tired of cheering me on along the way and believing in me.

Finally, I want to thank myself for balancing my own equation of motion by giving work and life an equal magnitude and reading all those self-care books.

Contents

Chapter 1

Introduction

The atmosphere is the most variable component of the climate system, driven by solar heating, gravitation and the Earth's rotation, where solar heating is the main source of energy for atmospheric motion. The Earth's surface absorbs solar radiation and converts it into heat energy, warming the atmosphere. However, this heating is strongly dependent on latitude. Annually averaged, it peaks at the equator and is minimal at the poles, creating an equator-to-pole temperature gradient and therefore a growing store of zonal mean available potential energy. This store is converted into kinetic energy by the atmosphere, developing a large-scale circulation to mitigate the temperature gradient by transporting heat from the equator to the poles. Therefore, the growth of the temperature gradient is restrained and the circulation is maintained against frictional dissipation. In this sense, the atmosphere can be seen as a heat engine, however, a very inefficient one, as only a small fraction of solar energy is converted into kinetic energy (Holton and Hakim, 2013a).

The atmospheric circulation shows variability on a broad range of spatial and temporal scales. The scales of interest start from aerosols and water vapour, impacting our daily weather as well as playing a key role in climate change, and the motions in the atmosphere are categorized as microscale (sub-daily, up to 1 kilometre), mesoscale (ranging days to weeks, up to 1000 kilometre), synoptic (up to a month, 1000s of kilometres) and global (months, years or even decades, spanning the entire globe). The choice of scales and processes incorporated in models of atmospheric dynamics is highly dependent on the scientific question that is asked, and the number of available atmospheric models has substantially increased in the last decades.

The connection between the most simple to the most complex models forms a hierarchy with the ultimate goal of understanding and predicting atmospheric motions. In simple models, the observed motions are reduced to their most fundamental components in order to understand the effect of isolated processes on the system, and they are validated against real atmospheric observations or more complex models

like general circulation models (GCMs), which are rather useful to realistically simulate the atmosphere on various time scales. It is therefore clear, that no single model can serve all purposes (Maher et al., 2019).

In their review on climate models, Schneider and Dickinson, 1974 highlight the importance of simple models by noting that an understanding of causal relationships is rather difficult in a GCM because of the large number of degrees of freedom, and the huge volume of output due to high resolution of space and time. They state that "solid progress toward an understanding of the dominant factors in climate change will require steady development of an almost continuous spectrum or hierarchy of models of increasing physical and mathematical complexity". In this work, they show that simple models are needed to estimate the sensitivity of the long-term behaviour of the atmosphere to changes in various thermodynamic and transport processes and that this step is essential to the development of more complex interactive models, which in turn are used to design realistic models like GCMs.

However, Hoskins, 1983 noted an "unhealthy" relation between idealised and complex numerical models, criticising the lack of connection of theoretical models to real atmospheric data or complex numerical models and therefore having no value for improving the high-resolution forecasting models. In terms of tackling climate change, the author emphasises that GCMs, although crucially important, are "only part of the weaponry at our disposal [and] equally, very simple low-order climate models are only one end of the complete and balanced attack that is needed". This gap between complex climate models and simple low-order models has not yet been successfully closed (Held, 2005), and the tension between understanding and simulating the dynamics of the atmosphere persists (Held, 2014).

According to Maher et al., 2019, the large-scale mid-latitude atmospheric circulation "provides one of the best success stories for hierarchical climate modelling", and even earlier, Hoskins, 1983 used it as an example to demonstrate the advantage of having low-order model informed GCMs. Although key concepts of the underlying dynamics of the mid-latitudes are well understood and part of textbook knowledge (e.g. Holton and Hakim, 2013a), there are still gaps which prevent complex climate models from accurately predicting the sensitivity of the climate to changes in external forcing.

One such area of active research is the non-linear dynamics related to the eddy-mean flow interaction in the mid-latitudes. This component of the atmospheric circulation is of great interest because the eddy-driven jet stream and its associated storm track is the main driver of extreme weather events like storms and blocking events in the mid-latitudes. Furthermore, this system has a profound impact on the general circulation by transporting heat, momentum and moisture from the equator

towards the poles. The location and intensity of the jet stream and storm tracks vary on different time scales, from several days to weeks, and even decades. This observed variability has been of interest since the beginning of climate modelling, and although a substantial amount of theories and models have been proposed and developed, the mechanisms controlling the observed variations are still not fully understood. Subsequently, there are still gaps in the corresponding model hierarchy leading to climate model biases which in turn result in large uncertainty in climate change predictions (Shepherd, 2014).

The above-described uncertainty is the motivation of this thesis, and the ultimate goal is to slightly narrow the gap between minimal models of eddy-mean flow interactions and their observed variability in the atmosphere. To fulfil this objective, the research is based on a simple model at the rather minimal end of the model hierarchy, yet incorporating observed properties of the real atmosphere by asking the following questions:

1. Can a simple model of the mid-latitudes capture some of the observed complex non-linear dynamics of the atmosphere?

2. With minimal ingredients and restricted flow properties, can a simple model exhibit a latitudinal shift of the jet stream?

3. How do changes in inherent parameters like surface friction or dissipation influence the behaviour of these systems?

4. How do these idealised models react to variations of external forcing like the equator-to-pole temperature gradient?

Despite being constructed for numerical weather forecasting (Phillips, 1954, Phillips, 1956), the quasi-geostrophic (QG) two-level model is the simplest turbulent climate model that can capture most of the complex dynamics in the mid-latitude atmosphere and is, therefore, a good compromise between simplicity and relevance (Held, 2007). In this model, the mid-latitude atmosphere is divided into two vertical layers, consisting of vorticity equations defined in the middle of the layers connected by the thermodynamic energy equation defined between them. For further simplicity, the equations are defined in a horizontal rectangular channel neglecting the purely kinematic effects of the curvature of Earth, however incorporating the effects of surface friction and diabatic heating (Phillips, 1956).

Despite obvious limitations and poor vertical resolution, this model is used in many studies, which often leads to the discovery of phenomena in the model solutions that are subsequently found in the atmosphere. However, although several theories

have been developed, there is still no consensus on a framework for describing the eddy-mean flow closure problem in this system. Zurita-Gotor, 2007 suspects that this is due to the fact that all of these theories had to incorporate some assumptions, so none can be universally valid. The closure problem in this model arises from averaging the nonlinear vorticity equations yielding equations containing again nonlinear terms describing the velocity perturbations. To close the system, these nonlinear eddy terms must be modeled as functions of the mean flow in order to remove any reference to the perturbation velocity.

Keeping this conditional validity in mind, we also used Phillips' two-level model in the pursuit to answer the above-stated questions. The first approach to achieve this is based on the assumption that the flow is meridionally symmetric and the eddies are of symmetric shape, so the eddy momentum flux cancels and thus the model does not incorporate direct non-linear eddy-eddy interaction. Despite being an extremely limiting and rather unrealistic representation of the real atmosphere, we discover properties of real atmospheric phenomena in the model behaviour as well. The derived system of six ordinary differential equations of zonally averaged mean flow and eddy quantities exhibits two steady states, one of which is the atmospheric equivalent to what is known in the oceanic scientific community as eddy saturation. In this state, the mean zonal flow is independent of the external thermal forcing, whereas the eddy energy increases with incoming heating. To our knowledge, the derived model is the first simple model of the atmosphere exhibiting these dynamics, which is a regime of the mid-latitudes that is supported by numerical models.

The second approach in this thesis is more directed towards the question regarding a possible latitudinal shift of the jet stream and associated storm tracks. So in contrast to the first approach, the mean zonal flow in this model is defined to consist of two latitudinal modes to enable variations of the latitudinal maximum. In accordance with that, we chose a southwest-northeast tilted eddy shape to allow nonlinear interactions in form of positive eddy momentum fluxes. These changes yield entirely different dynamics of the system and an almost-complete disappearance of the eddy saturation behaviour. Instead, this model exhibits competing eddy regimes with different impacts on the latitudinal maximum of the mean flow. These regimes closely resemble different phases of the life cycle of eddies and their impact on the jet stream location in the mid-latitude atmosphere.

Before the two derived models are presented, Chapter 2 of this thesis introduces some of the relevant features of the mid-latitude atmosphere that are used to substantially simplify the equations of motion. The concepts of barotropic and baroclinic instability are introduced in terms of early relevant literature which led to the development

of Phillips' QG two-level model, presented thereafter. Additionally, some aspects and properties of the life cycle of mid-latitude storm tracks are explained. In chapter 3 we present the first of the two modelling approaches described above. This work is published in Kobras, Ambaum, and Lucarini, 2021. Chapter 4 is dedicated to the second approach, which is accepted for publication with minor revisions in the Physica D journal "Nonlinear Phenomena" at the time of submission of this thesis. Chapter 5 summarises the results of the derived models, gives an outline of possibly interesting future research and shortly discusses some limitations in a broader view.

Chapter 2

Background

2.1 The general circulation of the atmosphere

Almost three hundred years ago a relatively unknown English scientist, George Hadley, wrote the perhaps most important early work on atmospheric circulation, seeking an explanation for the trade winds exploited by navigators even before his time. In the mean, these surface winds with a prevalent direction flow westward in low latitudes, eastward in the mid-latitudes, and westward or nearly vanishing in high latitudes. Hadley, 1735 realized "that the action of the sun is the original cause of these winds" by creating a temperature gradient between the equator and the poles. He visualised the heated air at the equator rising, flowing north, where it cools and sinks at the poles, and flowing back towards the equator along the Earth's surface, fulfilling one complete circulation across the hemisphere. He argues that by conservation of angular momentum and the Earth's rotation, the air moving from higher to lower latitudes, which have a higher angular momentum, will have a relative motion contrary to that of the Earth's rotation and is subsequently deflected to the west. This is consistent with the north-easterly (southwestward) and south-easterly trade winds in the tropics north and south of the equator, respectively. He used the same argument to explain the eastward motion of air when it flows poleward higher up in the atmosphere.

Although this theory is not the complete picture, this circulation pattern in the atmosphere is today called *Hadley cell*, see figure 2.1. In the early nineteenth century however, it was discovered that wind in the mid-latitudes has a poleward component instead of the equatorward motion suggested by Hadley (Thomson, 1892). Ferrel, 1856 explained these south-westerlies by a secondary, thermally indirect meridional circulation cell in the mid-latitudes, today called *Ferrel cell* (figure 2.1), and a third polar cell similar to the Hadley cell. However, these zonally symmetric circulation schemes were disproved by late nineteenth-century observations, where no consistent
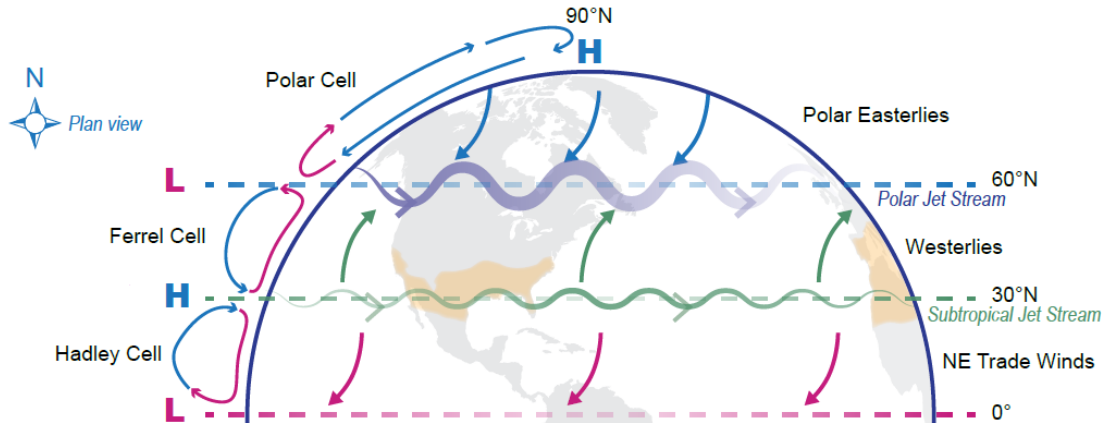
FIGURE 2.1: A schematic overview of the atmospheric circulation on the northern hemisphere, which is mirrored at the equator on the southern hemisphere; adapted from figure 5.1 in Wuebbles et al., 2017

theory of meridional cells could be found to explain the transport of the required angular momentum and heat (Lorenz, 1967).

Jeffreys, 1926 was able to show with mathematical arguments that no steady general circulation of the atmosphere is dynamically possible when friction is taken into account, and horizontal asymmetric eddies spanning the height of the troposphere are inevitable. It was realised in these times that large-scale eddies are not perturbations of a zonally symmetric circulation but are essential for the poleward transport of heat and momentum (Schneider, 2006). Today it is known that these large-scale eddies have a great influence on the zonally averaged circulation by transporting heat and momentum polewards. The eddies draw their energy from the zonally averaged flow in form of available potential energy by transporting heat polewards, and supply kinetic energy back by transporting momentum towards latitudes of higher angular velocity. Jeffreys' theory was later revisited by Starr, 1948, who emphasised the importance of finding a theory for the poleward transport of momentum that can explain the commonly observed southwest-northeast tilt of streamlines on meteorological maps.

In a quest to find an explanation for these observed south-westerly surface winds in the mid-latitudes, Rossby, 1941, relying upon the three-cell model proposed by Ferrel, argued that in the two direct circulation cells, (Hadley and polar cell in figure 2.1) strong westerly winds at high levels generate eddies with vertical axes on the boundaries of these cells to the middle cell. These eddies transport the upper-level momentum of the direct cells into the mid-latitudes, where the wind is diverted eastwards. He explains the mid-latitude westerlies on the surface as a result of the poleward and equatorward spread of air which sinks on the northern edge of the Hadley cell, where the poleward branch is again diverted westward by conservation

of angular momentum, later modified by Rossby, 1947 to conservation of vorticity.

During the same time, a research group, consisting of Charney, Rossby and Starr amongst others, and led by Erik Palmén obtained funding for a comprehensive study of the atmospheric circulation including the jet stream. The summary section of the published article (Staff Members, 1947) lists key features of the jet stream, including that "the jet stream is located in or just south of a zone in which a large fraction of the middle and upper troposphere temperature contrast between polar and equatorial regions is concentrated." They further describe the jet stream as a meandering band accompanied by cyclones of cold, high-latitude air on the north, and warm anticyclones on the south of the jet. Recalled later by Riehl, 1988, Palmén became convinced that the huge mass of air rising at the equator to the upper troposphere could not all descend in the subtropics, and proposed the existence of a second jet. Today it is differentiated between this subtropical jet and the polar or eddy-driven jet, see again figure 2.1, due to the different physical processes involved. Although there is often no spatial separation between the two jets, the conceptual separation can still be useful in many cases (Woollings, Hannachi, and Hoskins, 2010).

As a natural consequence of rapid advancements in this research area and a growing amount of observations, this period was also characterised by controversies in verbal and written form, see Lewis, 1998, especially about the mechanics and role of the eddies in the mid-latitudes. While a graduate student in the late 1940s and early 1950s, Norman Phillips was exposed to much of this controversy, also by being a research assistant for the project on the jet stream described above. This fuelled his interest in the general circulation problem and subsequently led to his first theoretical study on the two-level model described in the introduction of this thesis (Phillips, 1954), followed by his famous numerical experiment (Phillips, 1956), which was the first numerical medium range weather forecast at that time. Despite the simple and bold experimental design, to which Phillips was encouraged by Rossby and Charney, as he recalls in an interview (Phillips et al., 1989), the model was able to explain the interaction of the mean meridional circulation and the eddy transport in the mid-latitudes that gave rise to the south-westerly winds in these latitudes and therefore answered some major questions arising in the centuries before.

A key ingredient for Phillips' derivation of the model was laboratory experiments. Rotating containers of fluid produce circulations with eddies that are similar in structure to atmospheric eddies. This implies that the physical conditions yielding the eddies are similar for the atmosphere and the laboratory. Additionally, Phillips concluded that at least the main features of the general circulation can be simulated
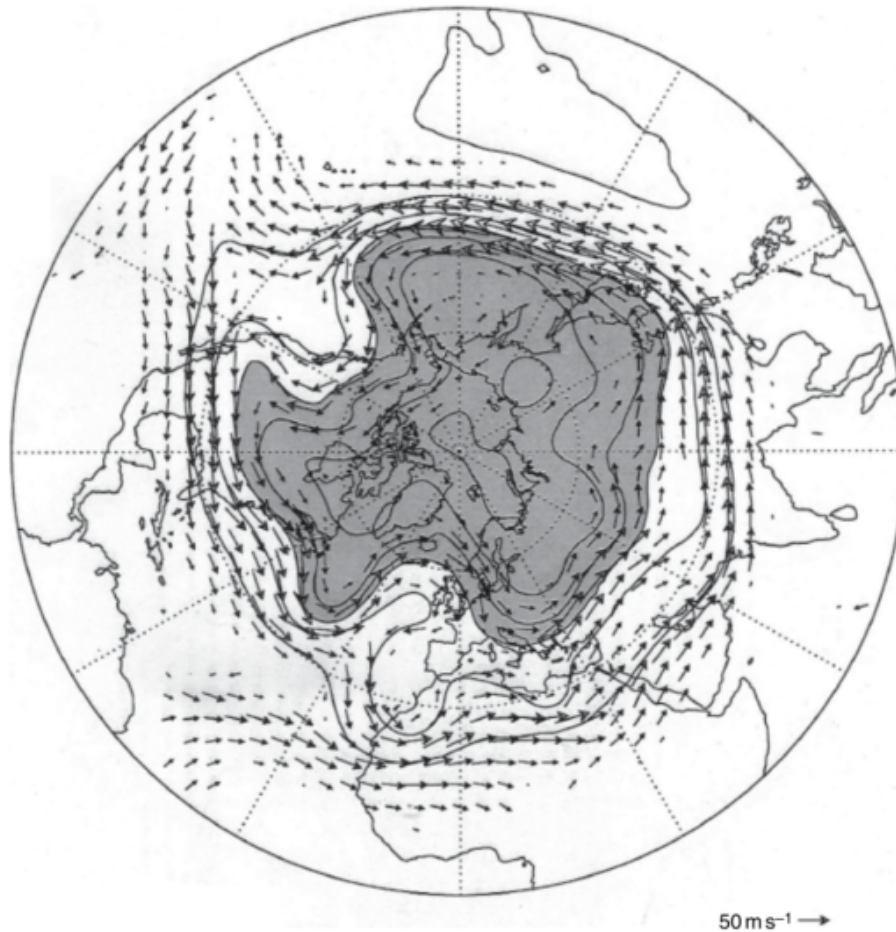
FIGURE 2.2: Contours of the geopotential height of the 250 hPa surface, contour interval 250 m, values below 10km are shaded, the arrows represent the horizontal component of the wind; an arbitrary day in the Northern Hemisphere winter; taken from Hoskins and James, 2014.

without specifying the diabatic heating and cooling in great detail (Lewis, 1998). In general, the flow in the mid-latitude atmosphere can be modelled by using assumptions that are valid for large-scale motions far enough away from the equator, or for laboratory experiments. These assumptions are the basis of the QG equations from which Phillips' two-level model was derived. To be able to understand the applicability and limitations of the model, and subsequently, the systems derived in this thesis, the next section briefly introduces these assumptions and some important theories about the mid-latitude atmosphere.

It should be noted that the above discussion is by no means a complete history of theories about the general circulation of the atmosphere, and famous contributing scientists are certainly missing since an extensive literature review is beyond the scope of this thesis. Instead, this section is a summary of some milestones that led to the understanding of the general and especially mid-latitude circulation, and

$50\,\mathrm{m\,s^{-1}} \longrightarrow$
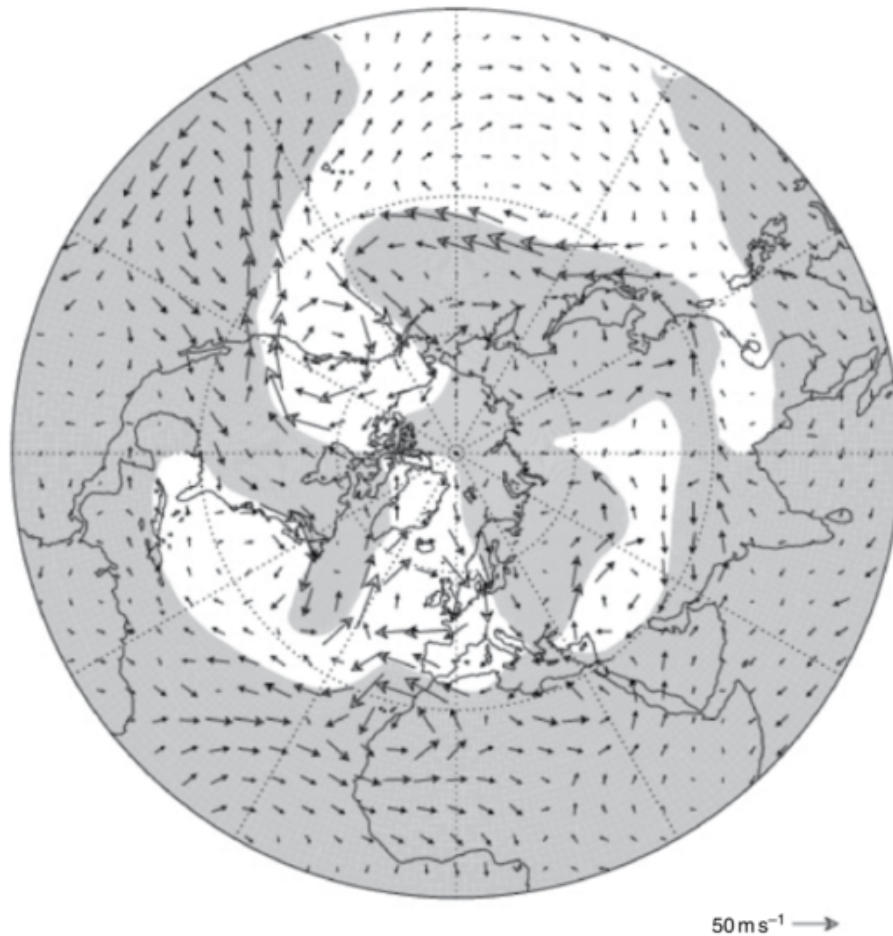
FIGURE 2.3: Horizontal component of the wind, as in figure 2.2, except that the zonal mean has been removed, the shading indicates regions where the 250 hPa geopotential height anomaly from its zonal mean is negative; again taken from Hoskins and James, 2014.

simultaneously a prelude to Phillips' numerical experiment on which the derived models in this thesis are based upon.

2.2 The dynamics of the mid-latitude atmosphere

The jet stream dominates the flow in the mid-latitude troposphere, especially in the Northern Hemisphere winter when the temperature gradients are strongest. Figure 2.2 shows the flow at 250 hPa for an arbitrary time in February, where the dominance of a westerly belt of strong winds in the mid-latitudes is obvious. It meanders from low to high latitudes, is highly asymmetric in form, and is influenced by orography like mountain ridges, and continent-ocean heating contrasts. This pattern is an extremely simple and effective way of transporting heat from the equator to the poles (Hoskins and James, 2014).

FIGURE 2.4: Polar stereographic projection of geopotential height contours in meter and isotachs (levels of equal wind speed) at 250 hPa for December to February (left) and June-August (right); adapted from Kållberg et al., 2005.

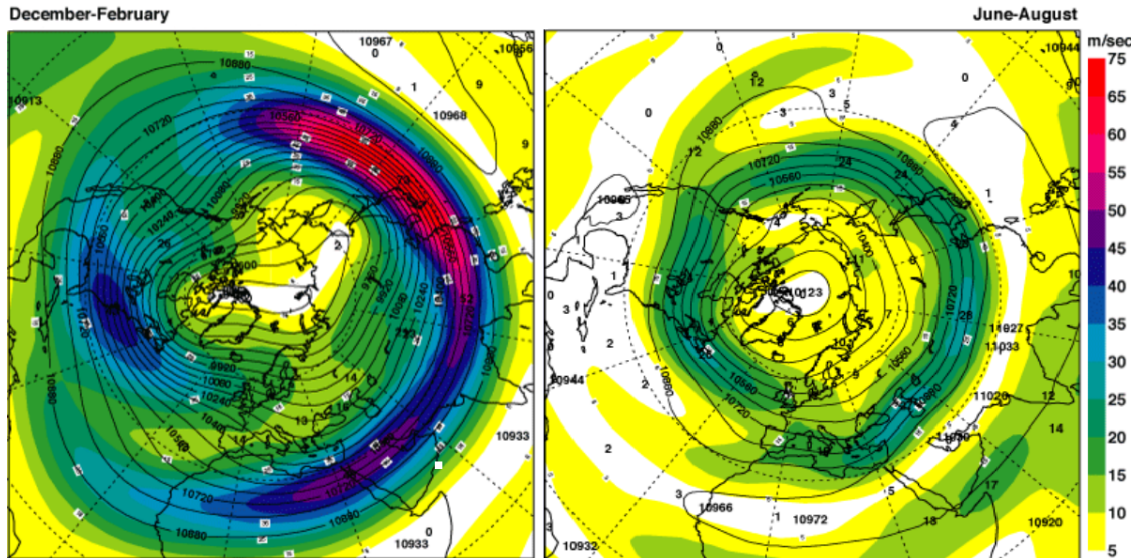The troughs and ridges of the jet stream are accompanied by large cyclonic and anticyclonic eddies of roughly circular shape. They are depicted in figure 2.3, which is the same point in time as figure 2.2, with the difference that the wind arrows show the flow without the zonal mean. This is in a way equivalent to viewing the flow in a frame of reference moving with the mean zonal flow. These eddies typically have a radius of around 1000 km and travel eastward at approximately 10 to 15 $\mathrm{m\,s^{-1}}$ (Holton and Hakim, 2013a).

The features of the jet stream in figure 2.2 and 2.3 live on different time scales, where some of them are rather short-lived or transient, whereas others persist throughout the season. This becomes evident by averaging the flow over 45 winter periods from December to February, as done with the European Centre for Medium-Range Weather Forecasts (ECMWF) ERA-40 reanalysis data in Kållberg et al., 2005, shown in figure 2.4 on the left. This field is smoother than that in figure 2.2, suggesting that the transients typically occur on smaller spatial scales compared to the longer-lasting characteristics of the flow. However, the flow is still highly dependent on longitude with strong zonal wind maxima east of the Asian and North American continents and above the Arabian peninsula, and minima west of North America and above Europe. The transient eddies develop preferentially in the regions of wind maxima, feeding on the mean flow energy, and propagating downstream along storm tracks that follow the jets. This flow is even smoother in summer, compare figure 2.4 on the right, when the equator-to-pole temperature gradient is smaller, and subsequently, the jets are slower and located further north.
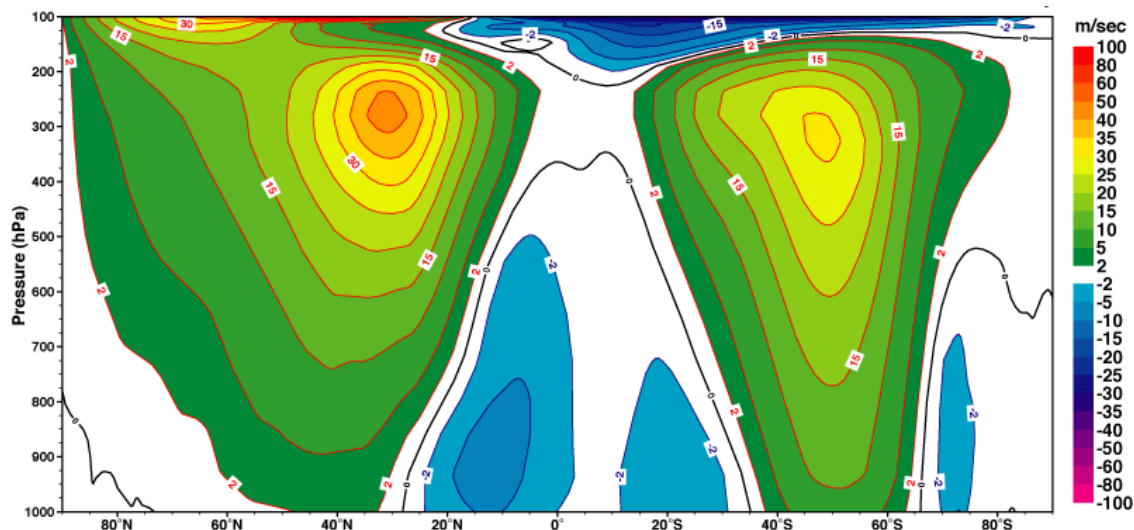
FIGURE 2.5: Meridional cross-section of longitudinally and time-averaged zonal wind for December to February; from Kållberg et al., 2005.

Although the mid-latitude atmospheric motion is highly asymmetric along longitudes and varies on different time scales, a zonal average of the flow can provide useful insights. Figure 2.5 shows a meridional cross-section of longitudinally and time-averaged zonal wind for December to February, calculated again from ECMWF ERA-40 reanalysis data in Kållberg et al., 2005. The height in this cross-section is in pressure coordinates and shows the mean zonal flow in the troposphere. The core of maximum zonal wind speed is located just below the tropopause, the boundary between the troposphere and stratosphere. This is due to the fact that the mid-latitude zonal wind is approximately in thermal wind balance with the temperature field, a property following from synoptic-scale flow being approximately in geostrophic and hydrostatic balance. These properties are the basis of the QG equations for the mid-latitude atmosphere, on which Phillips' two-level model is based, and therefore conceptually reviewed in the following subsections. For a detailed derivation, the reader is for example referred to Holton and Hakim, 2013b or Hoskins and James, 2014.

2.2.1 Geostrophic balance

Synoptic-scale systems in the mid-latitudes have a typical horizontal length scale of around 1000 km, the radius of the large-scale eddies accompanying the jet stream. These systems are confined to the troposphere with an average depth of 10 km, hence two orders of magnitude smaller than the horizontal scale. Additionally, the horizontal velocity is three orders of magnitude larger than the vertical velocity of synoptic scale motions. Applying these and additional pressure and time scaling

arguments to the horizontal momentum equation shows that the Coriolis and pressure gradient force terms are larger than all the other terms. Therefore, to a good approximation, there exists a balance between the two forces, called *geostrophic balance*, which can be written in vector notation as

$$\mathbf{V} = \mathbf{k} \times \frac{1}{\rho f_0} \nabla p, \tag{2.1}$$

where $\boldsymbol{V} = (u, v)$ is the horizontal velocity vector, ρ is the density and f_0 is a constant approximation of the Coriolis parameter valid in the mid-latitudes. The pressure is denoted by p, and ∇ is the horizontal gradient thereof. Defining the streamfunction ψ by

$$\mathbf{V} = \mathbf{k} \times \nabla \psi, \tag{2.2}$$

the geostrophic balance (2.1) can be written as

$$\psi = \frac{p}{\rho f_0}. \tag{2.3}$$

Hence, a fluid in geostrophic balance flows along contours of constant pressure, called isobars. Viewing along the flow, low pressure is to the left and high pressure is to the right of the flow in the Northern Hemisphere. Furthermore, from the balance equation (2.1) it follows

$$\frac{\partial u}{\partial x} + \frac{\partial v}{\partial y} = -\frac{1}{\rho f_0} \frac{\partial^2 p}{\partial x \partial y} + \frac{1}{\rho f_0} \frac{\partial^2 p}{\partial x \partial y} = 0, \tag{2.4}$$

so geostrophic flow is non-divergent, a property used for the derivation of the QG equations (see subsection 2.2.4).

2.2.2 Hydrostatic balance

Similar scaling arguments can be applied to the vertical component of the momentum equation. Since pressure decreases by about one order of magnitude from the ground to the tropopause, it can be shown that to a high degree of accuracy, the pressure field is in *hydrostatic balance*, that is, the pressure gradient force is balanced by the gravitational force and therefore, the pressure at any given point in the atmosphere is equal to the weight of air overlying this point. This approximation holds for the reference atmosphere as well as for deviations thereof and can be written as

$$\frac{\partial p}{\partial z} + \rho g = 0, \tag{2.5}$$

where g denotes the magnitude of gravity, and p and ρ denote the reference or perturbation pressure and density, respectively. Therefore, for synoptic-scale motions, vertical accelerations can be neglected, as done for the derivation of the QG equations in subsection 2.2.4.

For models describing the mid-latitudes, it is often useful to take pressure instead of height as the vertical coordinate, which is also the coordinate system of choice in this thesis. Defining the geopotential Φ by $d\Phi/dz = g$ and using the ideal gas law $p = \rho R T$, equation (2.5) can be written as

$$\frac{\partial \Phi}{\partial p} = -\frac{RT}{p},\tag{2.6}$$

where R is the gas constant for dry air ($R = 278$ J kg^{-1} K^{-1}) and T denotes the temperature. Thus, the variation of geopotential with respect to pressure depends only on temperature, a property used to derive the QG thermodynamic energy equation in subsection 2.2.4.

2.2.3   Thermal wind balance

Using pressure as the vertical coordinate, the thermodynamic state of the atmosphere must be specified by horizontal and vertical variations of the geopotential Φ and the temperature T. With the hydrostatic balance equation (2.5), the relation between horizontal variations of pressure and geopotential is given by

$$-\frac{1}{\rho}\left(\frac{\partial p}{\partial x}\right)_z = -\left(\frac{\partial \Phi}{\partial x}\right)_p \qquad \text{and} \qquad -\frac{1}{\rho}\left(\frac{\partial p}{\partial y}\right)_z = -\left(\frac{\partial \Phi}{\partial y}\right)_p,\tag{2.7}$$

where the subscripts denote the variables that remain constant when evaluating the derivative. Therefore, the geostrophic balance (2.1) can be written in pressure coordinates as

$$\mathbf{V} = \mathbf{k} \times \frac{1}{f_0}\nabla\Phi,\tag{2.8}$$

having the advantage that the density no longer appears explicitly in the pressure gradient force. Hence, a given geopotential gradient yields a constant geostrophic wind at any height, whereas a given horizontal pressure gradient yields different values of the geostrophic wind depending on the density.
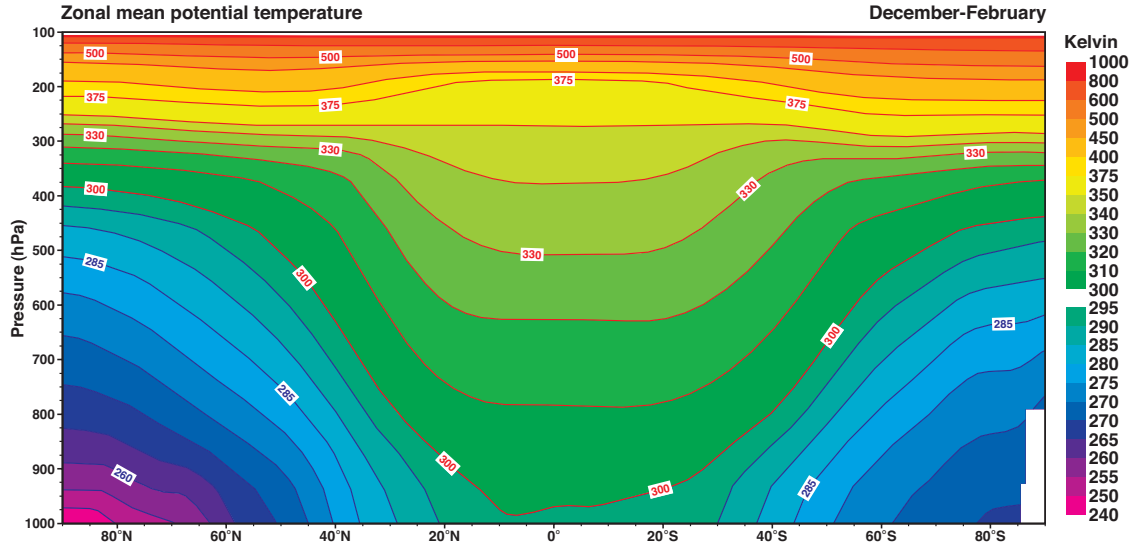
FIGURE 2.6: Meridional cross-section of longitudinally and time-averaged potential temperature field for December to February; from Kållberg et al., 2005.

Differentiating equation (2.8) and applying the hydrostatic balance equation (2.6) gives

$$\frac{\partial \mathbf{V}}{\partial \ln p} = -\mathbf{k} \times \frac{R}{f_0} \nabla T, \tag{2.9}$$

the equation commonly referred to as *thermal wind balance*. This relationship states that vertical variations of the geostrophic wind are proportional to horizontal variations of the temperature field.

Figure 2.6 shows a time-averaged field of potential temperature which is proportional to temperature by its definition

$$\theta = T(p_s/p)^{r/c_p}, \tag{2.10}$$

meaning that the potential temperature θ is simply the temperature that a parcel of dry air at pressure p and temperature T would have if it were expanded or compressed adiabatically to a standard pressure p_s, usually taken to be 1000 hPa (see e.g. Holton and Hakim, 2013a). Hence, comparing the zonal mean potential temperature field in figure 2.6 to the zonal mean wind in figure 2.5 indicates that the zonal flow is close to thermal wind balance. In the mid-latitudes, where the horizontal gradient of the potential temperature towards the poles is greatest, the zonal wind is westerly, increases with height and attains its maximum below the tropopause as mentioned before. Therefore, the thermal wind equation is a relationship for the vertical wind shear, i.e. the rate of change of the wind with height, with the greatest shear occurring at the location of greatest poleward gradients of

the temperature field, namely in the mid-latitudes.

2.2.4 The quasi-geostrophic equations

The former subsections have shown that mid-latitude synoptic-scale systems satisfy the geostrophic and hydrostatic balance equations, hence for these systems the equations of motion can be substantially simplified and are called *quasi-geostrophic* (QG). The governing equations are obtained by starting from the (approximate) zonal and meridional equation of motion and continuity in the pressure coordinate system

$$\frac{D\mathbf{V}}{Dt} + f\mathbf{k} \times \mathbf{V} = -\nabla\Phi + A\nabla^2\mathbf{V} + g\frac{\partial\boldsymbol{\tau}}{\partial p}, \tag{2.11a}$$

$$\nabla \cdot \mathbf{V} + \frac{\partial\omega}{\partial p} = 0, \tag{2.11b}$$

where ∇ is again the horizontal gradient, $\omega = dp/dt$ is the vertical velocity in isobaric coordinates, and the vertical advection of horizontal motion ($\omega\frac{\partial u}{\partial p}$, $\omega\frac{\partial v}{\partial p}$) in equation (2.11a) is neglected. The vector $\boldsymbol{\tau} = (\tau_x, \tau_y)$ denotes frictional stress across horizontal surfaces and A is the eddy diffusion parameter.

The QG vorticity equation used in Phillips, 1956 is obtained by taking $\nabla\times$ equation (2.11a) and introducing the geostrophic assumption $\partial u/\partial x + \partial v/\partial y = 0$ (equation 2.4) for all velocities besides in the term $f\nabla \cdot \mathbf{V}$, where the continuity equation (2.11b) was substituted. This incorporates the fact, that the mid-latitude flow is only approximately geostrophic, that is, having a small but significant ageostrophic component as well. Further, the β-plane approximation $f = f_0 + \beta y$ is used, which assumes a slowly varying f, such that $f = f_0$ is constant everywhere, except in the derivative with respect to y, where $\partial f/\partial y = \beta$ (Rossby, 1939), yielding

$$\left(\frac{\partial}{\partial t} + \mathbf{V} \cdot \nabla\right)(f + \nabla^2\psi) - f_0\frac{\partial\omega}{\partial p} = A\nabla^2\nabla^2\psi + g\frac{\partial}{\partial p}(\nabla \times \boldsymbol{\tau}), \tag{2.12}$$

where the geostrophic streamfunction was defined as $\psi = \Phi/f_0$.

The thermodynamic energy equation in pressure coordinates is defined as

$$\left(\frac{\partial}{\partial t} + \mathbf{V} \cdot \nabla\right)T - \Gamma\omega = \frac{J}{c_p} \tag{2.13}$$

where J is the diabatic heating, c_p is the isobaric specific heat capacity of dry air and the static stability Γ is defined as

$$\Gamma = \frac{RT}{pc_p} - \frac{\partial T}{\partial p}. \tag{2.14}$$

The QG thermodynamic energy equation is obtained by replacing Γ with the basic state static stability $\overline{\Gamma} = \frac{RT_0}{pc_p} - \frac{\partial T_0}{\partial p}$ and using the hydrostatic approximation (2.6) to write the temperature in terms of the streamfunction,

$$f_0 \frac{\partial \psi}{\partial p} = \frac{\partial \Phi}{\partial p} = -\frac{RT}{p}. \tag{2.15}$$

Thus, the QG thermodynamic energy equation reads

$$\left(\frac{\partial}{\partial t} + \mathbf{V} \cdot \nabla \right) \frac{\partial \psi}{\partial p} + \frac{R\overline{\Gamma}}{pf_0} \omega = -\frac{R}{pf_0 c_p} J. \tag{2.16}$$

Generalising the derivation in Charney, 1947, these equations were first introduced in a mathematically rigorous manner by Charney, 1948 (without the diffusion and friction terms), in a search for a set of simplifying principles governing the meteorologically significant motions of the mid-latitudes. Charney pointed out the necessity to "filter out the noise" from the equations of motion, that is, wave solutions describing small-scale phenomena like sound waves and other theoretically possible waves that do not influence the large-scale motions of the atmosphere, and that make integrating the equations impossible. Up to this study, it was known that the atmosphere on synoptic scales is to a high degree in hydrostatic and geostrophic balance and the motions are quasi-horizontal and quasi-adiabatic, but efforts to incorporate these properties together with the geostrophic approximation have failed.

The arguments in Charney, 1948 are based on dimensional analysis, specifically an extensive discussion of the scale arguments briefly mentioned in sections 2.2.1, 2.2.2 and 2.2.3. This enabled him to show that by eliminating the horizontal divergence and applying the synoptic approximations stated above, the large-scale motion of the atmosphere is governed by equations (2.12) and (2.16), which indeed filter out the meteorologically insignificant motions. During the times of very limited computing power, these results had important implications for numerical weather forecasting, since the integration of the simplified equations presupposed knowledge of the initial pressure field only, at that time directly available, instead of initial distributions of horizontal accelerations and divergence.

Although the technical development of computers quickly overcame the need for such

a limiting simplification, the QG equations are the starting point for most theoretical studies concerning the mid-latitude atmosphere. According to Phillips, 1954, one can differentiate between two principle types of these studies, namely *barotropic* and *baroclinic* ones. For barotropic studies, the basic current is assumed to be a function of latitude only, neglecting the vertical increase of the mid-latitude jet. In contrast to that, in baroclinic studies, only this vertical structure is considered but latitudinal variations of the zonal flow are neglected. In both types of studies, unstable (amplifying) and stable (damped) wave solutions are mathematically possible.

Phillips, 1954 noted that actual weather charts seem to be best described by a combination of amplifying baroclinic and damped barotropic waves. However, the combination of barotropic and baroclinic wave development has not been accomplished to that date but was always addressed separately. These two concepts will be touched upon in the next section, together with some assorted literature that inspired Phillips' design of his experiment, followed by the introduction of his two-level model.

2.3 Models of the mid-latitude atmosphere

In a barotropic atmosphere, the density is dependent on pressure only, $\rho = \rho(p)$. Hence, the isobaric surfaces are surfaces of constant density, and by the ideal gas law, surfaces of constant temperature. Therefore, $\nabla T = 0$ and the thermal wind balance equation (2.9) becomes

$$\frac{\partial \mathbf{V}}{\partial \ln p} = 0, \tag{2.17}$$

stating that the geostrophic wind does not vary with height in a barotropic atmosphere. In a baroclinic atmosphere, the density depends on both the pressure and temperature, $\rho = \rho(p, T)$. Thus, the geostrophic wind varies with height and the resulting wind shear is related to the horizontal temperature gradient by the thermal wind balance (2.9).

In the mid-latitude atmosphere, both barotropic and baroclinic instabilities determine the evolution of the flow. Superposed on a zonally symmetric basic flow field, barotropic instabilities are associated with asymmetries in the horizontal, gaining kinetic energy from the mean flow. Baroclinic instabilities, however, are variations in height, imposing a vertical shear onto the mean flow. They draw their energy from the potential energy resulting from the equator-to-pole temperature gradient that produces the vertical shear by thermal wind balance.

Although both of these instability types are important in synoptic-scale meteorology and barotrophy is a very strong constraint on the fluid motions, it proves useful to analyse a simpler barotropic atmosphere in order to gain some understanding of the mid-latitude atmospheric motions. Therefore, the next subsections touch upon relevant simple models regarding both instability types.

2.3.1 Barotropic instability

One of the simplest and most fundamental studies on barotropic perturbations is the work of Rossby, 1939 on large-scale planetary waves, today called *Rossby waves.* Considering a friction-less, homogeneous, incompressible atmosphere in a purely horizontal motion, that is, a barotropic atmosphere, the equations of motion reduce to a single equation expressing the conservation of absolute vorticity

$$\zeta + f = \text{constant}, \tag{2.18}$$

following a horizontal motion, where ζ is the vertical component of relative vorticity defined as

$$\zeta = \nabla^2 \psi = \frac{\partial v}{\partial x} - \frac{\partial u}{\partial y}. \tag{2.19}$$

Vorticity is positive for cyclonic (anti-clockwise) rotation and negative for anticyclonic rotation. Hence, equation (2.18) implies that relative to a reference latitude, air displaced towards higher latitudes will experience increased anticyclonic rotation, whereas air displaced towards lower latitudes will experience increased cyclonic rotation. This perturbation vorticity field induces a meridional velocity field where the air moves southward west of a vorticity maximum and northward west of a vorticity minimum, creating a barotropic wave structure.

Rossby showed with a simple perturbation analysis that latitudinal displacements of the flow are sufficient to create such a wave structure. These Rossby waves always travel westward relative to the mean zonal flow, whereas the wave can become stationary (in an absolute reference frame) for a certain wavelength relative to the mean zonal flow speed. However, for typical synoptic-scale disturbances, the Rossby wavelength is smaller than the stationary condition wavelength and therefore the wave travels eastward relative to the ground at a speed that is somewhat less than the mean zonal wind speed.

Another study of the character of nondivergent horizontal wave motion in a barotropic atmosphere was done by Kuo, 1949. In this work, it was assumed that the velocity

profile of the westerlies is meridionally symmetric with respect to some latitude and that the basic zonal velocity $u(y)$ is superposed by some simple wave structure with velocity c within a predefined latitudinal channel. The resulting singularity at $u = c$, where the wind velocity is equal to the wave velocity, of the derived vorticity evolution equation was obviated by introducing viscous stress terms into the equation, that can be neglected outside a thin belt around this singular point. Meteorologists had usually avoided this singularity by assuming that the wave velocity c is always smaller than u, which restricted the possible solutions to slowly moving long waves.

Analysing this model yields both amplified and damped perturbations as possible solutions, where the existence depends on the values of absolute vorticity within the latitudinal channel. If the absolute vorticity $\zeta + f$ is zero anywhere within the channel boundaries, neutral and amplified waves can exist with a velocity value between the minimum and maximum wind velocity, making the flow barotropically unstable. If no such critical point exists, then all perturbations must be damped and the flow is barotropically stable.

Phillips was exposed to both of these theories in his early career. As he recalls in the earlier mentioned interview (Phillips et al., 1989), Rossby used to talk a lot about his thoughts on vorticity mixing instead of angular momentum in his university courses. After his master's studies, Phillips worked for around two years with Kuo on a project supervised by Rossby, while Kuo was also writing his doctoral thesis on barotropic instability. Together with his experience in programming barotropic models, this exposure and subsequently in-depth knowledge obtained during his graduate time encouraged Phillips to conduct his first study on baroclinic unstable waves (Phillips et al., 1989).

2.3.2 Baroclinic instability

The work in Charney, 1948 on the set of generically applicable QG equations was based on his study of long waves in a baroclinic westerly current in Charney, 1947. Commenting on the work done by Rossby and others, he noted that studies of incompressible and barotropic atmospheres without vertical shear are not suitable to solve the instability problem since these models do not contain a source of potential energy that can convert into kinetic wave energy. Charney addressed this issue by setting up his model with a troposphere that is characterized by nearly constant values of the vertical lapse rate, that is, the rate of decrease of temperature with height, and a constant horizontal temperature gradient, and as a consequence a constant increase of the zonal wind with height. The total flow is then assumed to be superimposed by a small perturbation on the mean flow. However, in order to

be able to solve the equations explicitly, the author made the limiting assumption that the mean flow and perturbations are independent of the latitude.

For comparability, Charney first integrated the derived model equations for the special case of a barotropic atmosphere and re-derived the wave-velocity formula of Rossby, 1939. He further generalised this formula showing that it applies to baroclinic waves if the constant value of the zonal wind is the mean zonal wind averaged with respect to pressure from the top to the bottom of the baroclinic atmosphere. He found that for a given wavelength, the waves are neutral if the shear of the zonal wind lies below a certain critical value which increases with wavelength. For a greater shear than this value, the waves are unstable, that is, amplifying, and the instability becomes more pronounced with increasing shear, lapse rate and latitude. Longer waves are more stable and stability is almost independent of the value of the surface zonal wind speed.

The wave solutions of the baroclinic model in Charney, 1947 resemble many of the characteristics of the waves observed on daily weather maps in terms of speed of propagation and internal structure. The propagation speed is in general eastwards and is approximately equal to the speed of the surface zonal current, and the waves usually have a westward tilt with height. This tilt is an observation that is not explainable in terms of a barotropic atmosphere. Further, this theory predicts that waves of length less than 6000 km are amplified for a vertical shear of the zonal wind that is greater than about 1.5 m s^{-1} km^{-1}, a value usually exceeded in the mid-latitudes, especially in the Northern Hemisphere winter. Therefore, Charney concluded that the observed westerlies with vertical shear can be regarded as the origin of a constant amplification of perturbations.

When setting up the model, Charney also assumed that the stratosphere has specific flow and temperature profiles. However, by modifying these within the study he was able to show that the winds in the stratosphere have little influence on tropospheric weather phenomena, a result that is useful to justify respective model simplifications.

An even simpler baroclinic model, also based on the QG equations, is that of Eady, 1949. The main differences to Charney's model are that it is bounded by a rigid lid at the top of the troposphere, that the basic state density is constant, and that the Coriolis parameter is constant, that is, $\beta = 0$. Although these conditions only allow for a limiting representation of the real atmosphere, Eady's results are remarkably similar to the analysis in Charney, 1947, especially the growth rate and wavelength of the most unstable wave. The basic flow in this model has a uniform vertical shear and the interior potential vorticity gradient is zero. Therefore, the amplification of
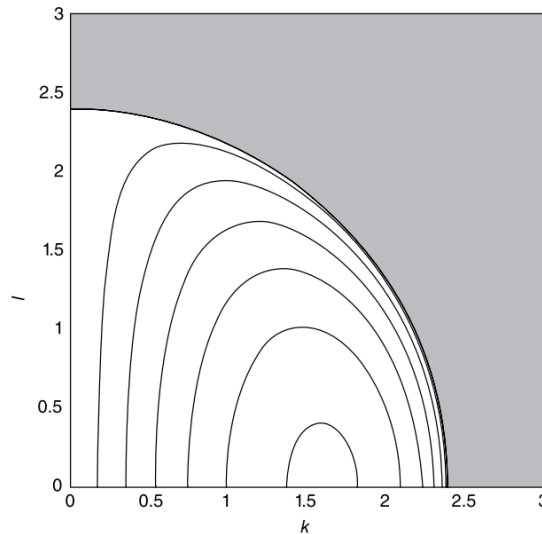
FIGURE 2.7: Growth rate for the Eady model as a function of the zonal wavenumber k and meridional wavenumber l, the shading indicates regions where there is no instability; from Hoskins and James, 2014.

waves relies on the interactions between two Rossby waves trapped at the top and bottom boundaries.

Similar to Charney, Eady found a critical wavelength, or *shortwave cut-off*, beyond which the baroclinic instability ceases, visualised by the shaded area in figure 2.7. Shorter waves are amplified and their growth rate dependence on the zonal and meridional wavenumber is depicted by the contours in figure 2.7. The shortwave cut-off resembles the fact that the mutual interaction of the waves over the depth of the model atmosphere is too weak to result in amplification because the vertical scale of the waves is too small. As in Charney, 1947, the waves become more unstable with increasing shear and lapse rate, in other words, the amplification of baroclinic waves is more pronounced for a basic flow with a higher available potential energy that the perturbation can grow on.

The most unstable wave in Eady's model has a similar vertical structure as the one in Charney's model and is of the type observed in the mid-latitudes. The meridional velocity wave is tilted westward with height and the upper- and lower-level waves are displaced relative to one another by exactly one-quarter of a wavelength. The vertical velocity wave is also tilted westward, whereas the temperature wave tilts eastward with height. A consequence of this variation of amplitude and phase with height is that the co-variance of the poleward velocity and temperature perturbation, that is, the poleward temperature flux is constant with height.

A short time after Eady's publication, in 1951, Phillips got the opportunity to present his first ideas on the two-level model in a meeting with Rossby and Charney,

where he elaborated on his difficulties with deriving the wave instability formula for his model. Encouraged to be bold with some of his assumptions by Rossby and Charney, he was finally able to derive the formula and since he hadn't heard of Eady's paper before that, he "remember[s] being elated" (Phillips et al., 1989) by the good match of his own with Eady's stability formula.

Shortly after, Phillips published his design of the two-level model, a prelude paper to his numerical experiment, with which he convinced Charney, his boss at the time (Phillips et al., 1989), to conduct the actual experiment. This two-level model is the basis of the research in this thesis and is introduced in the next subsection.

2.3.3   Phillips' quasi-geostrophic two-level model

In the two-level model, the Northern Hemisphere mid-latitudes are represented by a rectangular region, bounded latitudinally by fixed vertical walls at $y = 0$ and $y = W$, where W is set as the equator-to-pole distance. In the longitudinal direction, cyclic continuity is assumed, allowing for the life cycle of eddies since perturbations moving out of the domain on the eastern boundary enter the domain again on the western boundary. The vertical structure of the atmosphere is represented by two discrete layers bounded by surfaces, designated by 0, 2 and 4 as shown in figure 2.8. The QG vorticity equation including eddy diffusion and surface friction (2.12) is applied at the 250 and 750 hPa levels, denoted by 1 and 3 in figure 2.8. The derivative of the vertical wind with respect to pressure is evaluated by taking centred finite differences and noting that the vertical wind vanishes at the top and bottom surface, such that

$$\left(\frac{\partial \omega}{\partial p}\right)_1 = -\left(\frac{\partial \omega}{\partial p}\right)_3 = \frac{\omega_2}{\delta p}. \tag{2.20}$$

The surface friction stress $\boldsymbol{\tau} = (\tau_x, \tau_y)$ vanishes at the top layer, but according to Phillips, 1956, practically nothing is known about its value at 500 hPa. Therefore, it is assumed that $\boldsymbol{\tau}_2$ is much smaller than $\boldsymbol{\tau}_4$ and approximate $\boldsymbol{\tau}_2 = 0$, that is, the surface friction vanishes away from the surface compared to the friction on the actual surface. Further, the stress at the ground level is generally taken to be directed opposite to the surface wind C and proportional to the square of the wind speed at anemometer height, according to

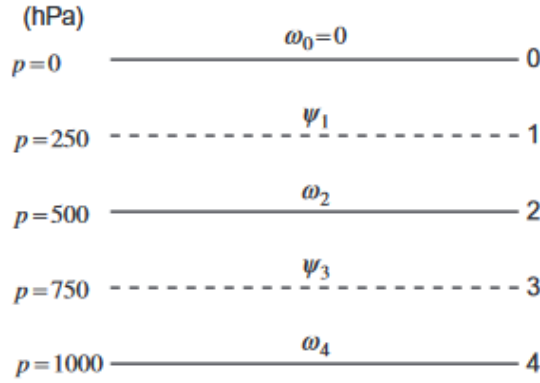$$|\boldsymbol{\tau}_4| = \hat{k}\rho C^2, \tag{2.21}$$

FIGURE 2.8: Visualisation of the vertical cross-section of the two-level model with relevant variables at each pressure level; from Holton and Hakim, 2013a.

where $\hat{k}$ is a non-dimensional constant. However, for simplicity, it is assumed, that τ_4 is directed at a constant angle to the surface geostrophic wind $\overline{C}_g$ and proportional to the wind speed. Assuming further that the anemometer (measurable) wind speed is about 70% of the geostrophic wind speed and using the ideal gas law, the friction term at level 3 can be rewritten as

$$g\nabla \left(\frac{\partial \boldsymbol{\tau}}{\partial p}\right)_3 = g\nabla \left(\frac{\boldsymbol{\tau}_4}{\delta p}\right) = \frac{g}{\delta p}\left(\frac{\partial \tau_y}{\partial x} - \frac{\partial \tau_x}{\partial y}\right)_4 = -\kappa\nabla^2\psi_4, \tag{2.22}$$

where $\kappa = 0.98g\hat{k}\overline{C}_g(RT_4)^{-1}$, and in the further derivation the vorticity on the ground level $\zeta_4 = \nabla^2\psi_4$ is defined by linear extrapolation from levels 1 and 3 according to $\zeta_4 = 3\zeta_3/2 - \zeta_1/2$.

The QG thermodynamic energy equation (2.16) is applied at level 2, where the derivative with respect to pressure is evaluated again by centred finite differences. The diabatic heating is set to be a linear and asymmetric function about $y = W/2$ (45°N latitude) and is defined in detail in section 3.2. Finally, the three equations on levels 1, 3 and 2 are

$$\left(\frac{\partial}{\partial t} + \boldsymbol{V}_1\cdot\boldsymbol{\nabla}\right)(\beta y + \nabla^2\psi_1) - f_0\frac{\omega_2}{\delta p} = A\nabla^2\nabla^2\psi_1, \tag{2.23a}$$

$$\left(\frac{\partial}{\partial t} + \boldsymbol{V}_3\cdot\boldsymbol{\nabla}\right)(\beta y + \nabla^2\psi_3) + f_0\frac{\omega_2}{\delta p} = A\nabla^2\nabla^2\psi_3 - \kappa\nabla^2\psi_4, \tag{2.23b}$$

$$\left(\frac{\partial}{\partial t} + \boldsymbol{V}_m\cdot\boldsymbol{\nabla}\right)\frac{\psi_3 - \psi_1}{\delta p} + \frac{R\overline{\Gamma}_2}{p_2 f_0}\omega_2 = -\frac{R}{p_2 f_0 c_p}J_2, \tag{2.23c}$$

where $\boldsymbol{V}_m = (\boldsymbol{V}_1 + \boldsymbol{V}_3)/2$ is the average wind vector between levels 1 and 3. These equations will be used in chapter 3 and 4 as the basis for the model derivation.

With these equations Phillips conducted his outstanding numerical weather forecast,
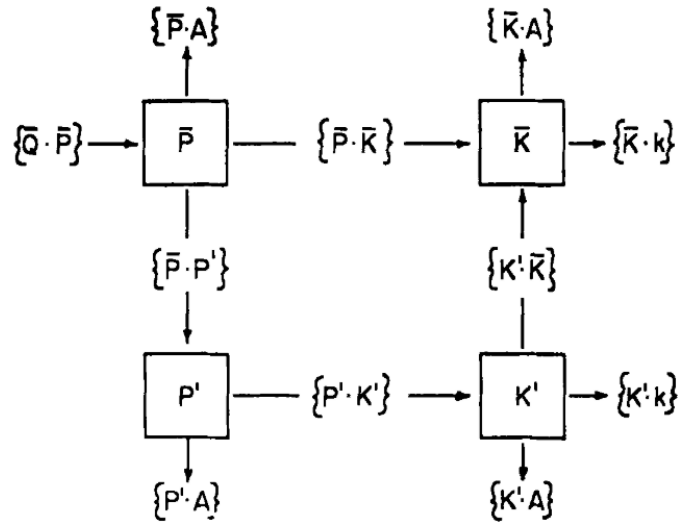
FIGURE 2.9: Energy flow diagram of Phillips' QG two-level model showing the reservoirs of kinetic (K) and potential (P) energy, where zonal mean components are denoted by overlines, eddy components by primes; $\overline{Q}$ denotes the adiabatic heating; the flow of energy is in the direction of the arrow if the associated transformation $\{\cdot\}$ is positive; taken from Phillips, 1956.

which attracted great attention and recognition by his colleagues, Charney and Eady amongst others, and inspired conferences and an international collaborative effort on numerical weather prediction (Lewis, 1998). In addition to that, Phillips derived the energetics of this model in the 1956 paper. Because the heating is asymmetric about the 45°N latitude, the total amount of energy added to the system is zero. However, the heating is positively correlated with the temperature in the total energy budget, and therefore the available potential energy of the system increases by adding heat at high temperatures and taking it away at low temperatures. The loss of energy from the system is due to eddy diffusion and surface friction.

The flow diagram in figure 2.9 shows the energy transformations between the kinetic (K) and potential (P) energy reservoirs of the mean zonal (denoted by overlines) and eddy (denoted by primes) components. Deriving explicit equations for the energy transformation terms $\{\cdot\}$ enabled Phillips to explain the diagram as follows. The heating in warm and cooling in cold latitudes increases the zonal potential energy $\overline{P}$ of the system and is transformed into eddy potential energy P' by horizontal transport of temperature by the eddies from warmer to colder regions. The transformations from potential into kinetic energy $\{\overline{P} \cdot \overline{K}\}$ and $\{P' \cdot K'\}$ represent the effect of vertical circulations in meridional and zonal planes, respectively. The transformation from eddy into zonal kinetic energy $\{K' \cdot \overline{K}\}$ denotes the eddy transport of horizontal momentum. The losses due to eddy diffusion are denoted by $\{X \cdot A\}$ and due to surface friction by $\{X \cdot k\}$.

The arrows in the diagram are drawn as if the transformations were all positive. This is true for all besides one transformation. Assuming the system to be in a steady state, the energy level in each of the reservoirs must be constant, so the flow into and out of each one must add up to zero. Phillips states that the classical theories of the general circulation would imply that the transformation $\{\overline{P} \cdot \overline{K}\}$ is positive, therefore maintaining the zonal kinetic energy against friction and dissipation because the effect of the large eddies in maintaining the zonal flow was disregarded. However, Phillips' experiment showed that $\{\overline{P} \cdot \overline{K}\}$ is actually slightly negative, and since the only other source of energy for the zonal kinetic energy is the eddy kinetic energy, this shows that in fact, it is the large scale eddies that maintain the zonal flow against dissipation. The negativity of $\{\overline{P} \cdot \overline{K}\}$ was also deferred from available wind statistics at that time and later verified by Oort, 1964.

This detailed treatment of the energy budget in the system allowed Phillips to verify the extent to which the model contains the physical processes that are known to be important in the real atmosphere. Although he recalls that he had been unaware of Lorenz's work at the time he finished the theoretical aspects of the numerical experiment (Phillips et al., 1989), Phillips acknowledges Lorenz's "beautiful attempt to reconcile the synoptic meteorologist's intuitive association of available potential energy with temperature gradients", a more general treatment of the energetics in the atmosphere in Lorenz, 1955, and concludes that both came to very similar results. Since it is referred to the energetics of the atmosphere in several parts of this thesis, the Lorenz energy cycle is presented in the following subsection.

2.3.4 Lorenz energy cycle

Lorenz, 1955 derived the energetics of the general circulation in a similar manner and his findings can be illustrated as an energy flow diagram as well, see figure 2.10. His calculations show that the net heating of the atmosphere at low latitudes and the net cooling at high latitudes results in a generation of zonal mean potential energy. All of this energy is converted into eddy potential energy by the horizontal eddy transport of heat, in other words, the transport of warm air poleward and cold air equatorward. Some of this energy is dissipated through the heating of the colder and cooling of the warmer parts of the eddies, but the main portion is converted to eddy kinetic energy by the vertical motion within the eddies, that is, the sinking of cold and rising of warm air. Again, some of this energy is dissipated by friction, but most of it is transformed into zonal mean kinetic energy by the horizontal momentum transport by the eddies. Most of the zonal mean kinetic energy is finally
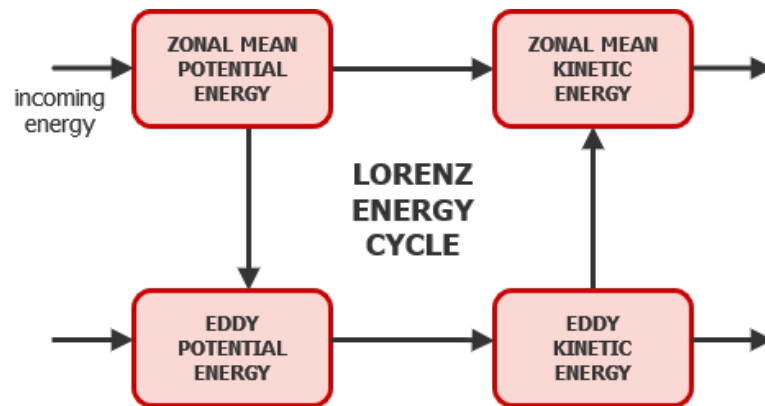
FIGURE 2.10: The Lorenz energy cycle, boxes denote the reservoirs of the energy types, arrows denote the transformation from one type of energy into another.

dissipated by friction, however, a small residual is converted into zonal available potential energy again by an indirect meridional circulation.

Lorenz concludes "that the large-scale eddies supply enough kinetic energy to the zonal flow to maintain it against the dissipative effects of small-scale eddies" (Lorenz, 1955). Additionally, the eddies are primarily responsible for the poleward heat transport to balance the temperature gradient imposed by the excess of radiation in the equatorial region.

One argument in Lorenz, 1955 states that the zonal winds and superposed eddies, a feature of the distribution of momentum and therefore possessing kinetic energy, are not identical with the meridional pressure gradient and the superposed pressure perturbations, which are features of the distribution of mass and therefore possess available potential energy. And although it is legitimate to study the exchanges of zonal mean and eddy kinetic energy separately, it is of value to include the study of available potential energy, because often zonal winds are identified with the meridional pressure gradient, and eddy circulations are identified with the pressure systems that almost always accompany them. In contrast to Lorenz, using this argument to support his analysis, this argument is partly reversed in the current thesis, since the systems derived in chapter 3 and 4 include primarily the kinetic energies but are interpreted in terms of the full energy cycle of the mid-latitude circulation.

2.4   The mid-latitude storm track

The objective of this thesis is to develop models that can capture some of the complex non-linear dynamics of the atmosphere, based on observed properties of the mid-latitudes and especially the storm tracks and the accompanying eddies. To

be able to do that, this last section is dedicated to shortly introducing some of these observed features, later used to support some modelling choices.

2.4.1 The storm track life cycle

Storm tracks are defined as the region in the mid-latitudes, especially the North Pacific and North Atlantic, where eddy activity is strongest. Their shape is zonally asymmetric with a distinct entrance, middle and exit region. The entrance region is characterised by a strong surface baroclinicity which generates the eddies. The middle region is dominated by strong eddy activity that weakens the mean flow baroclinicity, and finally in the exit region the eddies break or decay (Orlanski and Gross, 2000).

An early extensive study on the shape of eddies and their interaction with the mean flow is that of Hoskins, James, and White, 1983, providing a theory to quantify the feedback of the eddies onto the mean flow and the behaviour of the eddies themselves based on the famous Eliassen-Palm (EP) flux. This is a vector quantity in the meridional plane, thus non-zero components in the latitude and height coordinate, which is used to determine the relative importance of eddy heat flux and momentum flux. When the EP flux vector points upward, the poleward temperature flux dominates, when the vector points north- or southward, the meridional momentum flux dominates. The divergence of the EP-flux can be used to diagnose the zonal force exerted by synoptic-scale eddies on the mean flow.

Hoskins, James, and White, 1983 developed the three-dimensional extension of the EP flux vector

$$\mathbf{E} = (\overline{v'^2 - u'^2}, -\overline{u'v'}, \frac{f_0 c_p}{g}\overline{v'T'}), \tag{2.24}$$

where the overlines denote a time average and the primes a deviation from that average. The vertical component of the vector is proportional to the meridional eddy temperature flux. Applying this vector to flow fields of the Northern Hemisphere storm tracks, the authors found the following structure and influence of the eddies onto the mean flow. In the entrance region of the storm track, the eddies show a divergence of the horizontal components of $\mathbf{E}$, indicating a mean westerly forcing and a tendency by the eddies to extend the strong westerly flow. In the vertical, the eddies develop in low levels of the jet entrance and propagate upward, thus decreasing the vertical shear in this region. Towards the exit of the storm track, the eddies become more zonally elongated, tilted in the southwest-northeast direction, and travel at a speed slower than the mean flow. Hoskins, James, and White, 1983
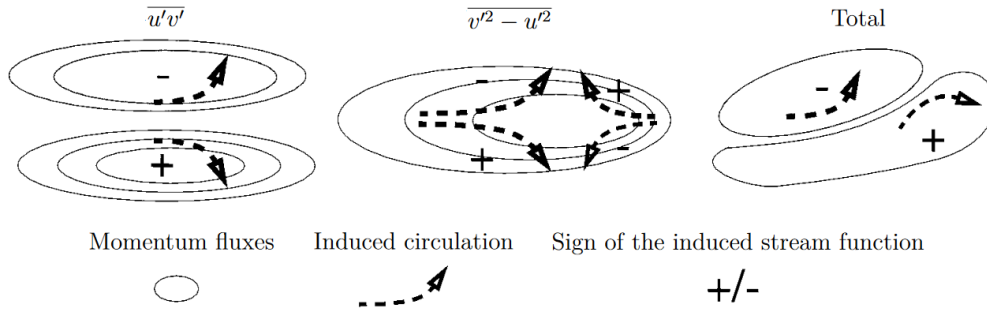
FIGURE 2.11: Correlation velocity patterns and the induced circulation and vorticity tendency of horizontal components of Hoskins' **E**-vector; the meridional flux of zonal momentum (left), the variance of the meridional minus the variance of the zonal wind component (middle), the total response if the eddy forcing (right); adapted from Orlanski, 1998.

also found the characteristic westward tilt with height in the entrance region of the storm track that he attributes to an increasing surface baroclinicity in these regions initially leading to eddy formation.

Energetically, these zonally elongated eddies exhibit a reducing force on the mean flow where it is strong, and an increasing force where it is weak. This implies an overall decrease of the mean zonal kinetic energy and in a theoretical absence of dissipation would increase the kinetic energy of the eddies.

2.4.2 Storm track variability

By analysing 11 years of vertically averaged ECMWF data, Orlanski, 1998 gave a detailed overview of the storm track barotropic variability on different time scales. On the scale of the winter storm track, the analysis shows that the eddies accelerate the westerlies in the middle of the storm track and deflect them poleward at the exit. Orlanski derived an expression for the eddy-induced tendency of the vertically averaged streamfunction to explain this deflection, containing the horizontal terms of Hoskins' **E**-vector (2.24), namely $(\overline{u'v'})$ and $(\overline{v'^2 - u'^2})$. The contributions of these terms to the streamfunction tendency are summarised in figure 2.11. The meridional momentum flux $(\overline{u'v'})$ (on the left), being positive on the poleward and negative on the equatorward side of the jet, induces an anticyclonic vorticity on the equatorward side and a cyclonic vorticity on the poleward side of the jet, yielding a streamfunction tendency with the same sign as the momentum fluxes. Since the magnitude of the positive flux is higher, the jet is strengthened and displaced poleward by the meridional momentum flux.

The contours of $(\overline{v'^2 - u'^2})$ (in the middle) have a maximum towards the exit region of the jet and the induced vorticity given by Orlanski's formula displays a quadrupole

deflection pattern, with anticyclonic streamfunction tendencies to the northeast and southwest and cyclonic tendencies to the northwest and southeast. The combined effect of the two terms (on the right) is to deflect the storm track axis to the north towards the exit region of the jet. These patterns and the described deflection can be seen in observations of both the Pacific and Atlantic storm tracks.

The seasonal life cycle of the storm tracks is characterised by intensifying eddies during the early fall, reaching its maximum by November and decaying for most of the winter months, where the storm track axis is deflected further poleward. A significant difference between November and December of the Pacific storm track is its extension across the Pacific Basin in November, whereas in December the eddy activity terminates further west. This is due to a similar pattern of the eddy forcing, where in the early season the eddy momentum flux $(\overline{u'v'})$ dominates, intensifying and elongating the jet, whereas in December, the effect of $(\overline{v'^2 - u'^2})$ becomes more prominent, the maximum thereof displaced westward and therefore deflecting the jet polewards at its exit region. This phenomenon has negative feedback on the eddy activity in the entrance as well as leading to a more abrupt termination of the eddies in the exit region of the jet.

The wintertime storm track, especially the Pacific one, also exhibits an interannual variability. In warm El Niño years, the extension of the storm track eastwards resembles that of fall conditions due to the source of low-level baroclinicity extending well into the eastern Pacific. In contrast, in cold La Niña years, the storm track terminates early and is deflected poleward, resembling the mid-to-end winter conditions. Although the authors note that it is not clear from their analysis what the source is for the enhanced baroclinicity in the warm phase, it prevents the westward deflection of the $(\overline{v'^2 - u'^2})$ maximum and therefore, the negative feedback on the eddies is inhibited during the warm and enhanced during the cold years.

Orlanski concludes this study by noting that although there are many consistencies between the eddy forcing and the time-mean circulation, it is difficult to prove cause and effect. A later study on a series of numerical experiments (Orlanski, 2003) shed light on the effect of the lower-level baroclinicity, showing that it influences the upper-level wave to such an extent that it can break cyclonically or anticyclonically, deflecting the jet position equatorward or poleward, respectively. In cold years, where the forcing is weak, anticyclonic wave breaking on the equatorward side of the jet dominates and a poleward shift of the jet occurs. For a slightly increased forcing the author found dominating anticyclones with very intense centres, leading to a southwest-northeast elongation of the cyclones and moving the jet poleward.

A further increase of the forcing leads to intensifying cyclones, thinning the anti-cyclones and thus moving the jet equatorward. This transition was found to occur very abruptly. In conclusion, Orlanski, 2003 found that the different wave breaking of the eddies indeed influences the time-mean circulation and its barotropic features.

Woollings, Hannachi, and Hoskins, 2010 used 45 years of daily ERA-40 reanalysis data for an extensive study on the latitudinal variation of the eddy-driven jet stream, where they zonally averaged and filtered the flow field to obtain jet maximum latitude anomalies. They found a trimodal distribution of the jet latitude in the North Atlantic, that is, a wind speed maximum at a central position, south and north thereof, whereas a bimodal distribution was found elsewhere. Using the horizontal component of Hoskins' **E**-vector as well, they further showed that in all three positions, the transient eddies act to reinforce the jet at its current location, and the eddy kinetic energy follows the jet stream and regions of diverging **E**-vectors closely. However, the significance of the central and southern jet positions is more dominant than that of the northern position. The central jet position at approximately 45°N was found to be the most frequented state and could therefore be interpreted as an unperturbed state, yielding a more suitable candidate for the basic state of the system than the mean state according to the authors.

2.5   Concluding remarks

Chapter 2 gave an introduction to the dynamic features of the mid-latitude atmosphere, the region of interest in this thesis. The scientific arguments upon which Phillips' QG two-level model was built were the reason to choose this model for further exploration of the observed variability. It should be noted that the literature introduced in this chapter should not be seen as a complete literature review, but rather an introduction to the theoretical basis of the questions asked in chapter 1.

The discussion above shows that the barotropic and baroclinic variability of the jet stream can be attributed to the anisotropy of the eddies in the storm tracks, but a definite explanation for cause and effect in this complex non-linear system is difficult. In addition, the storm tracks are influenced by many more factors not mentioned in the description above. Important factors determining the shape and location of the jet stream are orography, for example, the Rocky mountains, coastlines of continents, which imply a temperature gradient and therefore high baroclinicity, and many other features of the flow itself, like moist processes besides others. However, the goal of this thesis is to explore the mid-latitude flow by means of a minimal

model with minimal ingredients, so none of the mentioned factors is an ingredient of the developed models.

The first developed model in this thesis can be seen as an undirected exploratory model without any presumption of expected behaviour. Therefore, the zonal flow was chosen to have a latitudinally symmetric shape with a maximum in the middle of the channel defined by the two-level model, equal to the central position of the jet found by Woollings, Hannachi, and Hoskins, 2010. The perturbation flow was defined by circular eddies as seen in figure 2.3. The resulting behaviour unexpectedly resembled a mechanism called *eddy saturation*, which is usually found in models of the Antarctic Circumpolar Current and is explained in detail in the introduction to chapter 3.

The second model, presented in chapter 4, was a more directed approach with the goal to derive a simple model that can exhibit a shift of the zonally averaged flow. With that in mind, the zonal wind was defined to allow for a latitudinal shift of the mean flow maximum, and the perturbation streamfunction to allow for tilted and elongated eddies. The more complex behaviour of this system indeed resembles some of the above-described variability of the jet stream.

Chapter 3

Eddy saturation in a two-level model

3.1 Introduction

The Antarctic Circumpolar Current (ACC) is an ocean current that flows clockwise (seen from the South Pole) around the Antarctic. It is driven at the ocean surface by atmospheric winds, adding momentum to the flow, which is then transported vertically towards the ocean floor by eddies. There the energy is dissipated by the bottom drag, which acts as opposite force to the ocean surface wind (Munk and Palmén, 1951; Nadeau and Ferrari, 2015). Straub, 1993 was the first to suggest that the total amount of transported water within the ACC is independent of the wind stress at the ocean surface, meaning that an increase of energy added by the wind does not lead to an increase of water that is transported around the Antarctic. Since then more studies, using resolved turbulent ocean eddies, have confirmed this finding (e.g. Munday, Johnson, and Marshall, 2013; Nadeau and Ferrari, 2015). According to those studies, an increase in wind stress yields an increase of the vertical shear in the ocean and the flow becomes baroclinically unstable, thus generating stronger eddies instead of yielding a higher volume of water, a process called *eddy saturation.*

Marshall et al., 2017, inspired by a previous model of variability in atmospheric storm tracks (Ambaum and Novak, 2014), explained the physical principles of eddy saturation using a simple model with just three ingredients: a zonal momentum budget, a closure relation between the eddy form stress and eddy energy, and an eddy energy budget. In their model, both the vertical shear and the volume transport of the ACC are predicted to be independent of the forcing by the surface wind but instead controlled by the requirement of a sufficiently unstable vertical shear to overcome the stabilizing role of the eddy energy dissipation. Moreover, the model explains the increase of eddy energy with wind stress. Finally, they conclude an

analogy to the interaction between wave activity and baroclinicity in the original model of atmospheric storm tracks (Ambaum and Novak, 2014).

However, the process driving the variability of storm tracks in the mid-latitude atmosphere differs from the transport in the ocean in several ways. While mechanical stress dominates the oceanic processes described above, the baroclinic instability in the atmosphere is a result of the horizontal temperature gradient between the equator and poles, which is primarily due to the presence of a stronger radiative forcing at low rather than high latitudes. At all levels of the atmosphere, the meridional temperature gradient is proportional to the vertical shear of the mean flow by thermal wind balance and is the source of available potential energy for the eddies which are associated with the storm tracks. The corresponding poleward eddy heat fluxes in the storm tracks act to weaken the baroclinicity and therefore the mean flow (e.g. Pedlosky, 1979; Holton and Hakim, 2013a). The latter process is often referred to as baroclinic adjustment (Stone, 1978). The Lorenz energy cycle provides a comprehensive view of the energetics of the climate system that takes into account forcing, dissipation, and exchange of energy between available potential and kinetic form, and between energy pertaining to the mean flow and energy pertaining to eddy motions (Lorenz, 1967; Peixoto and Oort, 1992; Lucarini et al., 2014).

The heuristic model proposed by Ambaum and Novak, 2014 describes this baroclinic interaction between the mean flow and eddy activity. In its steady state, the model predicts a two-way equilibration of storm tracks to extratropical thermal forcing and eddy friction: baroclinicity is independent of the thermal forcing but proportional to the eddy dissipation, whereas storm track activity is independent of eddy dissipation but proportional to thermal forcing of large-scale baroclinicity and is therefore reminiscent of the eddy saturation phenomenon in the ACC (Novak, Ambaum, and Harvey, 2018).

Within the Lorenz energy cycle framework, one can see the eddy saturation mechanism as that a forcing acting on the zonal fields results in an increase of eddy energy (in both kinetic and available potential form), whereas the zonal energy stays largely unaffected. Additionally, one can view the eddy saturation mechanism as an extreme form of the baroclinic adjustment process; see also discussion in Lucarini, Speranza, and Vitolo, 2007.

The simplest model that can incorporate baroclinic processes together with diabatic heating and surface friction is Phillips' two-level QG model on the β-plane (Phillips, 1956), introduced in section 2.3.3. In this chapter, this model is used to derive a set of ordinary differential equations that are able to provide a minimal yet meaningful

model of the above-described interaction between the mean flow and eddy activity. As discussed below, our model does not represent direct non-linear eddy-eddy interactions.

The usual approach to an instability analysis of such simple models is called normal mode instability analysis (see e.g. Pedlosky, 1979; Hoskins and James, 2014). Therefore, it is assumed that a small perturbation consisting of a single Fourier wave mode of the form $\exp\left[ik(x-ct)\right]$ is introduced into the flow and determined for which conditions the phase velocity c has an imaginary part. If the conditions are met, the perturbations will amplify exponentially. This technique was also used by the studies introduced in section 2.3 like Kuo, 1949, Rossby, 1939, Charney, 1947, Eady, 1949 and Phillips, 1954 himself. Since this analysis only reveals growing normal mode baroclinic instabilities, we use here methods of dynamical systems theory, which allow us to show additionally the existence of a second attracting steady state. Another novel aspect is that this second steady state exhibits the above-described eddy saturation properties in a model with parameterised eddies.

In section 3.2 we briefly review the two-level model and its reduction which follows work by Phillips, 1956 and by Thompson, 1987. In section 3.3 we introduce the non-dimensionalisation used to define our reduced model and determine the steady states. The stability and dependence on relevant parameters thereof are analysed and physically explained in section 3.4 and compared to the normal mode baroclinic instability analysis of Phillips' two-level model in section 3.5. In section 3.6 a quality factor is introduced to describe the oscillatory behaviour of the model and section 3.7 summarizes the results and discusses them in comparison to the current literature.

3.2 The model equations

We use the QG two-level model in pressure coordinates of Phillips, 1956, introduced in section 2.3.3, consisting of two vorticity equations, coupled by a thermodynamic energy equation and including surface friction and a β-plane approximation, i.e. $f = f_0 + \beta y$. The equations are

$$\left(\frac{\partial}{\partial t} + \boldsymbol{V}_1 \boldsymbol{\cdot} \boldsymbol{\nabla}\right)\left(\beta y + \nabla^2 \psi_1\right) - f_0 \frac{\omega_2}{\delta p} = A\nabla^2 \nabla^2 \psi_1, \tag{3.1a}$$

$$\left(\frac{\partial}{\partial t} + \boldsymbol{V}_3 \boldsymbol{\cdot} \boldsymbol{\nabla}\right)\left(\beta y + \nabla^2 \psi_3\right) + f_0 \frac{\omega_2}{\delta p} = A\nabla^2 \nabla^2 \psi_3 - \kappa \nabla^2 \psi_4, \tag{3.1b}$$

$$\left(\frac{\partial}{\partial t} + \boldsymbol{V}_m \boldsymbol{\cdot} \boldsymbol{\nabla}\right)\frac{\psi_3 - \psi_1}{\delta p} + \frac{R\overline{\Gamma}_2}{p_2 f_0}\omega_2 = -\frac{R}{p_2 f_0 c_p}J_2, \tag{3.1c}$$

where ψ is the streamfunction, $\boldsymbol{V} = (u, v)$ the horizontal velocity vector, $\boldsymbol{V}_m = (\boldsymbol{V}_1 + \boldsymbol{V}_3)/2$ is the average velocity vector between levels 1 and 3, $\omega = dp/dt$ the vertical velocity and $\boldsymbol{\nabla}$ is the horizontal gradient. The pressure is denoted by p, where $\delta p = 500\,\text{hPa}$ is the pressure difference between the two vorticity levels as well as the pressure-thickness of each layer. Subscripts 1, 2, 3 and 4 denote the pressure levels 250, 500, 750, and 1000 hPa respectively and as in subsection 2.3.3 the vorticity on the ground level $\zeta_4 = \nabla^2 \psi_4$ is defined by linear extrapolation from levels 1 and 3 according to $\zeta_4 = 3\zeta_3/2 - \zeta_1/2$. The fields are defined in the spatial domain $(x, y) \in [0, L] \times [0, W]$, where L and W are the length and width of the β-plane channel. We remark that, as customary, the x coordinate is aligned with the longitude and the y coordinate is aligned with the latitude. The fields above are defined for non-negative times $t \geq 0$ starting from smooth initial conditions. The natural boundary conditions are $F(0, y, t) = F(L, y, t) \ \forall y \in [0, W]$ and $\forall t \geq 0$ for all fields F.

The parameters A and κ describe the eddy diffusion and the surface friction diffusion. Additionally, J is the diabatic heating and $\overline{\overline{\Gamma}} = RT/pc_p - \partial T/\partial p$ the basic state static stability, where T is the temperature, c_p the isobaric specific heat capacity of dry air and R the specific gas constant for dry air.

Next, we define barotropic and baroclinic potential vorticities

$$q_m = \nabla^2 \psi_m + \beta y \qquad \text{and} \qquad q_T = (\nabla^2 - \lambda_R^2)\psi_T, \qquad (3.2)$$

where the inverse square of the Rossby radius of deformation, which is the length scale at which rotational effects become as important as gravity wave effects in atmospheric motions, is defined as

$$\lambda_R^2 = 2p_2 f_0^2/(\delta p^2 \overline{\Gamma}_2 R). \qquad (3.3)$$

The barotropic and baroclinic streamfunctions are defined as $\psi_m = (\psi_1 + \psi_3)/2$ and $\psi_T = (\psi_1 - \psi_3)/2$. Using these definitions, taking half the sum and the difference of equations (3.1a) and (3.1b), and substituting equation (3.1c) we obtain the barotropic and baroclinic vorticity evolution equation as

$$\frac{\partial q_m}{\partial t} + \mathbf{V}_m \cdot \nabla q_m + \mathbf{V}_T \cdot \nabla q_T = A\nabla^2\nabla^2\psi_m - \frac{\kappa}{2}\nabla^2(\psi_m - 2\psi_T), \qquad (3.4a)$$

$$\frac{\partial q_T}{\partial t} + \mathbf{V}_T \cdot \nabla q_m + \mathbf{V}_m \cdot \nabla q_T = A\nabla^2\nabla^2\psi_T + \frac{\kappa}{2}\nabla^2(\psi_m - 2\psi_T) - \frac{f_0}{\delta p \overline{\Gamma}_2 c_p}J_2 \quad (3.4b)$$

where $\mathbf{V}_m = (\mathbf{V}_1 + \mathbf{V}_3)/2$, $\mathbf{V}_T = (\mathbf{V}_1 - \mathbf{V}_3)/2$. Here we used the geostrophic

assumption of horizontally non-divergent flow in all terms but the one containing the Coriolis parameter.

Since we want to obtain evolution equations for the longitudinally averaged or mean flow (denoted by overlines) and longitudinally varying flow or eddies (denoted by primes) separately, we introduce the zonal mean $\overline{F}(y,t) = 1/L \int_0^L \mathrm{d}x F(x,y,t)$ and define the deviation from such a mean as $F'(x,y,t) = F(x,y,t) - \overline{F}(y,t)$ for any field F. Taking the zonal mean of the flux form of equations (3.4a) and (3.4b) and incorporating the potential vorticity definitions (3.2) gives evolution equations for the zonally averaged barotropic and baroclinic vorticities as

$$\frac{\partial \overline{q}_m}{\partial t} - \frac{\partial^2}{\partial y^2}\overline{v'_m u'_m} - \frac{\partial^2}{\partial y^2}\overline{v'_T u'_T} = A\frac{\partial^4}{\partial y^4}\overline{\psi}_m - \frac{\kappa}{2}\frac{\partial^2}{\partial y^2}(\overline{\psi}_m - 2\overline{\psi}_T), \quad (3.5a)$$

$$\frac{\partial \overline{q}_T}{\partial t} - \frac{\partial^2}{\partial y^2}\overline{v'_T u'_m} - \frac{\partial^2}{\partial y^2}\overline{v'_m u'_T} - \lambda_R^2 \frac{\partial}{\partial y}\overline{v'_m \psi'_T} = A\frac{\partial^4}{\partial y^4}\overline{\psi}_T + \frac{\kappa}{2}\frac{\partial^2}{\partial y^2}(\overline{\psi}_m - 2\overline{\psi}_T) \quad (3.5b)$$

$$- \frac{f_0}{\delta p \overline{\Gamma}_2 c_p}\overline{J}_2.$$

Following again Phillips, 1956, the diabatic heating J is given by the sum of radiative and diffusive contributions. The radiative contribution represents the net local radiative energy gains and losses and is chosen to vary linearly in y,

$$J_{\mathrm{rad}} = 2H\left(1 - \frac{2y}{W}\right), \quad (3.6)$$

where H is the mean rate of heating per unit mass for $y \in [0, W/2]$ (or cooling for $y \in [W/2, W]$). The diffusive contribution represents the effect of lateral eddy diffusion of temperature at level 2:

$$J_{\mathrm{diff}} = c_p A \nabla^2 T_2 = \frac{2 f_0 c_p p_2}{\delta p R} A \nabla^2 \psi_T. \quad (3.7)$$

We remark that the parameters A and κ control the dissipation processes that remove energy from the system. The parameter H controls the input of energy in the form of an increase in temperature difference between low and high latitudes, hence fuelling the Lorenz energy cycle of the system by the production of zonal mean available potential energy. Subsequently, the dissipation and heating are opposite forces within the system, bounding the total amount of energy and determining the degree of instability and turbulence.

Finally, the evolution equations for the mean zonal wind and mean thermal wind or shear are obtained by taking the derivative with respect to y of equations (3.5a) and (3.5b), substituting the formulation for the diabatic heating and using the
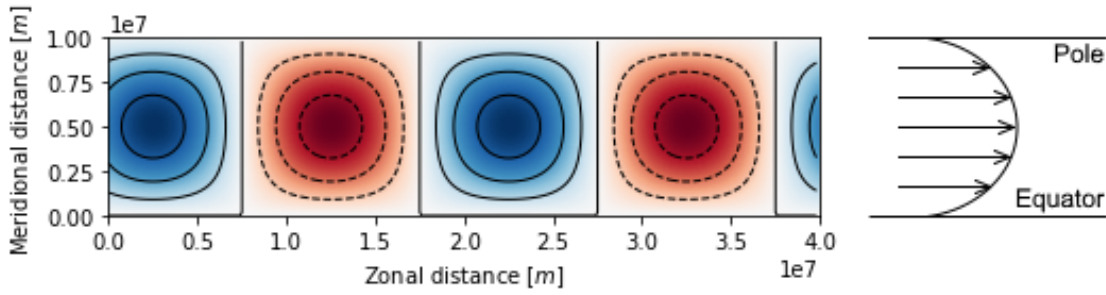
FIGURE 3.1: Eddy streamfunction shape, equation 3.9 (left) and meridional shape of the mean zonal wind $\overline{u}_m$ and shear $\overline{u}_T$ (right).

geostrophic relation $u = -\partial\psi/\partial y$ and $v = \partial\psi/\partial x$ to arrive at

$$\frac{\partial\overline{u}_m}{\partial t} - \frac{1}{\lambda_y^2}\frac{\partial^3}{\partial y^3}\overline{v'_m u'_m} - \frac{1}{\lambda_y^2}\frac{\partial^3}{\partial y^3}\overline{v'_T u'_T} = -\lambda_y^2 A\overline{u}_m - \frac{\kappa}{2}(\overline{u}_m - 2\overline{u}_T), \tag{3.8a}$$

$$\frac{\partial\overline{u}_T}{\partial t} - \frac{1}{\lambda_y^2 + \lambda_R^2}\frac{\partial^3}{\partial y^3}\overline{v'_T u'_m} - \frac{1}{\lambda_y^2 + \lambda_R^2}\frac{\partial^3}{\partial y^3}\overline{v'_m u'_T} - \frac{\lambda_R^2}{\lambda_y^2 + \lambda_R^2}\frac{\partial^2}{\partial y^2}\overline{v'_m\psi'_T} \tag{3.8b}$$

$$= -\lambda_y^2 A\overline{u}_T + \frac{\lambda_y^2}{\lambda_y^2 + \lambda_R^2}\frac{\kappa}{2}(\overline{u}_m - 2\overline{u}_T) + \frac{\lambda_R^2}{\lambda_y^2 + \lambda_R^2}\frac{2\delta p RH}{f_0 p_2 c_p W},$$

where $\overline{u}_m$ is the mean zonal wind and $\overline{u}_T$ the mean thermal wind or mean zonal shear. Here we additionally assumed a specific meridional shape of the mean wind, namely $\partial^2\overline{u}/\partial y^2 = -\lambda_y^2\overline{u}$ where λ_y^2 is an unspecified wavenumber.

Following Thompson, 1987, we next restrict the eddy component of the barotropic and baroclinic streamfunction to be of the form

$$\psi'_{m,T}(x, y, t) = A_{m,T}(t)\sin kx \sin ly + B_{m,T}(t)\cos kx \sin ly, \tag{3.9}$$

where the wavenumber k remains unspecified and $l = \pi/W$. We note that $\nabla^2\psi'_{m,T} = -\lambda_\nabla^2\psi'_{m,T}$ with $\lambda_\nabla^2 = k^2 + l^2 = k^2 + \pi^2/W^2$, see figure 3.1 on the left. Using this assumption, all eddy product terms in equations (3.8a) and (3.8b) besides the net poleward eddy temperature flux $\overline{v'_m\psi'_T}$ cancel. This amounts to neglecting the effect of direct eddy-eddy interactions and to focusing, instead, on the interaction between the zonal wind and waves. As discussed in Speranza and Malguzzi, 1988 and Lucarini, Speranza, and Vitolo, 2007, this assumption allows one to retain the essential ingredients of the process of baroclinic conversion and of the process of barotropic and baroclinic stabilization. Further support to our viewpoint comes from the fact that the statistical properties of both the general circulation of barotropic models of the atmosphere (Sawford and Frederiksen, 1983) as well as of the circulation of the actual atmosphere (Schneider, 2006) are only weakly affected by the presence of

eddy-eddy nonlinearities.

Note here that the streamfunction ψ_T is related to the temperature T_2 at level 2 by the hydrostatic balance equation 2.6 according to

$$\overline{v'_m \psi'_T} = \frac{R}{2f_0} \overline{v'_m T'_2}, \tag{3.10}$$

so $\overline{v'_m \psi'_T}$ is directly proportional to the poleward transport of heat by the eddies. Using now the explicit expression (3.9) for v'_m and ψ'_T we obtain

$$\overline{v'_m \psi'_T} = \frac{k}{2}(A_m B_T - A_T B_m)\sin^2\frac{\pi y}{W}, \tag{3.11a}$$

$$\frac{\partial^2}{\partial y^2}\overline{v'_m \psi'_T} = \frac{\pi^2 k}{W^2}(A_m B_T - A_T B_m)\left(\cos^2\frac{\pi y}{W} - \sin^2\frac{\pi y}{W}\right), \tag{3.11b}$$

so at $y = W/2$,

$$\frac{\partial^2}{\partial y^2}\overline{v'_m \psi'_T} = -\frac{2\pi^2}{W^2}\overline{v'_m \psi'_T}. \tag{3.12}$$

Since the sine function is zero at 0 and π and attains a maximum at $\pi/2$, it can be seen from equation (3.11a) that the net poleward heat transport attains its maximum at $y = W/2$ and vanishes at $y = 0$ and $y = W$. Indeed, this qualitatively corresponds to what is observed in more complex versions of the same model (Lucarini, Speranza, and Vitolo, 2007) and to what is observed in the actual climate (Peixoto and Oort, 1992). Following again Thompson, 1987, we assume that the mean thermal wind $\overline{u}_T$ has the same meridional structure as the net poleward heat transport, and inspecting equation (3.8a) we see that the same must be true for the mean zonal wind $\overline{u}_m$, visualised in figure 3.1 on the right. Additionally, from the assumption about the zonal mean wind, it follows that $\lambda_y^2 = 2\pi^2/W^2$. Finally, equations (3.8a) and (3.8b) can be substantially simplified to

$$\frac{\partial \overline{u}_m}{\partial t} = -\lambda_y^2 A\overline{u}_m - \frac{\kappa}{2}(\overline{u}_m - 2\overline{u}_T), \tag{3.13a}$$

$$\frac{\partial \overline{u}_T}{\partial t} = -\frac{\lambda_y^2 \lambda_R^2}{\lambda_y^2 + \lambda_R^2}\overline{v'_m \psi'_T} - \lambda_y^2 A\overline{u}_T + \frac{\lambda_y^2}{\lambda_y^2 + \lambda_R^2}\frac{\kappa}{2}(\overline{u}_m - 2\overline{u}_T) \tag{3.13b}$$

$$+ \frac{\lambda_R^2}{\lambda_y^2 + \lambda_R^2}\frac{2\delta p R H}{f_0 p_2 c_p W},$$

which is now a closed system if in addition we had an evolution equation for the net poleward temperature flux $\overline{v'_m \psi'_T}$. This equation can be derived by expanding all variables in the non-averaged form of the barotropic and baroclinic vorticity equations (3.4a) and (3.4b) in terms of the zonal mean and deviation thereof defined

above, yielding

$$-\lambda_\nabla^2 \frac{\partial \psi_m'}{\partial t} + (\lambda_y^2 - \lambda_\nabla^2)\overline{u}_m v_m' + (\lambda_y^2 - \lambda_\nabla^2)\overline{u}_T v_T' + \beta v_m'$$
$$- \lambda_\nabla^4 A \psi_m' - \lambda_\nabla^2 \frac{\kappa}{2}(\psi_m' - 2\psi_T') \tag{3.14a}$$
$$= \lambda_y^2 \frac{\partial \overline{\psi}_m}{\partial t} + \lambda_y^4 A \overline{\psi}_m + \lambda_y^2 \frac{\kappa}{2}(\overline{\psi}_m - 2\overline{\psi}_T),$$
$$-(\lambda_\nabla^2 + \lambda_R^2)\frac{\partial \psi_T'}{\partial t} + (\lambda_y^2 + \lambda_R^2 - \lambda_\nabla^2)\overline{u}_T v_m' + (\lambda_y^2 - \lambda_R^2 - \lambda_\nabla^2)\overline{u}_m v_T' + \beta v_T' - \lambda_\nabla^4 A \psi_T'$$
$$+ \lambda_\nabla^2 \frac{\kappa}{2}(\psi_m' - 2\psi_T') - \lambda_R^2 \lambda_\nabla^2 A \psi_T' \tag{3.14b}$$
$$= (\lambda_\nabla^2 + \lambda_R^2)\frac{\partial \overline{\psi}_T}{\partial t} - \lambda_R^2 \mathrm{J}(\psi_T', \psi_m') + \lambda_y^4 A \overline{\psi}_T - \lambda_y^2 \frac{\kappa}{2}(\overline{\psi}_m - 2\overline{\psi}_T)$$
$$+ \lambda_y^2 \lambda_R^2 A \overline{\psi}_T - \lambda_R^2 \frac{\delta p R H}{f_0 p_2 c_p}\left(1 - \frac{2y}{W}\right)$$

where the Jacobian $\mathrm{J}(\psi_T', \psi_m') = -\frac{k\pi}{W}(A_m B_t - A_T B_m)\left(\sin\frac{\pi y}{W}\cos\frac{\pi y}{W}\right)$ and therefore does not depend on x. Note here that the right-hand sides of both equations only depend on (y, t), not on x. Next we derive equations (3.14a) and (3.14b) with respect to x, yielding

$$\frac{\partial v_m'}{\partial t} + \left(\frac{\lambda_\nabla^2 - \lambda_y^2}{\lambda_\nabla^2}\right)\overline{u}_m \frac{\partial v_m'}{\partial x} + \left(\frac{\lambda_\nabla^2 - \lambda_y^2}{\lambda_\nabla^2}\right)\overline{u}_T \frac{\partial v_T'}{\partial x} + \lambda_\nabla^2 A v_m' \tag{3.15a}$$
$$+ \frac{\kappa}{2}(v_m' - 2v_T') - \frac{\beta}{\lambda_\nabla^2}\frac{\partial v_m'}{\partial x} = 0,$$
$$\frac{\partial v_T'}{\partial t} + \left(\frac{\lambda_\nabla^2 - \lambda_y^2 + \lambda_R^2}{\lambda_\nabla^2 + \lambda_R^2}\right)\overline{u}_m \frac{\partial v_T'}{\partial x} + \left(\frac{\lambda_\nabla^2 - \lambda_y^2 - \lambda_R^2}{\lambda_\nabla^2 + \lambda_R^2}\right)\overline{u}_T \frac{\partial v_m'}{\partial x} + \lambda_\nabla^2 A v_T' \tag{3.15b}$$
$$+ \frac{\kappa \lambda_\nabla^2}{2(\lambda_\nabla^2 + \lambda_R^2)}(2v_T' - v_m') - \frac{\beta}{\lambda_\nabla^2 + \lambda_R^2}\frac{\partial v_T'}{\partial x} = 0.$$

The evolution equation for $\overline{v_m' \psi_T'}$ can now be obtained by multiplying (3.14b) by $-v_m'/(\lambda_\nabla^2 + \lambda_R^2)$, multiplying (3.15a) by ψ_T', adding those equations and averaging the result with respect to x over one full wavelength $2\pi/k$. Here we note that the right-hand side of equation (3.14b) multiplied by v_m' vanishes when we take the x-average because it only contains averages over products of v_m' with averaged quantities, yielding

$$\frac{\partial}{\partial t}\overline{v_m' \psi_T'} = \frac{\lambda_R^2 + \lambda_y^2 - \lambda_\nabla^2}{\lambda_\nabla^2 + \lambda_R^2}\overline{u}_T \overline{v_m'^2} - \frac{\lambda_R^2}{\lambda_\nabla^2(\lambda_\nabla^2 + \lambda_R^2)}\left(\beta + \lambda_y^2 \overline{u}_m\right)\overline{v_m' v_T'} \tag{3.16}$$
$$+ \frac{\lambda_\nabla^2 - \lambda_y^2}{\lambda_\nabla^2}\overline{u}_T \overline{v_T'^2} - \left(2A\lambda_\nabla^2 + \frac{\kappa(3\lambda_\nabla^2 + \lambda_R^2)}{2(\lambda_\nabla^2 + \lambda_R^2)}\right)\overline{v_m' \psi_T'}.$$

This equation involves three other statistics, namely the mean meridional kinetic energy $\overline{v_m'^2}$, the temperature variance $\overline{v_T'^2}$ and the cross-correlation between temperature and geopotential $\overline{v_m' v_T'}$. Evolution equations for the first two statistics are obtained by multiplying (3.15a) by v_m', multiplying (3.15b) by v_T' and averaging both with respect to x. The third can be obtained by multiplying (3.15a) by v_T', multiplying (3.15b) by v_m', adding those two equations and averaging again with respect to x, yielding

$$\frac{\partial \overline{v_m'^2}}{\partial t} = \frac{2k^2(\lambda_\nabla^2 - \lambda_y^2)}{\lambda_\nabla^2}\overline{u}_T\overline{v_m'\psi_T'} - (2A\lambda_\nabla^2 + \kappa)\overline{v_m'^2} + 2\kappa\overline{v_m'v_T'}, \tag{3.17a}$$

$$\frac{\partial \overline{v_T'^2}}{\partial t} = \frac{2k^2(\lambda_y^2 + \lambda_R^2 - \lambda_\nabla^2)}{\lambda_\nabla^2 + \lambda_R^2}\overline{u}_T\overline{v_m'\psi_T'} - \left(2A\lambda_\nabla^2 + \frac{2\kappa\lambda_\nabla^2}{\lambda_\nabla^2 + \lambda_R^2}\right)\overline{v_T'^2} \tag{3.17b}$$

$$+ \frac{\kappa\lambda_\nabla^2}{\lambda_\nabla^2 + \lambda_R^2}\overline{v_m'v_T'},$$

$$\frac{\partial}{\partial t}\overline{v_m'v_T'} = \frac{\lambda_R^2 k^2}{\lambda_\nabla^2(\lambda_\nabla^2 + \lambda_R^2)}\left(\beta + \lambda_y^2\overline{u}_m\right)\overline{v_m'\psi_T'} + \frac{\kappa\lambda_\nabla^2}{2(\lambda_\nabla^2 + \lambda_R^2)}\overline{v_m'^2} + \kappa\overline{v_T'^2} \tag{3.17c}$$

$$- \left(2A\lambda_\nabla^2 + \frac{\kappa(3\lambda_\nabla^2 + \lambda_R^2)}{2(\lambda_\nabla^2 + \lambda_R^2)}\right)\overline{v_m'v_T'}.$$

The zonal mean equations (3.13a) and (3.13b) together with the evolution equations for the eddy statistics (3.16) and (3.17a)-(3.17c) comprise a closed system by a prescribed diabatic heating H.

3.3   The non-dimensional model

Up to this point, the longitudinal wavenumber k of the eddy component of the streamfunctions remained unspecified. In principle, one has that $k = 2n\pi/L$, where n is a non-vanishing natural number. Now, we let k be a multiple of the meridional wavenumber l and we define $k = jl = j\pi/W$ where j is a parameter describing the aspect ratio of the eddies, that is — for simplicity — assumed to be a non-negative number. Indeed, j can only assume discrete values, but since $L \gg W$, they are closely spaced and so the discrete nature of j is neglected in what follows. Hence, j larger than 1 means that the eddies are elongated in the meridional direction. If j is smaller than 1 but positive, the eddies are elongated in the longitudinal direction.

To simplify the notation, we introduce the dimensionless variables

$$M = \frac{\lambda_R^2}{2\beta}\overline{u}_m, \; S = \frac{\lambda_R^2}{2\beta}\overline{u}_T, \; T = \frac{\lambda_R^5}{2^3\beta^2}\overline{v_m'\psi_T'}, \; K = \frac{\lambda_R^4}{2^2\beta^2}\overline{v_m'^2}, \; V = \frac{\lambda_R^4}{2^2\beta^2}\overline{v_T'^2}, \; X = \frac{\lambda_R^4}{2^2\beta^2}\overline{v_m'v_T'}$$

and define the time variable $\tau = t\beta/\lambda_R$. The letters of the new dimensionless

variables were chosen in accordance to the meaning of the dimensional variable: the mean zonal wind is denoted by M, the mean zonal shear by S, the poleward eddy temperature flux by T, and for the three other eddy statistics K, V and X were chosen. With the new notation, equations (3.13a), (3.13b), (3.16) and (3.17a)-(3.17c) take the form

$$\frac{dM}{d\tau} = -aM + \alpha S, \tag{3.18a}$$

$$\frac{dS}{d\tau} = \frac{\gamma\alpha}{2}M - bS - 4\gamma T + \eta H, \tag{3.18b}$$

$$\frac{dT}{d\tau} = \mu SK - \frac{\delta\lambda_R^2}{2\lambda_y^2}X - \delta MX - cT + \frac{j^2-1}{j^2+1}SV, \tag{3.18c}$$

$$\frac{dK}{d\tau} = \frac{2^2 j^2(j^2-1)}{j^2+1}\frac{\lambda_y^2}{\lambda_R^2}ST - dK + 2\alpha X, \tag{3.18d}$$

$$\frac{dV}{d\tau} = \frac{2^2 j^2 \lambda_y^2 \mu}{\lambda_R^2}ST - eV + \alpha\zeta X, \tag{3.18e}$$

$$\frac{dX}{d\tau} = j^2\delta\left(1 + \frac{2\lambda_y^2}{\lambda_R^2}M\right)T - cX + \alpha V + \frac{\alpha\zeta}{2}K, \tag{3.18f}$$

with dimensionless constants

$$\alpha = \frac{\lambda_R}{\beta}\kappa, \quad \gamma = \frac{\lambda_y^2}{\lambda_y^2 + \lambda_R^2}, \quad \delta = \frac{\lambda_R^2}{\hat{j}(\hat{j}\lambda_y^2 + \lambda_R^2)}, \quad \epsilon = \frac{3\hat{j}\lambda_y^2 + \lambda_R^2}{\hat{j}\lambda_y^2 + \lambda_R^2}, \quad \nu = \frac{\lambda_R\lambda_y^2 A}{\beta},$$

$$\zeta = \frac{\hat{j}\lambda_y^2}{\hat{j}\lambda_y^2 + \lambda_R^2}, \quad \mu = \frac{\lambda_R^2 + (1-\hat{j})\lambda_y^2}{\hat{j}\lambda_y^2 + \lambda_R^2} \quad \eta = \frac{\lambda_R^5 R}{\beta^2 f_0 c_p W(\lambda_y^2 + \lambda_R^2)},$$

where

$$\hat{j} = \frac{j^2+1}{2}, \ a = \nu + \frac{\alpha}{2}, \ b = \nu + \gamma\alpha, \ c = 2\hat{j}\nu + \frac{\alpha\epsilon}{2}, \ d = 2\hat{j}\nu + \alpha, \ e = 2\hat{j}\nu + 2\alpha\zeta.$$

For a non-zero heating rate H this system exhibits three steady states. The first one is a zonal steady state where all eddy components are zero:

$$P^0 = (M^0, S^0, 0, 0, 0, 0) = \frac{2}{2ab - \gamma\alpha^2}\eta H(\alpha, a, 0, 0, 0, 0). \tag{3.19}$$

Here, M^0 and S^0 are always positive because the denominator of the pre-factor and all parameter values including the heating rate are positive within the considered parameter space (see tables 3.1 and 3.2).

The second steady state, denoted by $P^* = (M^*, S^*, T^*, K^*, V^*, X^*)$, is given by

$$M^* = \frac{\alpha}{a}S^*, \qquad\qquad S^* = \frac{j^2 a}{A}\left(\left(B^2 + 4CD\right)^{1/2} + B\right),$$

$$T^* = -\frac{2ab - \gamma\alpha^2}{8a\gamma}S^* + \frac{\eta}{4\gamma}H, \quad K^* = \frac{2^2 j^2(j^2-1)\lambda_y^2}{(j^2+1)d\lambda_R^2}S^*T^* + \frac{2\alpha}{d}X^*, \qquad (3.20)$$

$$V^* = \frac{2^2 j^2 \mu\lambda_y^2}{e\lambda_R^2}S^*T^* + \frac{\alpha\zeta}{e}X^*, \quad X^* = \left(\frac{2j^2\alpha\lambda_y^2 g}{a\lambda_R^2}S^* + j^2\delta\right)\left(c - \alpha\zeta\frac{d+e}{de}\right)^{-1}T^*,$$

with constants

$$B = 2\alpha\delta(g-f)\left(c - \alpha^2\zeta\frac{d+e}{de}\right)^{-1}, \quad C = \frac{\delta^2\lambda_R^2}{2\lambda_y^2}\left(c - \alpha^2\zeta\frac{d+e}{de}\right)^{-1} + c,$$

$$D = 8\frac{\lambda_y^2}{\lambda_R^2}\left(2a^2\mu\left(1 - \frac{1}{\hat{j}}\right)\frac{d+e}{de} + \alpha^2 fg\left(c - \alpha^2\zeta\frac{d+e}{de}\right)^{-1}\right),$$

$$f = \frac{2a\mu}{d} + (1 - \frac{1}{\hat{j}})\frac{a\zeta}{e} - \delta, \quad g = \delta + \frac{(j^2-1)a\zeta}{(j^2+1)d} + \frac{2a\mu}{e}.$$

Here, B, C and g are positive for the whole parameter space given by tables 3.1 and 3.2, D and f are non-negative for j larger than 1, and for the positivity of D additionally $\kappa \geq 3 \times 10^{-6}$ s^{-1} is required. Note that B, C and D are independent of the heating H and therefore the steady state mean zonal wind M^* and shear S^* are independent of the heating.

The third steady state of the system can be excluded as unphysical since the values of K and V are negative in the given parameter space despite being non-dimensional variables for $\overline{v_m'^2}$ and $\overline{v_T'^2}$, respectively, which being squared real quantities must always be non-negative. Therefore the system exhibits two physical solutions, in the following referred to as the zonal (P^0) and the eddy steady state (P^*).

3.4 Physical mechanisms of zonal and eddy saturated steady state

The linear stability of these two solutions is determined by numerically calculating the eigenvalues of the Jacobian matrix of system (3.18a)-(3.18f) at each steady state. Therefore, the parameters in table 3.1 were kept fixed, whereas the surface friction diffusion κ, the eddy diffusion A, the mean rate of heating H and the parameter j describing the eddy aspect ratio were varied within the ranges given in table 3.2.

In the following the notion of an attracting (stable) and repelling (unstable) steady state is used to describe the linear stability of the two steady states. Hence, if the

TABLE 3.1: Fixed parameter values for stability analysis.

Parameter	λ_R^2	λ_y^2	β	R	f_0	c_p	W
Value	4.39×10^{-12}	1.97×10^{-13}	1.6×10^{-11}	287	10^{-4}	1004	10^7
Unit	m^{-2}	m^{-2}	$\text{m}^{-1}\,\text{s}^{-1}$	$\text{J K}^{-1}\,\text{kg}^{-1}$	s^{-1}	$\text{J K}^{-1}\,\text{kg}^{-1}$	m

TABLE 3.2: Varying parameter values for stability analysis.

Parameter	κ	A	H	j
Minimum	10^{-7}	1	0	0.1
Standard	4×10^{-6}	10^5	3.5×10^{-3}	-
Maximum	8×10^{-6}	10^5	4×10^{-3}	6.8
Unit	s^{-1}	$\text{m}^2\,\text{s}^{-1}$	$\text{KJ ton}^{-1}\,\text{s}^{-1}$	-

eddy steady state is attracting, the model converges to the steady state with non-zero but finite eddy contributions. This state then breaks the zonal symmetry of the zonal state: the phase of the eddies is not determined but the eddy correlation statistics are fixed in time. On the other hand, an attracting zonal steady state describes a state of the atmosphere where eddy activity decays until the flow is purely zonal, and once in that state remains zonal.

The considered parameter space is divided into two opposite stability regions where either the zonal or the eddy steady state is attracting and the respective other state is repelling. Keeping κ, A and j fixed but increasing the heating rate H, a bifurcation occurs. To determine the type of bifurcation, the change of eigenvalues of the Jacobian at the steady states was analysed. At the bifurcation point, one eigenvalue at the zonal steady state has a real part becoming positive, whereas one eigenvalue at the eddy steady state changes its real part from positive to negative. Since this shows that the two steady states exchange stability at this point, the system undergoes a transcritical bifurcation, which is the only possible bifurcation for the observed stability switch (see for example Guckenheimer and Holmes, 1983).

From equation (3.19) it is clear that the mean zonal wind and shear of P^0 grow linearly with the heating H. However, this proportionality is lost for the eddy steady state, where M^* and S^* are independent of the heating rate. This can be seen directly from equation (3.20) and the left-hand side of figure 3.2, where contours of the mean zonal wind at the top level for the respective attracting steady state are shown. Such an insensitivity of the mean zonal wind to the forcing by the heating rate closely resembles the eddy saturation mechanism discussed in the introduction to the present section.

In contrast to that, the (non-dimensional) net poleward heat transport T^* grows
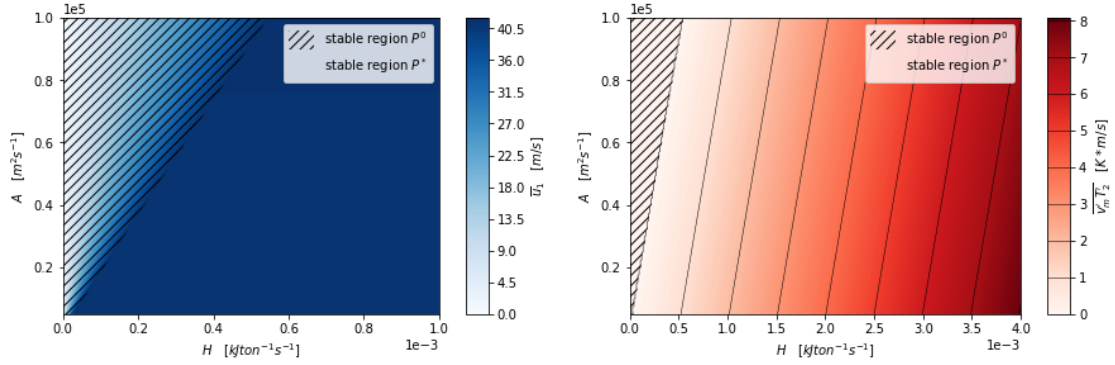
FIGURE 3.2: Contours of the mean zonal wind at the top level $\overline{u}_1$ (left) and the net poleward eddy temperature flux (right) for the respective attracting steady state; the dashed region is the parameter space where the zonal steady state P^0 is attracting, the non-dashed region where the eddy steady state P^* is attracting; note that the range of H in the right figure is four times the range in the left; $\kappa = 4 \times 10^{-6}$ s^{-1}, $j = 2.5$.

linearly with H (see again equation (3.20) and figure 3.2 on the right) and is non-negative in its attracting parameter region only. For values of H where the zonal steady state is attracting, T^* is negative and therefore the net eddy heat transport is equatorward for the eddy state. This would imply that the system transports heat from cold towards warm regions, which suggests a condition that is thermodynamically not realisable. This further clarifies that the eddy steady state is physically irrelevant in its repelling region. Furthermore, it is clear from equation (3.20) that the steady state value of the net poleward heat transport only depends on the shear and incoming heat but not on the three other eddy correlation variables K^*, V^* and X^*. Hence, the dynamics of the system are resembled by the mean zonal shear (proportional to the mean zonal wind) and the net poleward heat transport, and K^*, V^* and X^* do not need to be considered separately. An overview of the steady states and the respective flow properties is shown in table 3.3.

The above-described stability switch is also dependent on the eddy diffusion parameter A. This is illustrated in figure 3.2, where a higher eddy diffusion yields a larger heating rate at which the zonal steady state loses stability. The relation between eddy diffusion and heating rate in P^0 is determined by equation (3.19). Replacing S^0 by the mean poleward temperature gradient at the middle level $\overline{T}_2$ yields

$$G(A,\kappa)A\left(-\frac{\partial \overline{T}_2}{\partial y}\right) = H \quad \text{with} \quad G(A,\kappa) = \lambda_y^2 c_p W \frac{(\lambda_y^2 + \lambda_R^2)(2\lambda_y^2 A + (2\gamma+1)\kappa)}{4\lambda_R^2(2\lambda_y^2 A + \kappa)}.$$
(3.21)

By using the parameter values of tables 3.1 and 3.2 it can be shown that the derivative with respect to the diffusion parameter A of the function $G(A,\kappa)$ is of the order 10^{-30}, so almost zero, and therefore, the function $G(A,\kappa)$ is almost constant in A.

TABLE 3.3: Overview of flow properties in respective stable steady state.

	Purely zonal steady state P^0	Eddy steady state P^*
Mean zonal wind $\overline{u}_m$ and shear $\overline{u}_T$	positive, linear growth in H	positive, constant
Net poleward heat transport $\overline{v'_m T'_2}$	0	positive, linear growth in H

This means in physical terms that for a fixed equator-to-pole mean temperature gradient, a linear increase of the heating rate H can be balanced by a linearly increased eddy diffusion. In this sense, the stabilization of the zonal state against heating is always realized by an eddy heat transport, be it parameterised, as an eddy diffusion, or explicit, as in eddy heat transport.

It is also clear from (3.21) that the surface friction κ is not able to balance the heating and the stability analysis shows that a change in κ does not influence the critical value of heating for realistic values of κ (see figure 3.4 on the left).

These opposed roles of the zonal and eddy steady state describe two physically related mechanisms of the atmosphere to compensate for incoming heat. In the attracting region of the zonal steady state, the relatively low heating can be compensated by the eddy diffusion. However, this balance is no longer achievable for increasing H and decreasing A so that in the eddy steady state the eddies have to reach a finite size to perform poleward transport of heat and compensate for the atmospheric radiative energy imbalance. In the actual atmosphere — or in more complex models — this corresponds to the case where the flow is baroclinically unstable, and baroclinic cyclones grow and decay as a manifestation of an active Lorenz energy cycle and, at the same time, transport heat poleward. Although it is a similar mechanism, the compensation of the heating does not depend on the friction diffusion κ. This is explained later in this section.

Another parameter that influences the stability regions of the steady states is the aspect ratio $j \in \mathbb{R}^+$ of the eddy shape. For the previous analysis, $j = 2.5$ was chosen, which corresponds to eddies elongated by a factor of 2.5 in the meridional direction. For this aspect ratio, and even more meridionally elongated eddies, a stability switch always occurs and the larger j, the smaller the heating rate H at this switching point. In contrast to that, for j smaller than one, corresponding to zonally elongated eddies, there is no exchange of stability and the zonal steady state is attracting for the whole parameter space under consideration.

For an aspect ratio above one, the value of H at which the zonal state loses stability
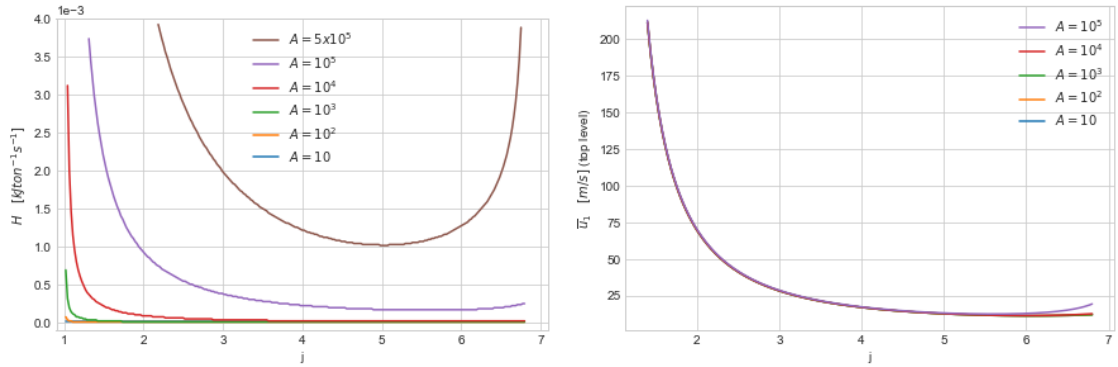
FIGURE 3.3: The value of the heating rate H at which the stability switch occurs (left) and the mean zonal wind at the top level $\bar{u}_1$ (right) as a function of the eddy shape aspect ratio j, shown for several values of the eddy diffusion A in m^2 s^{-1}; $H = 3.5 \times 10^{-3}$KJ ton^{-1} s^{-1} (right); $\kappa = 4 \times 10^{-6}$ s^{-1} (both).

is additionally dependent on the eddy diffusion parameter. The left-hand side of figure 3.3 shows the values of H at which the switch occurs as a function of j for several orders of magnitude of A. For a vanishing small eddy diffusion (e.g. A on the order of 10 m^2 s^{-1}) the eddy steady state is attracting for the whole range of H and an aspect ratio larger than one. Increasing A yields an exchange of stability for higher H, which was already seen in figure 3.2, and additionally, an increasing value of j is required for the eddy steady state to become attracting.

Hence, for meridionally more elongated eddies the eddy steady state becomes attracting at a lower heating rate. It is indeed well known that, in the full quasi-geostrophic flow, baroclinic instability is facilitated for these geometrical conditions (Pedlosky, 1979). Only for a very large aspect ratio j above five and for a large eddy diffusion the critical value of H increases again. As before, besides this behaviour at very high aspect ratios, a change in the surface friction does not change this critical heating rate.

The right-hand side of figure 3.3 shows the mean zonal wind at the top level of the eddy steady state as a function of the aspect ratio. Eddies close to a circular shape, i.e. j close to one, yield unrealistically high wind speeds just above 215 m s^{-1}. For more meridionally elongated eddies the wind speed decreases for an aspect ratio of up to 5 and thereafter increases again for very high eddy diffusion values. For $j \geq 2.5$ one gets reasonably realistic values for the wind speed. However, before this upward slope, the wind speed neither depends on the eddy diffusion nor the surface friction diffusion (the latter not shown).

For the net poleward heat transport, the opposite holds: the longer the eddies in the meridional direction, the higher the heat transport until it drops again for very large
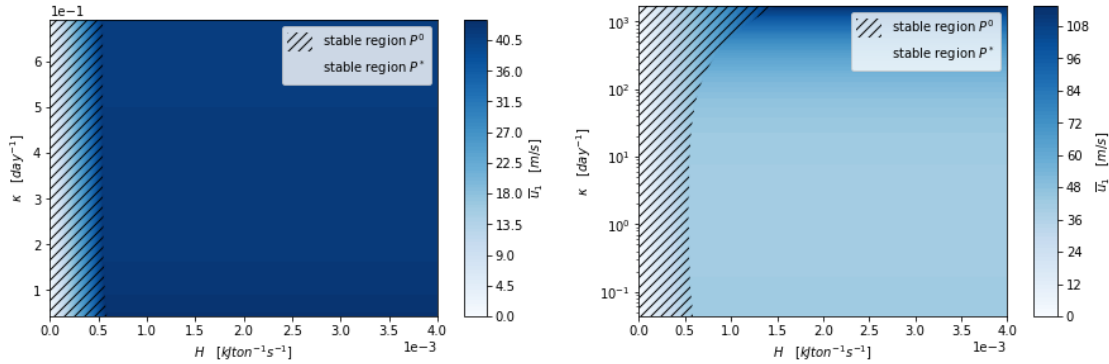
FIGURE 3.4: Contours of the mean zonal wind at the top level $\overline{u}_1$ for realistic (left) and extremely high (right) values of the surface friction parameter κ; the dashed region is the parameter space where the zonal steady state P^0 is attracting, the non-dashed region where the eddy steady state P^* is attracting; note that in the right panel the scale for the surface friction is logarithmic; $A = 10^5$ m^2 s^{-1}, $j = 2.5$.

j. Besides these very high aspect ratios, the surface friction diffusion κ has again no impact on the values, whereas a very high eddy diffusion A yields a decreased heat transport for the whole range of j.

As briefly mentioned earlier, the surface friction κ could perhaps be thought to act similarly to the eddy diffusion A, taking out energy from the system and thus compensating for the heating H. However, the heating forces a vertical zonal shear by thermal wind balance, but would not force a zonal wind directly at the surface. The model can develop very low surface winds but increase its shear by increasing upper-level zonal winds. In this sense, the surface friction does not directly compensate for the incoming heating H.

However, insofar as the heating induces surface winds, the surface friction would represent a sink for those surface winds. In that case, one would expect that higher surface friction is able to dissipate the incoming energy and therefore moves the stability switch to higher values of the heating. This frictional adjustment can not be seen for realistic values of κ (figure 3.4 on the left) but is observable for extremely high surface friction values (figure 3.4 on the right).

Additionally, and in contrast to the eddy diffusion A, extremely high surface friction increases the mean zonal wind to unrealistically high values. This behaviour of the mean flow was also observed by Novak, Ambaum, and Harvey, 2018 and Marshall et al., 2017 for the Antarctic Circumpolar Current.

3.5   Short and long wavelength cut-off

For sufficiently large eddy diffusion A, the left-hand side of figure 3.3 shows a short (large j) and long wavelength (small j) cut-off of the instability of the zonal solution. In other words, our model only exhibits finite-size eddies within a certain range of wavelengths and the zonal flow stabilizes for very short and long waves.

A similar result follows from the classical stability analysis of the Phillips model presented in, for example, Holton and Hakim, 2013a. This is done for a simpler version of the two-level model, without surface friction, eddy diffusion or external forcing due to heating, and is obtained by performing a linear perturbation analysis. Assuming wave-like solutions for the barotropic and baroclinic development of the streamfunction, they obtain a dispersion relation for the phase speed of the waves and from this derive conditions for instability of the zonal flow and the growth of perturbations. The zonal flow is stable for very short waves because they are inefficient in converting available into potential energy, and for very long waves, because they are stabilized by the differential rotation of the plane along latitudes (β-effect). This instability is similar to the repelling regime of the zonal steady state in our model and the results of Holton and Hakim, 2013a are compared to ours in the following.

The first condition in Holton and Hakim, 2013a for instability to occur is

$$\overline{u}_T > \frac{\beta}{\lambda_R^2}. \tag{3.22}$$

This is also Phillips' criterion for baroclinic instability of the two-level model, see Phillips, 1954. Using the values in table 3.1 we obtain a minimal shear of approximately 3.65 m s^{-1}, meaning that for a shear below this value, the zonal steady state must always be attracting. In fact, it can be shown that for values of $\overline{u}_T$ below this level, our model is always in the attracting region of the zonal steady state and as the shear is increased this state becomes repelling.

According to Holton and Hakim, 2013a, the minimum value of $\overline{u}_T$ for which P^0 becomes repelling occurs when $k^2 = \sqrt{2}\lambda_R^2/2$, where k is the meridional wavenumber. Using the relation $k = j\pi/W$, this condition becomes

$$j = \frac{2^{-1/4}W\lambda_R}{\pi} \approx 5.6, \tag{3.23}$$

where we used again the values in table 3.1. Analysing our model yields exactly that value of j at which the mean zonal shear is minimal. The corresponding minimum

is $\overline{u}_T \approx 4.1$ m s^{-1} and is similar to the value given by Holton and Hakim, 2013a. This value of j also yields the wavenumber of maximal instability of the purely zonal flow.

The short wavelength cut-off observed for large eddy diffusion A in figure 3.3 on the left is given in Holton and Hakim, 2013a by the critical wavelength

$$L_c = \frac{2\pi}{\lambda_R^2} \approx 3 \times 10^3 \text{ km.} \tag{3.24}$$

For waves shorter than this value, instability can not occur and the zonal steady state remains attracting. In our model, this value corresponds to $j > 6.6$ and matches roughly the value for which the zonal steady state becomes attracting again if the eddy diffusion is very high and the heating rate is approximately the standard value given in table 3.2.

3.6   Q factor

The quality factor Q is a dimensionless parameter that is used in mechanics and electronics to describe the oscillatory behaviour of a damped system. In general, the Q factor is defined as the ratio between the natural undamped frequency of a dynamical system and its damping coefficient. Therefore, a high Q factor indicates a larger number of oscillations before the system reaches the attracting steady state, in contrast to a low Q factor indicating that the damping is more dominant and the attracting steady state is reached after fewer oscillations. A Q factor below 1/2 corresponds to an overdamped system that does not oscillate at all when displaced from its steady state but returns to it by exponential decay.

This concept can be applied to the theory of damped oscillators, which satisfy the linear equation

$$\ddot{x} + \lambda \dot{x} + \omega_0^2 x = 0, \tag{3.25}$$

where ω_0^2 is the frequency of free oscillations and λ the damping coefficient. The general solution of equation (3.25) is

$$x = A \exp\left(-\frac{\lambda}{2}t\right) \exp\left(\pm i \left(\omega_0^2 - \frac{\lambda^2}{4}\right)^{1/2} t\right) = A \exp\left(pt\right), \tag{3.26}$$
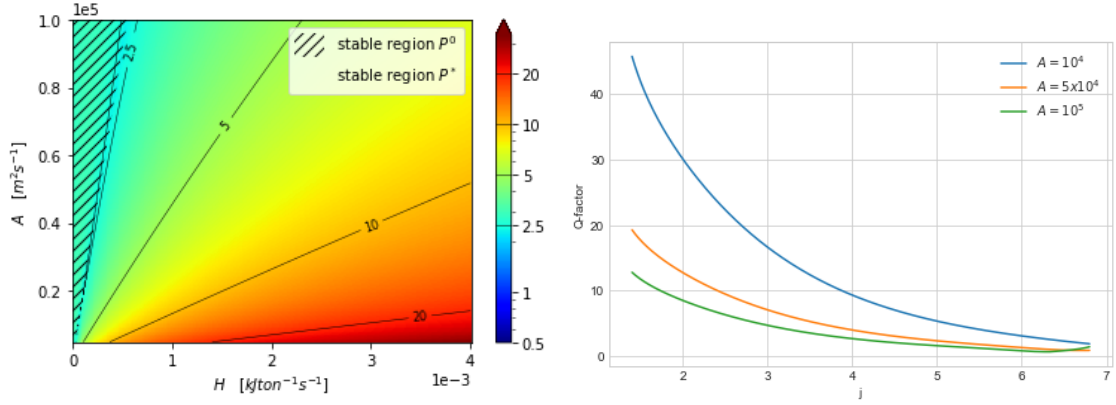
FIGURE 3.5: LEFT: Contours of the Q factor in the heating rate H versus eddy diffusion A plane, the dashed region is the parameter space where the zonal steady state P^0 is attracting, the non-dashed region where the eddy steady state P^* is attracting, $\kappa = 4 \times 10^{-6}$ s^{-1}, $j = 2.5$; RIGHT: Q factor as a function of j for various values of the eddy diffusion A in m^2 s^{-1}, $\kappa = 4 \times 10^{-6}$ s^{-1}, $H = 3.5 \times 10^{-3}$KJ ton^{-1} s^{-1}.

where A is a fixed complex amplitude and $p = -\lambda/2 \pm \mathrm{i}\left(\omega_0^2 - \lambda^2/4\right)^{1/2}$. The generally accepted definition of the Q factor for the damped oscillator is

$$Q = \frac{\omega_0}{\lambda}. \tag{3.27}$$

We now consider a linearised system obeying the differential equation $\mathrm{d}x/\mathrm{d}t = \alpha x$. This is associated with a linear damped oscillator if we take $p = \alpha = \alpha_R + \mathrm{i}\alpha_i$, where $\alpha_R < 0$ is the real and α_i the imaginary part of the eigenvalue. With this identification, we find $\alpha_R = -\lambda/2$ and $\alpha_i = \pm\left(\omega_0^2 - \lambda^2/4\right)^{1/2}$ and hence the Q factor of a linearised system can be expressed as

$$Q = \frac{\left(\alpha_i^2 + \alpha_R^2\right)^{1/2}}{-2\alpha_R} = \frac{|\alpha|}{-2\alpha_R}. \tag{3.28}$$

By construction, $Q \geq 1/2$ for eigenvalues with a non-zero imaginary part, which is associated with the oscillatory behaviour of the system. For real eigenvalues, the Q factor is exactly $1/2$ and the system is said to be critically damped. Similar to an over-damped system, the steady state is approached without oscillations.

For our analysis and the results shown in figure 3.5 the maximum of the fraction (3.28) calculated for each eigenvalue of the Jacobian at the steady state was used, where figure 3.5 depicts the respective stable region of each of the steady states.

The left-hand side of figure 3.5 shows contours of the Q factor in the heating rate H versus eddy diffusion A plane. As expected, Q is always greater than $1/2$ so the system oscillates everywhere in the considered parameter space. Furthermore, it

can be seen that an increase in the eddy diffusion parameter A leads to a decrease in the Q factor. This corresponds to the fact that diffusion acts as a damping and stabilizing factor of the system and leads to a reduction of the available energy. Therefore, the higher the diffusion, the less the initial transient relies on the eddy heat flux to compensate for the heat imbalance. In contrast to that, a larger heating rate H increases the Q factor since more heat needs to be transported away from the equator and therefore more oscillatory cycles of the eddies are needed during the initial transient. The contours of Q in the heating rate versus surface friction κ plane are similar (not shown) and can be interpreted in the same way.

On the right-hand side of figure 3.5 the Q factor is shown as a function of the eddy aspect ratio j for different values of A. The highest Q factor occurs for the smallest j, i.e. for the most symmetric eddy shape, and the larger j, the smaller the Q factor. Hence, for eddies that are more elongated in the meridional direction, the system undergoes fewer oscillatory cycles before it reaches the attracting steady state. In physical terms, meridionally elongated eddies are more efficient in balancing the heat in the atmosphere than eddies close to symmetric. This also coincides with the findings in the earlier chapters. Apart from that, the dependence on the diffusion parameter A is the same as in the contour plot on the left side.

3.7 Discussion and conclusion

We used Phillips' classical QG two-level model on the β-plane (Phillips, 1956) and performed a model reduction to develop a system of six ordinary differential equations describing the interaction between the mean flow and shear, and the eddy activity in the mid-latitude atmosphere. This has been achieved by imposing a specific shape on the eddy streamfunction and thus looking at the evolution of the amplitude of the atmospheric modes considered in our spectral projection. As a result, our model is able to deal with the interaction between the zonal wind and waves, but neglects, instead, direct wave-wave interactions. This approximation is well-known to bear value both in terms of representation of the baroclinic instability of the atmosphere (Speranza and Malguzzi, 1988) and in terms of the representation of its statistical properties (Schneider, 2006).

Instead of taking the usual approach of performing normal mode instability analysis, we used classical dynamical systems theory and determined two physically possible steady states, namely a zonal solution, where the flow is purely zonal and has no eddy contribution, and an eddy solution, where zonal flow and eddies coexist. The considered parameter space is divided into two separate regions where either the

zonal or the eddy solution is attracting, while the alternative solution is unstable and repels nearby initial conditions.

The two competing states are in close correspondence with two possible physical mechanisms that allow the atmosphere to reach a steady state in such a way that the imbalance in the diabatic heating between the equator to the poles is compensated. Relatively weak imbalances in the diabatic heating can be balanced by diffusion and no eddies need to develop to flatten the meridional temperature gradient. Indeed, the flow is, in this case, baroclinically stable. In this state, the mean flow increases for stronger forcing by diabatic heating, because the latter imposes a stronger temperature difference between low and high latitudes. This monotonicity is lost as soon as the heating reaches a certain threshold, where the eddies start growing to compensate for the incoming heat because the damping effect of the eddy diffusion is no longer sufficient. The zonal flow is then baroclinically unstable so that eddies grow and reach a finite steady-state amplitude, in such a way that the resulting poleward eddy heat flux weakens the baroclinicity and therefore the mean flow. This process is referred to as baroclinic adjustment (Stone, 1978).

In this baroclinically unstable eddy steady state, the zonal flow is independent of the external forcing by the heating. In contrast, the net poleward heat transport by the eddies and the eddy energy increase with incoming heat, so incoming energy in form of diabatic forcing of the zonal mean flow goes directly into the eddies in form of eddy kinetic energy, where it is dissipated. Therefore, the stability switch from zonal to eddy steady state describes a transfer of the location of dissipation of incoming energy. In terms of the Lorenz energy cycle, for sufficiently large heating, the zonal flow can no longer act as the reservoir for the incoming energy, so a new reservoir needs to develop, namely the eddies. This is visualised in figure 3.6. Thus, the reduced model is exhibiting complete eddy saturation.

In contrast to Munday, Johnson, and Marshall, 2013, stating that eddy-resolving models of the ACC lead to a much lower sensitivity of the volume transport to increased forcing, Marshall et al., 2017 suggested the possibility to capture the physics of eddy saturation in models with parameterised eddies. Thereafter, Mak et al., 2017 used a highly idealised model configuration of the ACC with parameterised eddies to obtain a near-total eddy saturation. For the atmosphere, Novak, Ambaum, and Harvey, 2018 found a model where the mean baroclinicity is nearly independent of the thermal forcing, whereas the eddy intensity responds more strongly to the forcing and is independent of the eddy dissipation. In this context, the model presented in this work is the first to exhibit complete eddy saturation in a model of the mid-latitude atmosphere with parameterised eddies.
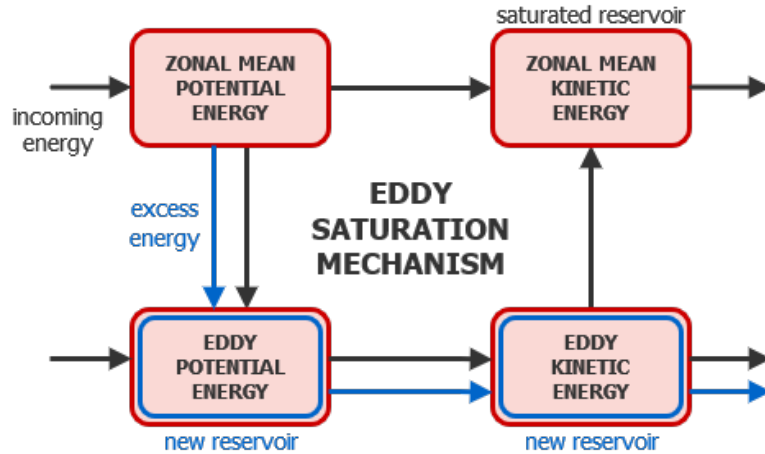
FIGURE 3.6: Eddy saturation mechanism in terms of the Lorenz energy cycle, where for sufficiently large incoming energy, the zonal kinetic energy can no longer act as an energy reservoir and instead the eddy energy develops as the new reservoir.

Another aspect of the eddy saturation mechanism described in Marshall et al., 2017 is the increase of the volume transport with the bottom drag, and one would expect a similar effect of the surface friction in our model, dissipating energy from the system and therefore compensating for the incoming heat. This would lead to a stability switch at higher values of the heating and to an increase in the zonal wind speed. However, this effect can only be seen for unrealistically high values of surface friction, perhaps indicating a limitation of our model. Due to the two-level setup, the model is able to develop a high wind shear induced by the incoming heating by increasing the upper-level zonal wind but maintaining a very low surface wind. Hence, the surface friction can not directly compensate for the incoming heating in the model, although in the atmosphere the heating actually induces stronger surface winds.

In addition to the zonal wind being independent of the incoming heating and the surface friction (for realistic values) in the baroclinically unstable eddy steady state, the wind speed is independent of the eddy diffusion as well. Instead, an increased diffusion leads to a decrease of eddy energy, indicating the damping effect of eddy dissipation which is known as *dissipative control* (e.g. Novak, Ambaum, and Harvey, 2018), and is in accordance with Marshall et al., 2017, stating that the equilibrium volume transport is controlled by the ACC requiring sufficiently strong vertical shear induced by external forcing to overcome the stabilising role of the eddy dissipation.

Despite the simplicity of the model and the limiting assumptions made on the shape of the eddies, our model exhibits complete eddy saturation, a regime of the mid-latitude atmosphere that appears to be supported by numerical models. The eddy saturation mechanism is explained as a switch of stability from a zonal mean state

to a mean state with finite eddy amplitude. Regarding the questions posed in the introduction to this thesis, we are able to answer the first one with yes: we developed a model that captures observed dynamics of the mid-latitudes. The stabilising effect on the zonal flow of the small scale eddy diffusion and large surface friction answers question three, whereas the destabilisation that results from increased forcing by heating gives an answer to question four of the thesis introduction.

Chapter 4

Latitudinal storm track shift in a two-level model

4.1 Introduction

The eddy-driven jet stream and associated storm track is the main location of extreme weather events in the mid-latitude atmosphere and has a profound impact on the general circulation of the atmosphere and oceans by transporting heat, momentum and moisture from the equator towards the poles. The strength and location of the jet stream vary on a vast range of time scales, from several days to weeks, and even decades (Holton and Hakim, 2013a). In order to explain these variations and eventually be able to predict them, it is crucially important to understand the driving mechanisms.

Numerous studies quantifying and describing the impact of the eddies on the zonal flow and its location developed around the work of Hoskins, James, and White, 1983, introduced in chapter 2, who developed a diagnostic time-mean quantity, which they called **E**-vector, to determine the relationship of mid-latitude eddies, their shape, and quantitative feedback onto the mean flow. Using data for the Northern Hemisphere 1979-80 winter from the ECMWF, the diagnostic showed that in the entrance region of the storm track non-tilted eddies with similar zonal and meridional wavenumber transport momentum and decrease the vertical shear in the zonal flow, and therefore increase the barotropic westerly flow near the entrance and middle. Whereas in the jet exit region, zonally elongated southwest-northeast tilted eddies decrease the kinetic energy of the mean flow.

The analysis by Woollings, Hannachi, and Hoskins, 2010, based on the 40-year ECMWF re-analysis (ERA-40) data, suggests that there are three preferred latitudinal positions of the North Atlantic eddy-driven jet stream in winter: south,

middle, and north. Using a non-linear oscillator relationship between the meridional temperature gradient (baroclinicity) and heat flux, and the above-mentioned diagnostic by Hoskins, James, and White, 1983, Novak, Ambaum, and Tailleux, 2015 found that high heat flux is likely to deflect the jet northward, whereas low heat flux is associated with a more southward deflected jet.

On climate time scales, the growing consensus is a poleward shift of the mid-latitude storm track as the climate warms, which was both found in re-analysis data of recent years (e.g. Fyfe, 2003) and ensembles of 21st-century climate simulations by different coupled climate models (e.g. Yin, 2005). Lucarini, Speranza, and Vitolo, 2007 chose a rather simplified two-level quasi-geostrophic model with a few hundred degrees of freedom to study the behaviour of the mid-latitude atmospheric climate with respect to changes in a forced equator-to-pole temperature gradient T_E. For an increase of T_E, their system moves from a stable purely zonal state through stable periodic orbits into a chaotic regime. For this transition, the zonally averaged momentum and temperature difference between the equator and poles, which is the zonally averaged mean shear by geostrophy, are monotonically increasing with T_E. However, when the system enters the chaotic regime, the averages have a much smaller value and grow sub-linear with T_E.

Despite the efforts on various relevant time scales, a generally accepted theory for the dynamical mechanisms driving observed and modelled shifts is still absent. Instead of using re-analysis data or large model simulations, this study aims to qualitatively describe jet shifts by posing the question of whether it is possible to obtain this behaviour in a minimal model of the atmosphere. Our objective is not to create a realistic model of atmospheric dynamics but rather to capture the essential nonlinear processes responsible for the latitudinal vacillation of the jet by distilling the minimal components needed to observe such behaviour.

In chapter 3, based on Phillips' QG two-level model on the β-plane, we developed a set of ordinary differential equations that are able to provide a minimal yet meaningful model of the interaction between mean flow and eddy activity. However, due to the circular shape of the eddies in this model, direct non-linear eddy-eddy interactions were not represented and the latitudinal maximum of the mean flow did not vary. In the current chapter, we redefine the shape of the mean flow to enable variations of the latitudinal maximum and accordingly adapt the shape of the eddies to allow non-linear interactions in form of poleward eddy momentum fluxes. These changes yield substantially richer dynamics as compared to the model in chapter 3. Apart from a purely zonal regime, the new model exhibits competing barotropic

and baroclinic eddy regimes with different impacts on the latitudinal maximum of the mean flow.

In section 4.2 we briefly review the model derived in section 3.2, followed by above mentioned definitions of the mean flow and eddy shape, and the derivation of evolution equations for the flow amplitudes defining our model. In section 4.3 the steady state and stability thereof are determined and the model is compared to the non-tilted eddy case in section 3.4. The complete dynamics of the system for tilted eddies is described in section 4.4, and section 4.5 summarises the results and discusses them in light of the current literature.

4.2   The model equations

We use again the two-level quasi-geostrophic model in pressure coordinates of Phillips, 1956 and follow the derivation in chapter 3.2 to arrive at evolution equations for the mean zonal wind $\overline{u}_m$ and shear $\overline{u}_T$, being half the sum and difference of the wind at the 250 and 750 hPa levels respectively,

$$\frac{\partial \overline{u}_m}{\partial t} - \frac{1}{l^2}\frac{\partial^3}{\partial y^3}\overline{v'_m u'_m} - \frac{1}{l^2}\frac{\partial^3}{\partial y^3}\overline{v'_T u'_T} = -l^2 A\overline{u}_m - \frac{\kappa}{2}(\overline{u}_m - 2\overline{u}_T), \tag{4.1a}$$

$$\frac{\partial \overline{u}_T}{\partial t} - \frac{1}{l^2 + \lambda_R^2}\frac{\partial^3}{\partial y^3}\overline{v'_T u'_m} - \frac{1}{l^2 + \lambda_R^2}\frac{\partial^3}{\partial y^3}\overline{v'_m u'_T} - \frac{\lambda_R^2}{l^2 + \lambda_R^2}\frac{\partial^2}{\partial y^2}\overline{v'_m \psi'_T} \tag{4.1b}$$

$$= -l^2 A\overline{u}_T + \frac{l^2}{l^2 + \lambda_R^2}\frac{\kappa}{2}(\overline{u}_m - 2\overline{u}_T) + \frac{\lambda_R^2}{l^2 + \lambda_R^2}\frac{2RH}{f_0 c_p W},$$

which are equal to equations (3.8a) and (3.8b). $\boldsymbol{V} = (u, v)$ is the horizontal velocity vector, the overline denotes the zonal mean $\overline{F}(y, t) = (1/L)\int_0^L \mathrm{d}x\, F(x, y, t)$ and the prime denotes the deviation from such a mean as $F'(x, y, t) = F(x, y, t) - \overline{F}(y, t)$ for any field F. These equations are defined on the spatial domain $(x, y) \in [0, L] \times [0, W]$, where L and W are the length and width of the β-plane channel with $f = f_0 + \beta y$.

The parameters A and κ describe the eddy diffusion and the surface friction diffusion, hence controlling the dissipation processes that remove energy from the system. The parameter c_p is the isobaric specific heat capacity of dry air and R is the specific gas constant for dry air. H is the mean rate of heating per unit mass for $y \in [0, W/2]$ (or cooling for $y \in [W/2, W]$) and therefore controlling the input of energy in the form of an increase in the temperature gradient between low and high latitudes. The profile of the diabatic heating is linear in y, and antisymmetric with respect to the central latitude. Diabatic forcing of this form increases the mean available potential energy of the system by imposing a gradient subsequently balanced by atmospheric motions and the transport of momentum and heat poleward.
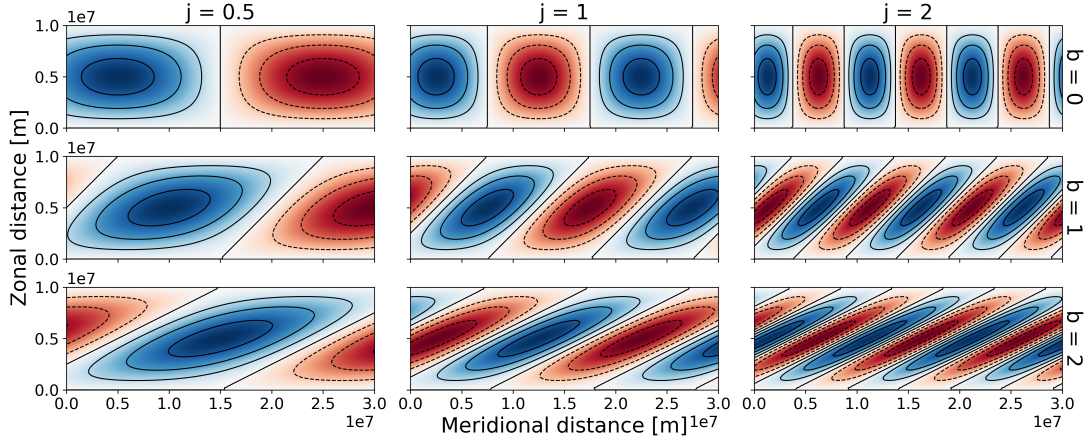
FIGURE 4.1: Eddy streamfunction shape for different values of the tilt b and the aspect ratio j; blue denotes positive, red denotes negative values.

The parameter $\lambda_R^2 = 2f_0^2/(\delta p \overline{\Gamma}_2 R)$ is the inverse square of the Rossby radius of deformation, where δp is the pressure difference between levels 1 and 3 and the basic state static stability is defined as $\overline{\Gamma} = RT/pc_p - \partial T/\partial p$ with temperature T.

To obtain a zonally averaged mean flow with a variable latitudinal maximum, we defined the mean zonal wind and shear as

$$\overline{u}_{m,T}(t) = \overline{U}_{m,T}(t)\sin ly - \overline{L}_{m,T}(t)\cos ly, \tag{4.2}$$

with time-dependent amplitudes $\overline{U}_{m,T}(t)$, determining the flow speed and (positive) $\overline{L}_{m,T}(t)$ shifting the latitudinal maximum y_{max} of the flow (northwards) according to

$$\tan(ly_{max}) = -\frac{\overline{U}_{m,T}}{\overline{L}_{m,T}} \tag{4.3}$$

(for $\overline{U}_{m,T}$ and $\overline{L}_{m,T}$ non-zero). The meridional wavenumber is $l = \pi/W$, yielding the following property, which was used to obtain equations (4.1a) and (4.1b):

$$\frac{\partial^2}{\partial y^2}\overline{u}_{m,T} = -l^2\left(\overline{U}_{m,T}\sin ly - \overline{L}_{m,T}\cos ly\right) = -l^2\overline{u}_{m,T}. \tag{4.4}$$

Based on the findings introduced in chapter 2 by Hoskins, James, and White, 1983 and Orlanski, 1998, showing that during their life cycle, the mid-latitude eddies in the storm track associated with the eddy-driven jet stream evolve to become meridionally elongated and southwest-northeast tilted, the eddy component of the

barotropic and baroclinic streamfunction is defined to be of the shape

$$\psi'_{m,T}(x,y,t) = A_{m,T}(t)\sin k(x - by)\sin ly + B_{m,T}(t)\cos k(x - by)\sin ly \qquad (4.5)$$

where $A_{m,T}(t)$ and $B_{m,T}(t)$ are time-dependent amplitudes, the meridional wavenumber $l = \pi/W$ equal to above, and k is a multiple of l defined as $k = jl = j\pi/W$ where j is a parameter describing the aspect ratio of the eddies, that is — without loss of generality — assumed to be a non-negative number. In the following, eddies with equal zonal and meridional wavenumber and thus aspect ratio $j = 1$ are referred to as being circular. The parameter b describes the slope of the tilt, see figure 4.1.

In comparison to the zonally and meridionally symmetric eddy shape in section 3.2, this shape of the eddy streamfunction components does not lead to a cancellation of the eddy product terms in equations (4.1a) and (4.1b). This is due to the eddies being not meridionally symmetric and therefore the system exhibits non-zero momentum and mixed momentum fluxes defined by

$$\overline{u'_m v'_m} + \overline{u'_T v'_T} = \frac{1}{2}j^2 l^2 b \left(A_m^2 + B_m^2 + A_T^2 + B_T^2 \right) \sin^2 ly, \qquad (4.6a)$$

$$\overline{u'_m v'_T} + \overline{u'_T v'_m} = j^2 l^2 b \left(A_m A_T + B_m B_T \right) \sin^2 ly, \qquad (4.6b)$$

where the sum of these fluxes is the momentum flux at the upper level 1 of the two-level model and the difference is the momentum flux at the lower level 3. The net poleward temperature flux produced by the eddy shape (4.5) can be calculated as

$$\overline{v'_m T'_2} = \frac{jlf_0}{R} \left(A_m B_T - A_T B_m \right) \sin^2 ly, \qquad (4.7)$$

where the temperature at level 2 is related to the streamfunction ψ_T by the hydrostatic balance equation (2.6). The meridional shape of the fluxes closely resembles the zonally averaged reanalysis data as shown in Kållberg et al., 2005.

Next, we derive time evolution equations for the mean flow amplitudes $\overline{U}_{m,T}(t)$ and $\overline{L}_{m,T}(t)$, and for the eddy streamfunction amplitudes $A_{m,T}(t)$ and $B_{m,T}(t)$. The former can be obtained by first replacing the mean zonal wind and shear in equations (4.1a) and (4.1b) by its definitions (4.2), additionally calculating the zonally averaged eddy momentum and heat fluxes occurring in these equations by replacing the eddy variables by their definitions (4.5) and projecting both equations onto the two meridional modes of $\overline{u}_m$ and $\overline{u}_T$. This is done by multiplying the result by either $\sin ly$ or $\cos ly$ and taking the meridional average from the equator to the pole. The detailed derivation can be found in appendix A.1.

To obtain evolution equations for the eddy amplitudes $A_{m,T}$ and $B_{m,T}$ we project the non-averaged evolution equations for the barotropic and baroclinic vorticities (3.4a) and (3.4b) onto the two zonal modes ($\sin k(x - by)$ and $\cos k(x - by)$) and the meridional mode ($\sin ly$) of the barotropic and baroclinic streamfunction (4.5), yielding four equations, see appendix A.2 for a detailed derivation.

Finally, the eight evolution equations for the mean flow and eddy amplitudes are

$$\frac{\partial}{\partial t}\overline{U}_m = - l^2 A\overline{U}_m - \frac{\kappa}{2}\left(\overline{U}_m - 2\overline{U}_T\right), \tag{4.8a}$$

$$\frac{\partial}{\partial t}\overline{L}_m = \frac{16j^2l^2b}{3W}\left(A_m^2 + B_m^2 + A_T^2 + B_T^2\right) - l^2 A\overline{L}_m - \frac{\kappa}{2}\left(\overline{L}_m - 2\overline{L}_T\right), \tag{4.8b}$$

$$\frac{\partial}{\partial t}\overline{U}_T = - \frac{4jl^2\lambda_R^2}{3W\left(l^2 + \lambda_R^2\right)}\left(A_mB_T - A_TB_m\right) - l^2 A\overline{U}_T \tag{4.8c}$$
$$\qquad + \frac{l^2}{l^2 + \lambda_R^2}\frac{\kappa}{2}\left(\overline{U}_m - 2\overline{U}_T\right) + \frac{\lambda_R^2}{l^2 + \lambda_R^2}\frac{8RH}{f_0c_p\pi W},$$

$$\frac{\partial}{\partial t}\overline{L}_T = \frac{16j^2l^4b}{3W\left(l^2 + \lambda_R^2\right)}\left(A_mA_T + B_mB_T\right) - l^2 A\overline{L}_T + \frac{l^2}{l^2 + \lambda_R^2}\frac{\kappa}{2}\left(\overline{L}_m - 2\overline{L}_T\right) \tag{4.8d}$$

$$\frac{\partial}{\partial t}A_m = - \frac{\alpha_m\beta j}{l}B_m + \frac{8\alpha_m j^3(1+b^2)}{3W}\left(B_m\overline{U}_m + B_T\overline{U}_T\right) - \frac{\kappa}{2}\left(A_m - 2A_T\right) \tag{4.8e}$$
$$\qquad - \widetilde{A}_m\alpha_m A_m - \frac{8\alpha_m j^2b}{3W}\left(A_m\overline{L}_m + A_T\overline{L}_T\right),$$

$$\frac{\partial}{\partial t}B_m = \frac{\alpha_m\beta j}{l}A_m - \frac{8\alpha_m j^3(1+b^2)}{3W}\left(A_m\overline{U}_m + A_T\overline{U}_T\right) - \frac{\kappa}{2}\left(B_m - 2B_T\right) \tag{4.8f}$$
$$\qquad - \widetilde{A}_m\alpha_m B_m - \frac{8\alpha_m j^2b}{3W}\left(B_m\overline{L}_m + B_T\overline{L}_T\right),$$

$$\frac{\partial}{\partial t}A_T = - \frac{\alpha_T\beta j}{l}B_T + \frac{8\alpha_T j^3(1+b^2)}{3W}\left(B_m\overline{U}_T + B_T\overline{U}_m\right) + \frac{\kappa\alpha_T}{2\alpha_m}(A_m - 2A_T) \tag{4.8g}$$
$$\qquad - \widetilde{A}_T\alpha_T A_T - \frac{8\alpha_T j\lambda_R^2}{3l^2W}\left(B_m\overline{U}_T - B_T\overline{U}_m\right) - \frac{8\alpha_T j^2b}{3W}\left(A_m\overline{L}_T + A_T\overline{L}_m\right),$$

$$\frac{\partial}{\partial t}B_T = \frac{\alpha_T\beta j}{l}A_T - \frac{8\alpha_T j^3(1+b^2)}{3W}\left(A_m\overline{U}_T + A_T\overline{U}_m\right) + \frac{\kappa\alpha_T}{2\alpha_m}(B_m - 2B_T) \tag{4.8h}$$
$$\qquad - \widetilde{A}_T\alpha_T B_T + \frac{8\alpha_T j\lambda_R^2}{3l^2W}\left(A_m\overline{U}_T - A_T\overline{U}_m\right) - \frac{8\alpha_T j^2b}{3W}\left(B_m\overline{L}_T + B_T\overline{L}_m\right),$$

where $\widetilde{A}_m = (j^4l^2 + b^4j^4l^2 + 6b^2j^2l^2 + l^2)A$ and $\alpha_m = (j^2 + j^2b^2 + 1)^{-1}$, $\widetilde{A}_T = (j^4l^2 + j^4b^4l^2 + 6j^2b^2l^2 + l^2 + (j^2 + j^2b^2 + 1)\lambda_R^2)A$ and $\alpha_T = (j^2 + j^2b^2 + 1 + \lambda_R^2/l^2)^{-1}$ for better readability.

4.3   Purely zonal flow and non-tilted eddies

For a non-zero positive heating rate H this system exhibits only one steady state, namely a purely zonal state where all eddy components are zero and the maximum

TABLE 4.1: Fixed parameter values for stability analysis.

Parameter	λ_R^2	β	A	κ	R	f_0	c_p	W
Value	$4.39{\times}10^{-12}$	$1.6{\times}10^{-11}$	10^5	$4{\times}10^{-6}$	287	10^{-4}	1004	10^7
Unit	m^{-2}	$\mathrm{m}^{-1}\mathrm{s}^{-1}$	$\mathrm{m}^2\mathrm{s}^{-1}$	s^{-1}	$\mathrm{JK}^{-1}\mathrm{kg}^{-1}$	s^{-1}	$\mathrm{JK}^{-1}\mathrm{kg}^{-1}$	m

TABLE 4.2: Varying parameter values for stability analysis.

Parameter	H	b	j
Range	$(0, 4{\times}10^{-3}]$	$[0, 2]$	$0.5, 1, 2$
Unit	KJ ton^{-1} s^{-1}	-	-

of the mean zonal flow is positive and in the middle of the meridional channel:

$$P^0 = (\overline{U}_m^0, 0, \overline{U}_T^0, 0, 0, 0, 0, 0) = \alpha H(1, 0, \frac{l^2 A}{\kappa} + \frac{1}{2}, 0, 0, 0, 0, 0), \qquad (4.9)$$

with $\alpha = 16(A(l^2 + \lambda_R^2)(2l^2 A + \kappa) + 2\kappa l^2 A)^{-1}\kappa\lambda_R^2 R/(f_0 c_p l^3 W^2)$ is a linear function in H. As expected, this state is the same as the zonal steady state (3.19) in section 3.3. The linear stability of this solution is determined by numerically calculating the eigenvalues of the Jacobian matrix of system (4.8a)-(4.8h) at this steady state. Therefore, the parameters in table 4.1 were kept fixed, whereas the mean rate of heating H, the eddy streamfunction tilt parameter b and the parameter j describing the eddy aspect ratio were varied within the ranges given in table 4.2. Since the behaviour of both the current and previous model is identical for changes in the eddy diffusion parameter A and surface friction parameter κ, these parameters are kept constant for the following study.

For eddies that are not tilted ($b = 0$), this system's stability behaviour is identical to that of the model in section 3.2, as expected. Keeping j fixed, the above-defined purely zonal state grows linearly with the heating H. For a further increase of H, a complex conjugate pair of eigenvalues of the Jacobian matrix of system (4.8a)-(4.8h) at the steady state (4.9) crosses the imaginary axis such that their real part turns positive. It follows that the steady state loses its stability at this threshold value of H and numerical simulations show that in this region of the parameter space a stable periodic limit cycle of the eddy amplitudes $A_{m,T}$ and $B_{m,T}$ appears. This suggests a Hopf bifurcation because only for this type of bifurcation a steady states exchanges stability with a limit cycle. Since these appearing orbits are stable after the switch, the Hopf bifurcation is supercritical. As the purely zonal steady state loses its stability, the wind speed remains constant, called *eddy saturation*.

The stable limit cycle of the eddy amplitudes appears to be a different behaviour to

the previous model, where the system exhibits a second steady state, the eddy steady state (3.20), which exchanges stability with the zonal steady state (3.19). However, it is the same: in the previous model, the evolution equation for the net poleward temperature flux in addition to three other eddy correlation terms was analysed. Here, the equations describe the evolution of the individual eddy amplitudes of (4.5), from which the net poleward temperature flux can be calculated by equation (4.7). This quantity is zero in the stable region of the purely zonal state and grows linearly with H in the unstable region. It is therefore equal to the eddy steady state (3.20) found in section 3.3. The zonally averaged momentum flux (4.6a) and mixed momentum flux (4.6b) are zero in the entire parameter space for $b = 0$, because non-tilted eddies are symmetric in both directions and therefore the momentum fluxes cancel in the zonal average. Subsequently, the amplitudes $\overline{L}_{m,T}$ are zero and therefore the mean flow remains meridionally symmetric. This behaviour can alternatively be seen from equations (4.8a)-(4.8d) directly: it is the heat flux that decreases the baroclinicity ($\overline{U}_T$) of the model and the momentum fluxes act on the cosine mode of the mean flow ($\overline{L}_{m,T}$) and therefore push the mean flow poleward.

4.4 Barotropic and baroclinic eddy regime

For tilted eddies ($b > 0$), the system exhibits an entirely different behaviour compared to the case where eddies are not tilted. As soon as the tilt is non-zero, that is, the tilting parameter b is greater than zero as shown in the second and third row of figure 4.1, the eddy-saturated state of the model with non-tilted eddies vanishes completely: in each of the regimes described in the following, the zonal wind speed increases with the heating H and is never independent of it. Increasing the tilt from zero leads to a decrease in the critical value of the heating H at which the zonal state loses its stability. Moreover, for larger values of H than this critical value, the dynamics of the system features two different regimes.

As before, in both of these unstable regimes the eddy amplitudes $A_{m,T}$ and $B_{m,T}$ exhibit stable periodic orbits, whereas the mean flow amplitudes $\overline{U}_{m,T}$ and $\overline{L}_{m,T}$ are non-zero and constant for constant parameters. Therefore, the poleward heat flux and momentum fluxes remain constant as well. The stability of the periodic orbits was determined by numerical experiments. Therefore, the dynamical system was simulated for a dense range of the parameter values in table 4.2 until the solution converged to the constant values of the mean flow amplitudes, poleward heat flux and momentum fluxes. The solutions were verified by simulating the system for a range of different initial conditions, which did not change the final constant values of the solutions. The black areas in figure 4.2 are the regions of the parameter
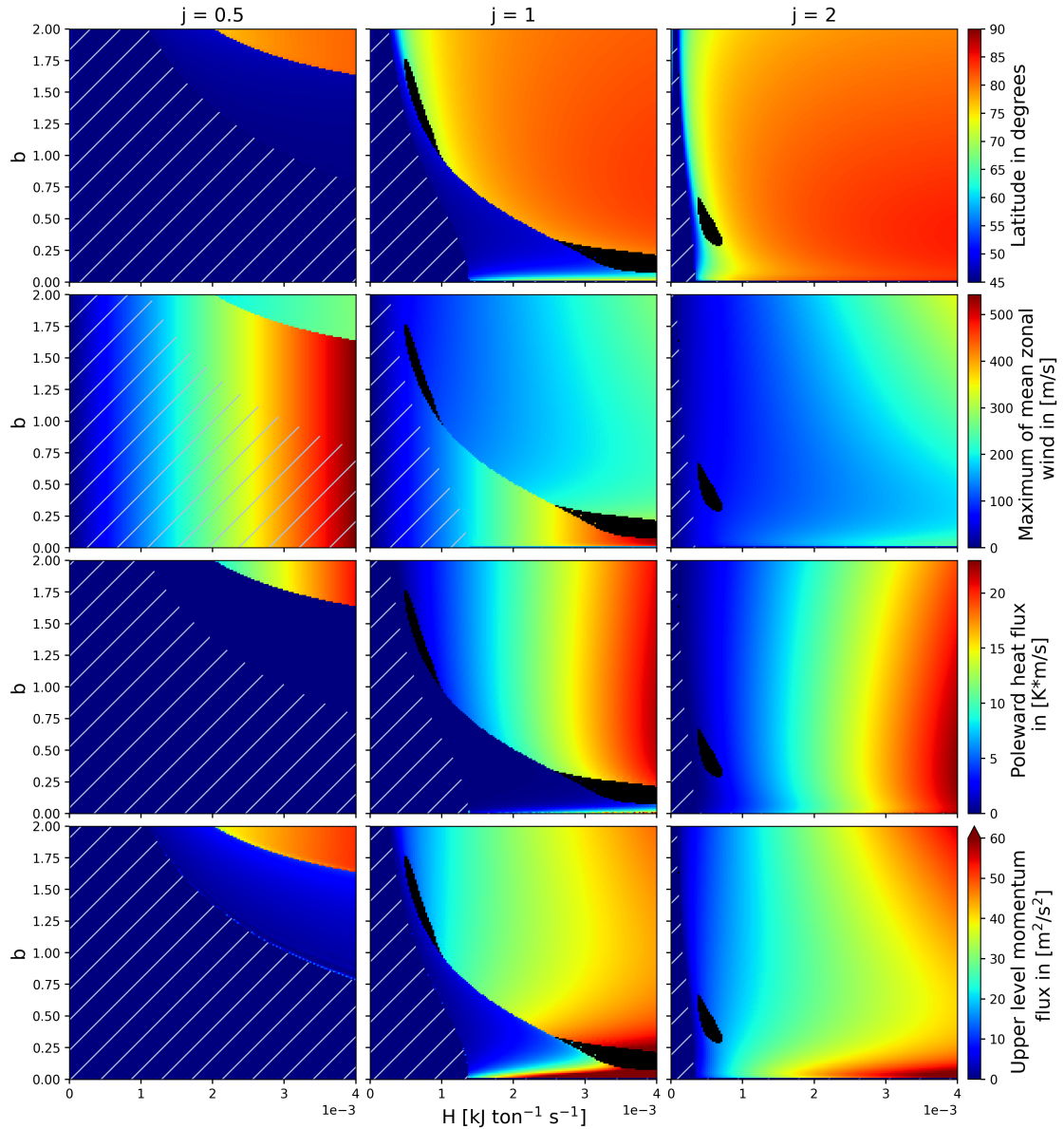
FIGURE 4.2: Contours of model diagnostics in the H-b-parameter space; for the left column $j = 0.5$, the middle $j = 1$, the right $j = 2$; the first row shows the latitude of the mean zonal wind maximum, the second row shows the maximum values of the mean zonal wind, the third row shows the poleward heat flux, and the fourth row the momentum flux; the dashed areas denote the stable region of the zonal steady state; the black areas are the regions where the zonal flow regime and baroclinic eddy regime compete.

TABLE 4.3: Overview of flow properties in respective regimes.

	Purely zonal flow regime	Barotropic eddy regime	Baroclinic eddy regime
Mean zonal wind $\overline{u}_m$ and shear $\overline{u}_T$	positive, growth in H	growth in H, pushed north	reduced growth in H pushed further north
Net poleward heat flux $\overline{v'_m T'_2}$	0	0	positive, growth in H
Eddy momentum flux $\overline{u'v'}$	0	positive, growth in H	positive, reduced growth in H

space were the solution did not converge and the behaviour of the model for these parameter combinations is explained later in this section.

For the following analysis the latitudinal maximum strength and position of the mean zonal wind and shear (4.2) together with the poleward temperature flux (4.7) and the momentum flux on the upper level of the two-level model (4.6a)+(4.6b) are the quantities of interest. Therefore, we describe the behaviour of these diagnostics directly instead of the evolution of the single amplitudes.

Unlike the non-tilted case, for increasing the tilt b of the eddies, the maximum of the zonal flow moves poleward as soon as the zonal state loses stability. This can be seen in the first row of figure 4.2, where the latitude of the mean zonal wind maximum is shown as dependent on the heating H and the tilt b. First, solely the column in the middle is considered, where j was set to one, meaning that the eddy streamfunction has the same zonal and meridional wavenumber, compare figure 4.1. The dashed region, where the latitude is homogeneously 45°, is the stable region of the zonal steady state. Increasing the heating H and/or the eddy tilt b leads to a switch of the system to the next state, where the mean flow is slightly pushed northward and still growing linearly with H, see figure 4.2 in the middle of the second row and compare also the top middle plot in figure 4.3. In this state, the momentum flux (bottom row) is positive and nearly linearly increasing with H in a similar manner as the mean flow moves poleward, whereas the poleward heat flux (third row) remains zero. In the absence of poleward heat flux by the eddies the diffusion within the zonal flow is the sole mechanism to balance the equator-to-pole temperature forcing, so the zonal wind speed is highly sensitive to the magnitude of the diabatic forcing, H. Therefore, this regime is called the barotropic eddy regime in the following.

The region in the top right of the plot shows the third regime of the system, where the mean flow is pushed much further north, so the depicted latitude is very high.
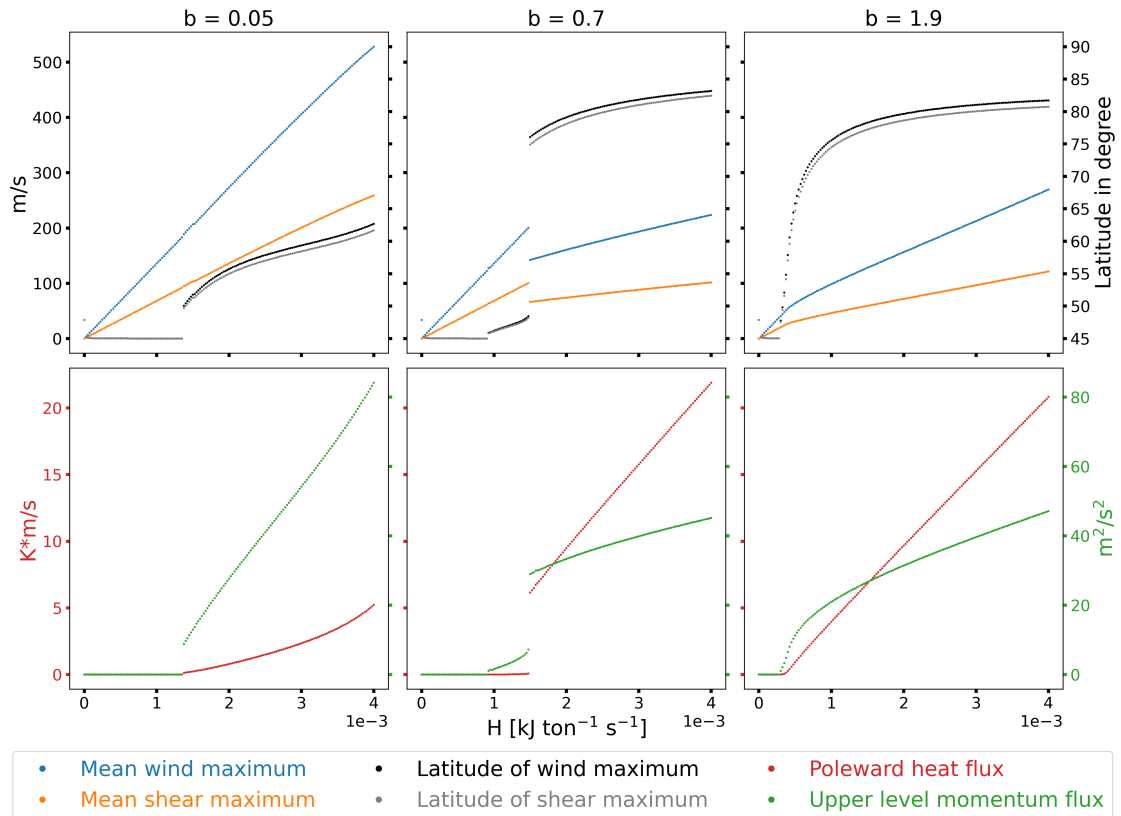
FIGURE 4.3: Diagnostics of the model as functions of H; the top row plots show the maximum value of the mean zonal wind and shear and their respective latitudinal position, the bottom row shows the poleward heat flux and upper-level momentum flux; for the left plots the tilt is $b = 0.05$, for the middle ones $b = 0.7$, for the right ones $b = 1.9$; for all three scenarios the eddy aspect ration $j = 1$.

In this regime, the zonal wind still grows almost linearly with the heating, but now with a lower rate, and the poleward heat flux and the momentum flux increase with higher values of the heating rate. Since the heat flux is not zero anymore, this regime is named the baroclinic eddy regime. An overview of the three flow regimes and the respective flow properties is shown in table 4.3.

The switch from the stable state through the barotropic to the baroclinic eddy regime for increasing heating can happen in four different ways, depending on the magnitude of the tilt b. Three of these transitions are shown in figure 4.3 for $j = 1$. For b in the interval $[0.34, 0.99]$ (values rounded to two digits) this transition happens in two stages, see plots in the middle. First, the zonal state loses stability, leading to growing eddies and therefore an increase in momentum flux, whereas the poleward heat flux remains zero. The second transition into the baroclinic eddy regime is non-continuous, the momentum flux and also heat flux jump to a higher value, whereas the zonal flow abruptly slows down and is relocated much further north. After this jump, the mean flow continues growing, but with a smaller sensitivity,
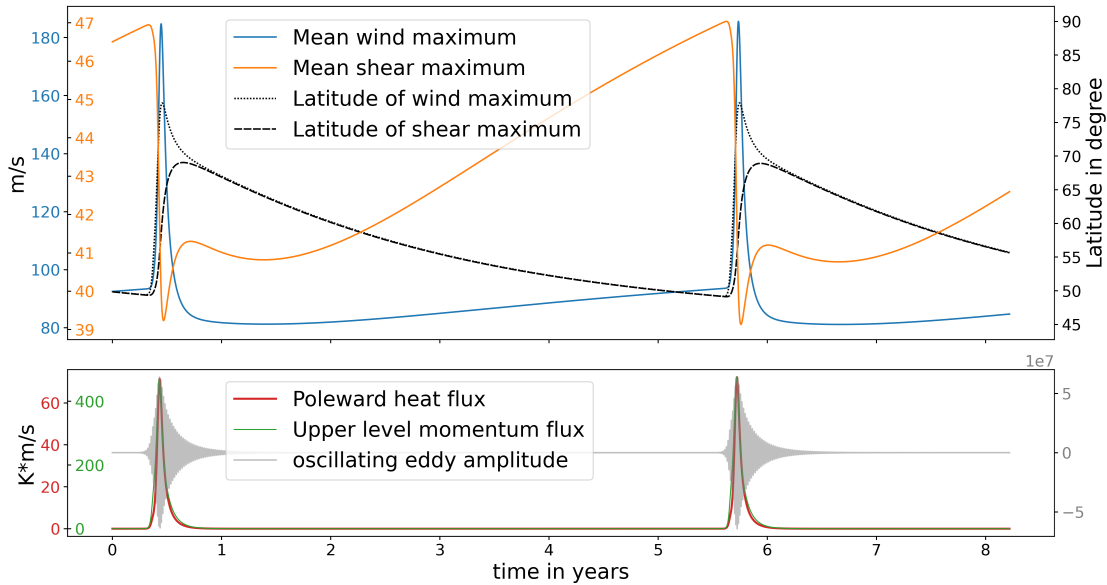
FIGURE 4.4: Diagnostics of the model as a function of time; $j = 1$, $b = 1.3$, $H = 7.5 \times 10^{-4}$, as an example of the recharged oscillator of the model in certain regions of the considered parameter space.

and the momentum flux and heat flux rise with increased heating.

This regime is a close resemblance to the eddy saturation state in the non-tilted model. Although the growth rate of the mean flow is not zero and not independent of the heating, it is particularly low compared to the other regimes, and the heat flux is growing linearly with the heating. The reason for this is the non-zero momentum flux increasing with H and therefore generating additional momentum of the mean flow. In contrast to the complete eddy saturation with zero mean flow growth rate in the model with non-tilted eddies, here the tilt of the eddies yields a positive poleward momentum flux which increases with H and subsequently generates additional momentum of the mean flow, leading to a small remaining sensitivity of the mean flow to the forcing despite positive poleward heat flux.

The plots on the right of figure 4.3 show the transition behaviour for values of the tilt b higher than 1.76. Here, the system continuously moves from the stable region through the barotropic eddy regime and immediately to the baroclinic eddy regime without a jump. However, the mean zonal wind and shear and the momentum flux show again a reduced growth rate. Similarly, for a very weak tilt b below 0.06, the system directly shifts from the zonal to the baroclinic eddy regime, shown in the left plots of figure 4.3. In this transition, the mean flow exhibits no change in growth rate but is non-continuously relocated polewards. The momentum flux jumps from zero to positive growth, whereas the heat flux rises monotonically from zero.

The fourth possible switch is a variation of the first one and occurs in the black regions of the heating rate - tilt - plane in figure 4.2. Here the model exhibits a charge and discharge behaviour where the system oscillates between the purely zonal state and the baroclinic eddy regime on a very long time scale. One cycle of this behaviour for an example set of parameters is shown in figure 4.4. In the charging phase of the cycle, the mean zonal wind and shear built up and grow over time, building up the baroclinicity in the atmosphere. Starting from further towards the pole, the latitudinal maximum of the flow moves south during this phase almost to the middle of the channel at 45°. In this phase of the cycle, the eddy amplitudes oscillate in such a way that the heat and momentum fluxes remain zero.

After a certain amount of time, the magnitudes of the eddy amplitudes increase rapidly, yielding a sudden peak of the heat and momentum flux magnitudes, which in turn cause the shear and therefore the baroclinicity to collapse, but dramatically increase the mean wind speed and simultaneously push the mean flow far poleward. After this short peak, the fluxes drop again back to zero, the wind speed drops to a lower level than before the peak and the system starts to recharge again. Depending on the tilt b, the eddy aspect ratio j and the heating rate H, this cycle can vary in magnitude of the different diagnostics and also frequency, ranging from a return time of around one year to up to ten years.

Finally, the eddy aspect ratio j has a noteworthy impact on the three different regimes of the model. This can be seen in figure 4.2 in the left and right columns. The left column shows the regimes for $j = 0.5$, meaning that the eddies are zonally elongated, see also figure 4.1, and therefore resemble planetary waves rather than eddies. Such waves have a stabilising effect on the purely zonal flow and also favour the barotropic eddy regime of the model, which can be seen by the increased area of those two regimes compared to the column in the middle. This stabilising effect on the zonal flow for long meridional waves is well known as the shortwave cut-off introduced in section 2.3.2 discovered by both Charney, 1947 and Eady, 1949 for waves with small wave numbers in simple baroclinic models of the mid-latitudes. In contrast to that, in the column on the right, the meridionally elongated eddies for $j = 2$ destabilise the purely zonal flow and favour the baroclinic eddy regime, whereas the barotropic eddy regime almost vanishes. Thus, eddies of this shape, which are also observed in the atmosphere, seem to be more effective in transporting heat poleward.

For low values of the heating H, meridionally elongated eddies produce a mean wind with reasonably realistic values for the wind speed of up to $50 \, \text{ms}^{-1}$ in the baroclinic regime of the model, whereas for more symmetric and zonally elongated eddies the

obtained wind speed is only feasible in the stable zonal regime. This behaviour was already observed in the former model, section 3.4. The poleward temperature flux and upper-level momentum flux values are mostly realistic for the considered parameter space: the maximum of the temperature flux in the atmosphere ranges from 7 to 20 $\mathrm{K\,m\,s^{-1}}$, and the mean upper-level momentum flux can reach 50 $\mathrm{m^2\,s^2}$, where values are taken from Kållberg et al., 2005.

4.5　Discussion and conclusion

Starting from Phillips' classical two-level quasi-geostrophic model on the β-plane (Phillips, 1956) and modifying the derivation and model reduction in section 3.2 we developed a system of eight ordinary differential equations describing the latitudinal modification of the mean flow and shear by the large-scale eddies in the mid-latitude atmosphere. This was accomplished by defining the shape of the mean wind and shear to consist of two modes, allowing for variations in the latitudinal maximum thereof. The accordingly constructed eddy streamfunction allows eddy shapes that yield the defined mean flow and were chosen in agreement to Hoskins, James, and White, 1983 to be tilted southwest-northeast. By projecting the non-averaged flow equations onto the eddy modes, we were able to obtain isolated evolution equations for the eddy amplitudes and therefore a closed system under predefined diabatic heating.

Similar to the analysis in 3, we avoided the usual normal mode instability analysis and instead used dynamical systems theory to determine a single zonal steady state and stable periodic orbits in different regions of the considered parameter space. As expected, the purely zonal state (4.9) is equal to the zonal state (3.19) of the former model, and for non-tilted eddies, the stability behaviour dependent on the parameters is the same. In the repelling regime of the zonal steady state, the eddy amplitudes exhibit stable periodic orbits, yielding constant mean wind and shear, and heat and momentum flux values for a fixed set of parameters. Therefore, the stable periodic orbits can be treated as steady states of the system comprised of mean flow, heat and momentum flux, independent of the tilt of the eddies.

The eddy saturation behaviour of the non-tilted case, where the zonal flow is completely independent of the diabatic heating, is lost for even the smallest tilt. This results from tilted eddies exhibiting a non-zero momentum flux and subsequently feeding back kinetic energy into the mean flow, as described in the Lorenz energy cycle (Lorenz, 1955). The perfect eddy saturation result from chapter 3 can therefore be considered a singular limit of the system for vanishing tilt, where the new

eddy saturation regime found in the model of the current chapter is less complete and more in accordance with observations (Novak, Ambaum, and Harvey, 2018).

In the repelling region of the purely zonal flow, the considered parameter space is divided into two regimes resembling two theoretically possible mechanisms of the atmosphere to compensate for the imbalance of the diabatic heating between the equator and the poles. The first regime, which is more pronounced for zonally elongated or circular and rather non-tilted eddies, is dominated by a positive momentum flux increasing with heating and simultaneously speeding up the mean flow. In this regime, the poleward heat flux remains zero, so the imbalance due to the diabatic heating at the equator is compensated by the dissipation within the mean flow and the eddy momentum flux alone, which leads to unrealistically high values of the zonal wind speed. Therefore, this regime is called the barotropic eddy regime.

For meridionally elongated eddies, the system is mainly in the second, the baroclinic eddy regime for the considered parameter space. The eddies exhibit a positive heat flux which increases with intensifying heat imbalance, and the momentum flux together with the zonal flow speed increases at a significantly lower rate than in the barotropic regime. For some choices of parameters, the system eventually exhibits incomplete eddy saturation, having a dominant growth rate of the heat flux compared to small growth rates of the momentum flux and zonal flow speed. Compared to a slight shift northwards of the mean flow maximum in the barotropic regime, the heat flux coincides with a significantly greater northward shift in the baroclinic regime. This correlation was also found in Novak, Ambaum, and Tailleux, 2015, to which a comparison is drawn in the following.

Despite the simplicity of the model and the limiting assumptions made on the eddy streamfunction, especially having a constant tilt, the model resembles the characteristics of the mid-latitude eddies found by Hoskins, James, and White, 1983 described earlier. Their diagnosed effect of the eddies onto the mean flow is reminiscent of the effect the aspect ratio j in our model has on the two eddy regimes: For almost non-tilted and circular eddies, the model exhibits the barotropic eddy regime with a positive momentum flux enhancing the zonal flow. However, for zonally elongated southwest-northeast tilted eddies, the model mainly exhibits the baroclinic regime with a depleted mean flow growth rate.

Based on a simple oscillator model of baroclinicity (or wind shear) and eddy activity (or heat flux) (Ambaum and Novak, 2014), Novak, Ambaum, and Tailleux, 2015 used Hoskins' diagnostic to draw a connection between the eddy anisotropy and the three preferred latitudinal positions of the North Atlantic jet stream, which were found by Woollings, Hannachi, and Hoskins, 2010 analysing North Atlantic winter season

ERA-40 data. Coinciding with Franzke, Woollings, and Martius, 2011, the study by Novak, Ambaum, and Tailleux, 2015 also finds the preferred transitions between the south, middle and north regimes of the jet stream and describes the life cycle of the North Atlantic storm track as follows.

In the jet entrance region in the western Atlantic, diabatic forcing increases the baroclinicity, which in turn starts to form round and coherent eddies. In this phase, the jet is steered south, which coincides with the low latitude of the mean flow maximum in the barotropic eddy regime of our model, which is exhibited for this particular shape of eddies. Further increases in baroclinicity (or wind shear in our model) will further enhance the eddies and at the same time, the eddies become stronger and propagate downstream. This leads to enhanced eddy deformation to meridionally elongated southwest-northeast tilted shapes and therefore pushes the jet northward into the middle regime.

Further in their development, the eddies become so large that the eddy mixing rapidly reduces the baroclinicity of the zonal flow, overriding the replenishing effect of the diabatic forcing. Since the reduced baroclinicity inhibits the production of new storms, this enables the eddies to deform farther upstream and push the mean flow farther polewards into the northern jet regime. This phase is similar to the baroclinic eddy regime in our model, where the jet is pushed northwards and instead of the jet stream the eddies grow. This can be seen by the dominating poleward heat flux in our model, which agreed with the findings by Novak, Ambaum, and Tailleux, 2015, who was able to relate regions of high heat flux to a northward deflection of the jet. As the eddy activity decays, the mean zonal shear in the flow is replenished by the diabatic forcing and the cycle repeats from the south regime.

To highlight the novelty of our work, it is noteworthy that the studies by Hoskins, James, and White, 1983, Woollings, Hannachi, and Hoskins, 2010 and Novak, Ambaum, and Tailleux, 2015 describing the effect of the eddies onto the mean flow are data driven approaches based on atmospheric observations, whereas our study is a modeling approach. Instead of analysing data, our derived model features properties of the atmosphere as intrinsic behaviour of the model dynamics itself. Therefore, our results can broaden the understanding of cause and effect of the observed dynamics in the mid-latitude atmosphere.

It is also noteworthy, that the diagnostic quantities by Hoskins, James, and White, 1983 and Novak, Ambaum, and Tailleux, 2015 are averaged in time, whereas the model in the present study deals with a zonally averaged flow without variation in the eddy shape. Therefore, instead of an evolution of the flow in time, the barotropic

and baroclinic regimes of our model can rather be interpreted as a snapshot in time of the life cycle of the eddies in the mid-latitude storm track.

On climate timescales, the dependence of the mean flow on the forcing determined by Lucarini, Speranza, and Vitolo, 2007 in their two-level model can similarly be observed in our system for a substantial tilt of the eddy shape: when moving from the barotropic into the baroclinic eddy regime, the growth rate of the mean zonal wind and shear is lower than before the transition and in some regions of the parameter space even the magnitude is lowered after the stability switch. This observation is expected due to the geostrophic assumption incorporated into the system. While the mean zonal wind and shear grow monotonically with the diabatic heating H, their actual value is reduced by the eddy activity in the baroclinic compared to the barotropic eddy regime. This is due to the onset of the poleward heat flux, necessary to balance and reduce the increased equator-to-pole temperature gradient, therefore weakening the baroclinicity or mean shear and subsequently the mean flow. This process is known as the baroclinic adjustment of the mid-latitude atmosphere (Stone, 1978).

To conclude, this study presents a minimal model of the mid-latitude atmosphere exhibiting eddy-mean flow interaction, jet shifts, and partial eddy saturation and therefore question two of the introduction to this thesis can be answered with yes. Despite the minimal setup, the model captures processes of the mid-latitude atmosphere on different time scales, which are commonly observed in re-analysis data and atmospheric climate models. Additionally, the model shows how the systems reacts to variations of external forcing by heating, answering again question four of the introduction to this thesis. Therefore, the significance of this work lies in atmospheric modelling, where it is still not fully understood how the mid-latitude storm tracks respond to variations in the forcing and how this affects the zonal flow.

Chapter 5

Conclusion

The goal of this thesis is to shed some light on the complex non-linear dynamics of the mid-latitude atmosphere by developing simple models with minimal ingredients based on Phillips' QG two-level model (Phillips, 1956). Two models, each a set of ordinary differential equations, describing the interaction between the mean flow and the eddies were developed and analysed by means of linear stability analysis. The results were found to resemble features of other models and observations of the real mid-latitude atmosphere.

The first model derived in chapter 3 is based on an extremely simple shape of the zonally averaged mean flow with a fixed maximum location in the middle of the channel. Accordingly, the eddy streamfunction is defined to be of non-tilted shape, possibly elongated in the zonal or meridional direction. This specific perturbation streamfunction shape neglects direct eddy-eddy interactions and does therefore not exhibit eddy momentum flux. The developed set of ordinary differential equations describes the evolution of the zonally averaged mean wind and shear, that is, baroclinicity, the net poleward temperature flux and three other eddy statistics. This model exhibits two physically possible steady states, a purely zonal state and a steady state with developed eddies, with opposite stability regions describing two principal physical mechanisms of the atmosphere to balance the imposed equator-to-pole temperature gradient.

For relatively low values of heating, that is, a weak equator-to-pole temperature gradient, the purely zonal steady state, where all the eddy statistics remain zero, is attracting. In this state, the temperature gradient is balanced by diffusion of the zonal flow and no eddies need to develop, thus the atmosphere is baroclinically stable. The mean zonal wind speed increases for a stronger forcing by heating until a certain threshold, where the zonal state loses stability and the eddy steady state becomes attracting. In this second state, the eddies grow to a finite amplitude in order to compensate for the growing temperature gradient that can no longer be

balanced by diffusion. Above this threshold of the stability switch, the zonal wind speed remains constant and no longer increases with the heating, a property of the flow called eddy saturation.

The second model derived in chapter 4 can be viewed as an extension of the first one since the mean flow in this model is defined to have a latitudinally varying maximum within the model channel. The eddy streamfunction is modelled more realistically to be possibly tilted in the southwest-northeast direction and again elongated in the zonal or meridional direction, allowing for a positive poleward eddy momentum flux. In this model, the developed set of ordinary differential equations describes the evolution of the zonal mean wind and shear amplitudes and the eddy amplitudes, yielding eight equations in total. As expected, for non-tilted eddies this system behaves equally to the first model. However, for tilted eddies, only the zonal steady state remains the same, whereas the repelling regime thereof is divided into two regions of different behaviour.

As the zonal steady state loses stability, the system enters the barotropic eddy regime, where the maximum of the zonal flow moves slightly poleward while, in contrast to non-tilted eddies, the zonal wind keeps increasing with incoming heating. In this state, the poleward heat flux remains zero, whereas the eddy momentum flux grows nearly linearly with the heating. Further increasing the forcing pushes the system into the baroclinic eddy regime, where the poleward temperature flux in addition to the momentum flux increases with growing heating. The zonal flow is pushed further poleward in this state, whereas the zonal wind speed is reduced but still increases at a lower rate with the heating than before. This resembles the eddy saturation mechanism of the first model, but in the second model the saturation is not complete.

The ultimate goal of this thesis was to develop minimal models to better understand the complex dynamics of the mid-latitude atmosphere, especially the interaction of the zonal flow and the eddies. In the introduction to this thesis we therefore posed four specific questions to achieve this goal. The first and second question, asking whether it was possible to capture some of these complex dynamics, the latitudinal shift of the jet amongst others, can now be answered with yes. Additionally, both models were analysed in terms of their behaviour to changing internal and external parameters, giving answers to questions three and four.

Probably the most limiting assumption in this work is the constant shape of the eddy streamfunction. As described in section 2.4, the tilt and elongation of the eddies vary during their lifetime within a storm track. A possibly interesting undertaking and further extension of the work in this thesis could be to allow for such a variation

by deriving a ninth differential equation describing the evolution of the eddy tilt and shape. This could give further insight into the storm track life cycle and the preferred tendency of the eddies.

Further to that, the results and conclusions, such as the extent of the eddy saturation or the sensitivity of the jets and eddy fluxes to various internal and external parameters, are all in the context of the simple models derived in this thesis. The robustness of these results is difficult to assess a priori, since there are many different ways in which the models can be perturbed or extended to more complexity. To show such robustness, one would need to consider a hierarchy of models with an increasing number of modes and analyse their behaviour compared to each other. One example of such a result is the eddy saturation mechanism, which is also observed in more comprehensive models (e.g. Novak, Ambaum, and Harvey, 2018) of the atmosphere and ocean. Therefore, eddy saturation is a robust result and it can be expected in any model with a representation of baroclinic instability that the zonal state will become unstable for large enough forcing, enabling eddies to develop and to balance the poleward temperature gradient. However, the extent of eddy saturation found in our first model of chapter 3 is not that robust. Already a small change of the mean flow and eddy properties as in our second model in chapter 4 yielded a weakening - but not a full disappearance - of the mechanism.

A final comment should be made on the applicability of the presented models to the real atmosphere regarding climate change. Despite great similarities between the two models and observed behaviour in the mid-latitudes, the defined diabatic forcing by a linearly declining heating which is zero in the middle of the channel is a great simplification, being fulfilled neither in the laboratory nor in the atmosphere according to Phillips, 1956. Although it is a reasonable first approximation for the purpose of the model, this makes interpreting the model behaviour in terms of a warming climate more difficult. Present-day observations and future climate projections agree that in the currently changing climate, the near-surface air temperature in the Arctic region will increase at a faster rate relative to lower latitudes and the global mean (see e.g. Previdi, Smith, and Polvani, 2021), a mechanism called *Arctic amplification*. This would lead to a decreasing equator-to-pole temperature gradient and attempting to model the diabatic heating like in the models presented in this thesis, the linearly declining function of heating would be zero further towards the poles. Since this possibility is not included in either of the two models, the results should be treated with caution in light of climate change.

Despite the limiting assumptions imposed on the possible shape of the flow, both models exhibit features that can be found in the mid-latitude atmosphere. To the

author's knowledge, the model derived in chapter 3 is the first minimal model of the atmosphere to exhibit complete eddy saturation, the model in chapter 4 is the first minimal model that incorporates a latitudinal shift of the zonal flow maximum in such a manner. Therefore, this thesis contributes to increasing the basic understanding of the interaction between the mean flow and the eddies, and in light of the questions asked in the introduction of this thesis, it is indeed possible to develop models with minimal ingredients that still resemble some features observed in the mid-latitude atmosphere.

Appendix A

Derivation of evolution equations in section 4.2

A.1 Mean wind and shear amplitude equations

The different components in equations (4.1a) and (4.1b) either project on the $\sin ly$ mode, on the $\cos ly$ mode or on both modes of the mean zonal wind and shear. Therefore, these equations can be separated into two equations each, one equation for each time-dependent amplitude $\overline{U}_{m,T}(t)$ and $\overline{L}_{m,T}(t)$. This is done by replacing $\overline{u}_{m,T}$ by its definition (4.2), multiplying by either $\sin ly$ or $\cos ly$, and taking the meridional average from the equator to the pole.

We start with equation (4.1a) and replace $\overline{u}_m$ by its definition (4.2), yielding

$$\sin ly \frac{\partial}{\partial t}\overline{U}_m - \cos ly \frac{\partial}{\partial t}\overline{L}_m = \frac{1}{l^2}\frac{\partial^3}{\partial y^3}\left(\overline{u'_m v'_m} + \overline{u'_T v'_T}\right) \tag{A.1}$$
$$- l^2 A\left(\overline{U}_m \sin ly - \overline{L}_m \cos ly\right)$$
$$- \frac{\kappa}{2}\left(\overline{U}_m \sin ly - \overline{L}_m \cos ly - 2\overline{U}_T \sin ly + 2\overline{L}_T \cos ly\right).$$

To obtain the evolution equation for $\overline{U}_m$, we take the integral with respect to y from 0 to W. All terms multiplied by $\cos ly$ vanish as well as the third derivative of the eddy momentum fluxes since they are proportional to $\sin 2ly$. Note here that multiplying by $\sin ly$ before taking the integral would give the same result because the eddy momentum fluxes do not project on this mode. Therefore, we obtain

$$\int_0^W \sin ly \, dy \frac{\partial}{\partial t}\overline{U}_m = -l^2 A\overline{U}_m \int_0^W \sin ly \, dy - \frac{\kappa}{2}\left(\overline{U}_m - 2\overline{U}_T\right)\int_0^W \sin ly \, dy$$
$$\Leftrightarrow \frac{\partial}{\partial t}\overline{U}_m = -l^2 A\overline{U}_m - \frac{\kappa}{2}\left(\overline{U}_m - 2\overline{U}_T\right).$$

Multiplying (A.1) by $\cos ly$ and taking again the integral with respect to y gives the evolution equation for $\overline{L}_m$. Here, all terms multiplied by $\sin ly$ vanish and we obtain

$$
-\int_0^W \cos^2 ly\, dy \frac{\partial}{\partial t}\overline{L}_m = \frac{1}{l^2}\int_0^W \cos ly \frac{\partial^3}{\partial y^3}\left(\overline{u'_m v'_m} + \overline{u'_T v'_T}\right) dy
$$
$$
+ l^2 A \overline{L}_m \int_0^W \cos^2 ly\, dy + \frac{\kappa}{2}\left(\overline{L}_m - 2\overline{L}_T\right)\int_0^W \cos^2 ly\, dy
$$
$$
\Leftrightarrow \frac{\partial}{\partial t}\overline{L}_m = \frac{16j^2 l^2 b}{3W}\left(A_m^2 + B_m^2 + A_T^2 + B_T^2\right) - l^2 A \overline{L}_m - \frac{\kappa}{2}\left(\overline{L}_m - 2\overline{L}_T\right).
$$

The same separation can be done with equation (4.1b). First, we replace $\overline{u}_T$ by its definition (4.2):

$$
\sin ly \frac{\partial}{\partial t}\overline{U}_T - \cos ly \frac{\partial}{\partial t}\overline{L}_T = \frac{1}{l^2 + \lambda_R^2}\frac{\partial^3}{\partial y^3}\left(\overline{u'_m v'_T} + \overline{u'_T v'_m}\right) + \frac{\lambda_R^2}{l^2 + \lambda_R^2}\frac{\partial^2}{\partial y^2}\overline{v'_m \psi'_T} \quad \text{(A.2)}
$$
$$
- l^2 A \left(\overline{U}_T \sin ly - \overline{L}_T \cos ly\right) + \frac{\lambda_R^2}{l^2 + \lambda_R^2}\frac{2\delta p R H}{f_0 p_2 c_p W}
$$
$$
+ \frac{l^2}{l^2 + \lambda_R^2}\frac{\kappa}{2}\left(\overline{U}_m \sin ly - \overline{L}_m \cos ly - 2\overline{U}_T \sin ly + 2\overline{L}_T \cos ly\right).
$$

Multiplying by $\sin ly$ and taking the integral with respect to y from 0 to W gives the evolution equation for $\overline{U}_T$. Again, all terms multiplied by $\cos ly$ and the eddy momentum flux term vanish because they are not projecting on the $\sin ly$ mode, yielding

$$
\int_0^W \sin^2 ly\, dy \frac{\partial}{\partial t}\overline{U}_T = \frac{\lambda_R^2}{l^2 + \lambda_R^2}\int_0^W \sin ly \frac{\partial^2}{\partial y^2}\overline{v'_m \psi'_T}\, dy - l^2 A \overline{U}_T(t)\int_0^W \sin^2 ly\, dy
$$
$$
+ \frac{l^2}{l^2 + \lambda_R^2}\frac{\kappa}{2}\left(\overline{U}_m - 2\overline{U}_T\right)\int_0^W \sin^2 ly\, dy
$$
$$
+ \frac{\lambda_R^2}{l^2 + \lambda_R^2}\frac{2\delta p R H}{f_0 p_2 c_p W}\int_0^W \sin ly\, dy
$$
$$
\Leftrightarrow \frac{\partial}{\partial t}\overline{U}_T = -\frac{4kl\lambda_R^2}{3W(l^2 + \lambda_R^2)}\left(A_m B_T - A_T B_m\right) - l^2 A \overline{U}_T
$$
$$
+ \frac{l^2}{l^2 + \lambda_R^2}\frac{\kappa}{2}\left(\overline{U}_m - 2\overline{U}_T\right) + \frac{\lambda_R^2}{l^2 + \lambda_R^2}\frac{8\delta p R H}{f_0 p_2 c_p l W^2}.
$$

Similarly, multiplying equation (A.2) by $\cos ly$ and integrating give the evolution equation for $\overline{L}_T$. Terms multiplied by $\sin ly$ and the net poleward temperature flux term vanish because they are not projecting on the $\cos ly$ mode. The term describing the constant heating also vanishes because the integral of $\cos ly$ over the domain is

zero, yielding

$$
\begin{aligned}
-\int_0^W \cos^2 ly\, dy \frac{\partial}{\partial t}\overline{L}_T =& \frac{1}{l^2+\lambda_R^2}\int_0^W \cos ly \frac{\partial^3}{\partial y^3}\left(\overline{u'_m v'_T}+\overline{u'_T v'_m}\right)\,dy \\
&+ l^2 A\overline{L}_T \int_0^W \cos^2 ly\, dy \\
&- \frac{l^2}{l^2+\lambda_R^2}\frac{\kappa}{2}\left(\overline{L}_m - 2\overline{L}_T\right)\int_0^W \cos^2 ly\, dy \\
\Leftrightarrow \frac{\partial}{\partial t}\overline{L}_T =& \frac{16 j^2 l^4 b}{3W\left(l^2+\lambda_R^2\right)}\left(A_m A_T + B_m B_T\right) - l^2 A\overline{L}_T \\
&+ \frac{l^2}{l^2+\lambda_R^2}\frac{\kappa}{2}\left(\overline{L}_m - 2\overline{L}_T\right).
\end{aligned}
$$

A.2 Eddy streamfunction amplitude equations

To obtain evolution equations for the eddy amplitudes $A_{m,T}$ and $B_{m,T}$, we replace the vorticities in the non-averaged evolution equations for the barotropic and baroclinic vorticities (3.4a) and (3.4b) by their definitions (3.2) and expand all variables in terms of the Eulerian mean, yielding for (3.4a)

$$
\begin{aligned}
\left(\frac{\partial^2}{\partial y^2}-k^2\right)\frac{\partial \psi'_m}{\partial t} &+ \left(l^2-k^2+\frac{\partial^2}{\partial y^2}\right)v'_m \overline{u}_m + \left(l^2-k^2+\frac{\partial^2}{\partial y^2}\right)v'_T \overline{u}_T + \beta v'_m \quad\text{(A.3)}\\
&+ \frac{\kappa}{2}\left(-k^2+\frac{\partial^2}{\partial y^2}\right)(\psi'_m - 2\psi'_T) - A\left(k^4+\frac{\partial^4}{\partial y^4}\right)\psi'_m \\
&+ u'_m\frac{\partial^2}{\partial y^2}v'_m - v'_m\frac{\partial^2}{\partial y^2}u'_m + u'_T\frac{\partial^2}{\partial y^2}v'_T - v'_T\frac{\partial^2}{\partial y^2}u'_T \\
&= l^2\frac{\partial \overline{\psi}_m}{\partial t} + l^4 A\overline{\psi}_m + \frac{\kappa}{2}l^2\left(\overline{\psi}_m - 2\overline{\psi}_T\right)
\end{aligned}
$$

and for (3.4b)

$$
\begin{aligned}
-\left(k^2+\lambda_R^2-\frac{\partial^2}{\partial y^2}\right)\frac{\partial \psi'_T}{\partial t} &+ \left(l^2-k^2+\lambda_R^2+\frac{\partial^2}{\partial y^2}\right)v'_m \overline{u}_T + \beta v'_T \quad\text{(A.4)}\\
&+ \left(l^2-k^2-\lambda_R^2+\frac{\partial^2}{\partial y^2}\right)v'_T \overline{u}_m - A\left(k^4+\frac{\partial^4}{\partial y^4}\right)\psi'_T \\
&+ u'_m\frac{\partial^2}{\partial y^2}v'_T - v'_T\frac{\partial^2}{\partial y^2}u'_m + u'_T\frac{\partial^2}{\partial y^2}v'_m - v'_m\frac{\partial^2}{\partial y^2}u'_T \\
&+ \lambda_R^2 A\left(-k^2+\frac{\partial^2}{\partial y^2}\right)\psi'_T + \frac{\kappa}{2}\left(k^2-\frac{\partial^2}{\partial y^2}\right)(\psi'_m - 2\psi'_T) \\
&= \left(l^2+\lambda_R^2\right)\frac{\partial \overline{\psi}_T}{\partial t} - \lambda_R^2\,\mathrm{J}\left(\psi'_T,\psi'_m\right) + l^4 A\overline{\psi}_T - l^2\frac{\kappa}{2}(\overline{\psi}_m - 2\overline{\psi}_T) \\
&\quad + l^2\lambda_R^2 A\overline{\psi}_T - \lambda_R^2\frac{RH}{f_0 c_p}\left(1-\frac{2y}{W}\right).
\end{aligned}
$$

Next, we want to replace the second derivatives with respect to y in equations (A.3) and (A.4) and note that

$$\frac{\partial^2}{\partial y^2}\psi'_{m,T} = -\left(b^2 k^2 - l^2\right)\psi'_{m,T} - 2bkl\left(A_{m,T}\cos k(x - by) - B_{m,T}\sin k(x - by)\right)\cos ly.$$

By defining

$$\widetilde{\psi}_{m,T} = 2bkl\left(A_{m,T}\cos k(x - by) - B_{m,T}\sin k(x - by)\right)\cos ly,$$

we are able to replace the second derivatives in the following way:

$$\frac{\partial^2}{\partial y^2}\psi'_{m,T} = -\left(b^2 k^2 + l^2\right)\psi'_{m,T} - \widetilde{\psi}_{m,T},$$

$$\frac{\partial^2}{\partial y^2}v'_{m,T} = -\left(b^2 k^2 + l^2\right)v'_{m,T} - \frac{\partial}{\partial x}\widetilde{\psi}_{m,T},$$

$$\frac{\partial^2}{\partial y^2}u'_{m,T} = -\left(b^3 k^2 + bl^2 + 2bl^2\right)v'_{m,T} - \left(\frac{b}{2} + \frac{l^2}{2bk^2} + b\right)\frac{\partial}{\partial x}\widetilde{\psi}_{m,T},$$

$$\frac{\partial^4}{\partial y^4}\psi'_{m,T} = \left(b^4 k^4 + 6b^2 k^2 l^2 + l^4\right)\psi'_{m,T} + 2\left(b^2 k^2 + l^2\right)\widetilde{\psi}_{m,T}.$$

Replacing these in equation (A.3) and (A.4) gives

$$-\left(j^2 + b^2 j^2 + 1\right)\frac{\partial\psi'_m}{\partial t} - \frac{1}{l^2}\frac{\partial\widetilde{\psi}_m}{\partial t} - \left(j^2 + b^2 j^2\right)\left(v'_m\overline{u}_m + v'_T\overline{u}_T\right) + \frac{\beta}{l^2}v'_m \qquad\text{(A.5)}$$

$$- \left(b^2 j^2 + 1\right)\left(u'_m v'_m + u'_T v'_T\right) + \left(b^3 j^2 + 3b\right)\left(v'^2_m + v'^2_T\right)$$

$$- \frac{1}{l^2}\left(\frac{\partial\widetilde{\psi}_m}{\partial x}\overline{u}_m + \frac{\partial\widetilde{\psi}_T}{\partial x}\overline{u}_T + \frac{\partial\widetilde{\psi}_m}{\partial x}u'_m + \frac{\partial\widetilde{\psi}_T}{\partial x}u'_T\right) + \frac{3b^2 j^2 + 1}{2bj^2 l^2}\left(\frac{\partial\widetilde{\psi}_m}{\partial x}v'_m + \frac{\partial\widetilde{\psi}_T}{\partial x}v'_T\right)$$

$$- \left(j^4 l^2 + b^4 j^4 l^2 + 6b^2 j^2 l^2 + l^2\right)A\psi'_m - 2(b^2 j^2 + 1)A\widetilde{\psi}_m$$

$$- \frac{\kappa}{2}\left(j^2 + b^2 j^2 + 1\right)\left(\psi'_m - 2\psi'_T\right) - \frac{\kappa}{2l^2}\left(\widetilde{\psi}_m - 2\widetilde{\psi}_T\right)$$

$$= \frac{\partial\overline{\psi}_m}{\partial t} + l^2 A\overline{\psi}_m + \frac{\kappa}{2}\left(\overline{\psi}_m - 2\overline{\psi}_T\right)$$

and

$$-\left(j^2 + j^2 b^2 + 1 + \frac{\lambda_R^2}{l^2}\right)\frac{\partial\psi'_T}{\partial t} - \frac{1}{l^2}\frac{\partial\widetilde{\psi}_T}{\partial t} - \left(j^2 + j^2 b^2\right)\left(v'_m\overline{u}_T + v'_T\overline{u}_m\right) + \frac{\beta}{l^2}v'_T \quad\text{(A.6)}$$

$$+ \frac{\lambda_R^2}{l^2}\left(v'_m\overline{u}_T - v'_T\overline{u}_m\right) - \left(j^2 b^2 + 1\right)\left(u'_T v'_m + u'_m v'_T\right)$$

$$+ \frac{\lambda_R^2}{l^2}\left(u'_T v'_m - u'_m v'_T\right) + 2b\left(j^2 b^2 + 3\right)v'_m v'_T$$

$$- \frac{1}{l^2}\left(\frac{\partial\widetilde{\psi}_m}{\partial x}\overline{u}_T + \frac{\partial\widetilde{\psi}_T}{\partial x}\overline{u}_m + \frac{\partial\widetilde{\psi}_m}{\partial x}u'_T + \frac{\partial\widetilde{\psi}_T}{\partial x}u'_m\right) + \frac{3b^2 j^2 + 1}{2bj^2 l^2}\left(\frac{\partial\widetilde{\psi}_m}{\partial x}v'_T + \frac{\partial\widetilde{\psi}_T}{\partial x}v'_m\right)$$

$$- \left(j^4 l^2 + j^4 b^4 l^2 + 6j^2 b^2 l^2 + l^2 + (j^2 + j^2 b^2 + 1)\lambda_R^2 \right) A\psi_T'$$

$$- \left(2(j^2 b^2 + 1) + \frac{\lambda_R^2}{l^2} \right) A\tilde{\psi}_T + \frac{\kappa}{2}(j^2 + j^2 b^2 + 1)\left(\psi_m' - 2\psi_T' \right) + \frac{\kappa}{2l^2} \left(\tilde{\psi}_m - 2\tilde{\psi}_T \right)$$

$$= \frac{l^2 + \lambda_R^2}{l^2} \frac{\partial \overline{\psi}_T}{\partial t} + l^2 A\overline{\psi}_T - \frac{\kappa}{2} \left(\overline{\psi}_m - 2\overline{\psi}_T \right) + \lambda_R^2 A\overline{\psi}_T - \frac{\lambda_R^2 R H}{l^2 f_0 c_p} \left(1 - \frac{2y}{W} \right).$$

Now we project these equations onto the sine and cosine modes in the x and sine mode in the y direction, giving us four evolution equations for the eddy amplitudes A_m, B_m, A_T and B_T. Note here that all terms on the right-hand sides of equations (A.5) and (A.6) vanish as functions of y only, and that all products of two eddy quantities are sums of the products $\sin^2 k(x - by)$, $\cos^2 k(x - by)$ and $\sin k(x - by) \cos k(x - by)$, and projected on one full wavelength in the x direction they vanish, since

$$\int_0^{2W/j} \sin^3 k(x - by) \, dx = \int_0^{2W/j} \cos^3 k(x - by) \, dx = 0,$$

$$\int_0^{2W/j} \sin^2 k(x - by) \cos k(x - by) \, dx = \int_0^{2W/j} \sin k(x - by) \cos^2 k(x - by) \, dx = 0.$$

Therefore, the final evolution equations obtained by the projections of equation (A.5) are

$$\text{Projection 1:} \int_0^W \sin ly \int_0^{2W/j} \sin k(x - by) \, (A.5) \, dx \, dy \Leftrightarrow$$

$$\frac{W(j^2 + j^2 b^2 + 1)}{2j} \frac{\partial A_m}{\partial t} = -\frac{\beta W^2}{2\pi} B_m + \frac{4(j^2 + j^2 b^2)}{3} \left(B_m \overline{U}_m + B_T \overline{U}_T \right)$$

$$- \frac{4bj}{3} \left(A_m \overline{L}_m + A_T \overline{L}_T \right) - \left(j^4 l^2 + b^4 j^4 l^2 + 6b^2 j^2 l^2 + l^2 \right) \frac{AW}{2j} A_m$$

$$- \frac{\kappa W(j^2 + j^2 b^2 + 1)}{4j} \left(A_m - 2A_T \right),$$

$$\text{Projection 2:} \int_0^W \sin ly \int_0^{2W/j} \cos k(x - by) \, (A.5) \, dx \, dy \Leftrightarrow$$

$$\frac{W(j^2 + j^2 b^2 + 1)}{2j} \frac{\partial B_m}{\partial t} = \frac{\beta W^2}{2\pi} A_m - \frac{4(j^2 + j^2 b^2)}{3} \left(A_m \overline{U}_m + A_T \overline{U}_T \right)$$

$$- \frac{4bj}{3} \left(B_m \overline{L}_m + B_T \overline{L}_T \right) - \left(j^4 l^2 + b^4 j^4 l^2 + 6b^2 j^2 l^2 + l^2 \right) \frac{AW}{2j} B_m$$

$$- \frac{\kappa W(j^2 + j^2 b^2 + 1)}{4j} \left(B_m - 2B_T \right),$$

and the evolution equations of projected equation (A.6) are

$$\text{Projection 1:} \int_0^W \sin ly \int_0^{2W/j} \sin k(x - by) \, (A.6) \, dx \, dy \Leftrightarrow$$

$$\frac{W(j^2 + j^2 b^2 + 1 + \lambda_R^2/l^2)}{2j} \frac{\partial A_T}{\partial t} = -\frac{\beta W^2}{2\pi} B_T + \frac{4(j^2 + j^2 b^2)}{3} \left(B_m \overline{U}_T + B_T \overline{U}_m \right)$$

$$- \frac{4\lambda_R^2}{3l^2} \left(B_m \overline{U}_T - B_T \overline{U}_m \right) - \frac{4jb}{3} \left(A_m \overline{L}_T + A_T \overline{L}_M \right)$$

$$- \left(j^4 l^2 + j^4 b^4 l^2 + 6j^2 b^2 l^2 + l^2 + (j^2 + j^2 b^2 + 1)\lambda_R^2 \right) \frac{AW}{2j} A_T$$

$$+ \frac{\kappa W(j^2 + j^2 b^2 + 1)}{4j}(A_m - 2A_T),$$

Projection 2: $\displaystyle\int_0^W \sin ly \int_0^{2W/j} \cos k(x - by) \ (A.6) \ dx \ dy \Leftrightarrow$

$$\frac{W(j^2 + j^2 b^2 + 1 + \lambda_R^2/l^2)}{2j} \frac{\partial B_T}{\partial t} = \frac{\beta W^2}{2\pi} A_T - \frac{4(j^2 + j^2 b^2)}{3} \left(A_m \overline{U}_T + A_T \overline{U}_m \right)$$

$$+ \frac{4\lambda_R^2}{3l^2} \left(A_m \overline{U}_T - A_T \overline{U}_m \right) - \frac{4jb}{3} \left(B_m \overline{L}_T + B_T \overline{L}_M \right)$$

$$- \left(j^4 l^2 + j^4 b^4 l^2 + 6j^2 b^2 l^2 + l^2 + (j^2 + j^2 b^2 + 1)\lambda_R^2 \right) \frac{AW}{2j} B_T$$

$$+ \frac{\kappa W(j^2 + j^2 b^2 + 1)}{4j}(B_m - 2B_T).$$

Bibliography

Ambaum, Maarten H. P. and Lenka Novak (2014). "A nonlinear oscillator describing storm track variability". In: *Quarterly Journal of the Royal Meteorological Society* 140.685, pp. 2680–2684.

Charney, J. G. (1947). "The dynamics of long waves in a baroclinic westerly current". In: *Journal of Meteorology* 4.5, pp. 136–162.

– (1948). "On the scale of atmospheric motions". In: *Geof. Publ.* 17.2, pp. 3–17.

Eady, E. T. (1949). "Long waves and cyclone waves". In: *Tellus* 1.3, pp. 33–52.

Ferrel, William (1856). "An essay on the winds and the currents of the ocean". In: *Nashville Journal of Medicine and Surgery* 11, pp. 287–301.

Franzke, Christian, Tim Woollings, and Olivia Martius (2011). "Persistent Circulation Regimes and Preferred Regime Transitions in the North Atlantic". In: *Journal of the Atmospheric Sciences* 68.12, pp. 2809–2825.

Fyfe, John C. (2003). "Extratropical Southern Hemisphere Cyclones: Harbingers of Climate Change?" In: *Journal of Climate* 16.17, pp. 2802–2805.

Guckenheimer, John and Philip Holmes (1983). *Nonlinear oscillations, dynamical systems, and bifurcations of vector fields.* 1st ed. Applied Mathematical Sciences. Springer, New York, NY.

Hadley, Geo. (1735). "VI. Concerning the cause of the general trade-winds". In: *Philosophical Transactions of the Royal Society of London* 39.437, pp. 58–62.

Held, Isaac (2014). "Simplicity amid complexity". In: *Science* 343.6176, pp. 1206–1207.

Held, Isaac M. (2005). "The Gap between Simulation and Understanding in Climate Modeling". In: *Bulletin of the American Meteorological Society* 86.11, pp. 1609–1614.

Held, Isaac M (2007). "Progress and problems in large-scale atmospheric dynamics". In: *The Global Circulation of the Atmosphere* 1, p. 21.

Holton, James R. and Gregory J. Hakim (2013a). *An Introduction to Dynamic Meteorology.* 5th ed. Academic Press.

– (2013b). "Chapter 10 - The General Circulation". In: *An Introduction to Dynamic Meteorology (Fifth Edition).* Ed. by James R. Holton and Gregory J. Hakim. Boston: Academic Press, pp. 325–375.

Hoskins, B. J. (1983). "Dynamical processes in the atmosphere and the use of models". In: *Quarterly Journal of the Royal Meteorological Society* 109.459, pp. 1–21.

Hoskins, Brian J. and Ian M. James (2014). *Fluid Dynamics of the Midlatitude Atmosphere*. 1st ed. John Wiley & Sons, Ltd.

Hoskins, Brian J., Ian N. James, and Glenn H. White (1983). "The shape, propagation and mean-flow interaction of large-scale weather systems". In: *Journal of the Atmospheric Sciences* 40.7, pp. 1595–1612.

Jeffreys, Harold (1926). "On the dynamics of geostrophic winds". In: *Quarterly Journal of the Royal Meteorological Society* 52, pp. 85–104.

Kållberg, P. et al. (2005). *ERA-40 Atlas*. Number 19. ECMWF.

Kobras, Melanie, Maarten H. P. Ambaum, and Valerio Lucarini (2021). "Eddy saturation in a reduced two-level model of the atmosphere". In: *Geophysical & Astrophysical Fluid Dynamics*, pp. 1–18.

Kuo, Hsiao-Lan (1949). "Dynamic instability of two-dimensional nondivergent flow in a barotropic atmosphere". In: *Journal of Meteorology* 6.2, pp. 105–122.

Lewis, John M. (1998). "Clarifying the Dynamics of the General Circulation: Phillips's 1956 Experiment". In: *Bulletin of the American Meteorological Society* 79.1, pp. 39–60.

Lorenz, Edward N. (1955). "Available Potential Energy and the Maintenance of the General Circulation". In: *Tellus* 7.2, pp. 157–167.

– (1967). *The nature and theory of the general circulation of the atmosphere*. Vol. 218. World Meteorological Organization Geneva.

Lucarini, Valerio, Antonio Speranza, and Renato Vitolo (2007). "Parametric smoothness and self-scaling of the statistical properties of a minimal climate model: What beyond the mean field theories?" In: *Physica D: Nonlinear Phenomena* 234.2, pp. 105–123.

Lucarini, Valerio et al. (2014). "Mathematical and physical ideas for climate science". In: *Reviews of Geophysics* 52.4, pp. 809–859.

Maher, Penelope et al. (2019). "Model Hierarchies for Understanding Atmospheric Circulation". In: *Reviews of Geophysics* 57.2, pp. 250–280.

Mak, J. et al. (2017). "Emergent eddy saturation from an energy constrained eddy parameterisation". In: *Ocean Modelling* 112, pp. 125–138.

Marshall, David P. et al. (2017). "Eddy saturation and frictional control of the Antarctic Circumpolar Current". In: *Geophysical Research Letters* 44.1, pp. 286–292.

Munday, David R., Helen L. Johnson, and David P. Marshall (2013). "Eddy saturation of equilibrated circumpolar currents". In: *Journal of Physical Oceanography* 43.3, pp. 507–532.

Munk, W. H. and E. Palmén (1951). "Note on the dynamics of the antarctic circumpolar current". In: *Tellus* 3.1, pp. 53–55.

Nadeau, Louis-Philippe and Raffaele Ferrari (2015). "The role of closed gyres in setting the zonal transport of the Antarctic Circumpolar Current". In: *Journal of Physical Oceanography* 45.6, pp. 1491–1509.

Novak, Lenka, Maarten H. P. Ambaum, and Ben J. Harvey (2018). "Baroclinic adjustment and dissipative control of storm tracks". In: *Journal of the Atmospheric Sciences* 75.9, pp. 2955–2970.

Novak, Lenka, Maarten H. P. Ambaum, and Rémi Tailleux (2015). "The life cycle of the North Atlantic storm track". In: *Journal of the Atmospheric Sciences* 72.2, pp. 821–833.

Oort, Abraham H. (1964). "On estimates of the atmospheric energy cycle". In: *Monthly Weather Review* 92.11, pp. 483–493.

Orlanski, Isidoro (1998). "Poleward Deflection of Storm Tracks". In: *Journal of the Atmospheric Sciences* 55.16, pp. 2577–2602.

– (2003). "Bifurcation in Eddy Life Cycles: Implications for Storm Track Variability". In: *Journal of the Atmospheric Sciences* 60.8, pp. 993–1023.

Orlanski, Isidoro and Brian Gross (2000). "The Life Cycle of Baroclinic Eddies in a Storm Track Environment". In: *Journal of the Atmospheric Sciences* 57.21, pp. 3498–3513.

Pedlosky, Joseph (1979). *Geophysical Fluid Dynamics*. Springer Study Edition. Springer-Verlag Berlin Heidelberg, pp. XII, 626.

Peixoto, Jose P. and Abraham H. Oort (1992). *Physics of Climate*. American Institute of Physics.

Phillips, Norman A. (1954). "Energy transformations and meridional circulations associated with simple baroclinic waves in a two-level, quasi-geostrophic model". In: *Tellus* 6.3, pp. 274–286.

– (1956). "The general circulation of the atmosphere: A numerical experiment". In: *Quarterly Journal of the Royal Meteorological Society* 82.352, pp. 123–164.

Phillips, Norman A. et al. (1989). "Transcript of oral history interview with Norman Phillips". In: *American Meteorological Society Oral History Project*.

Previdi, Michael, Karen L Smith, and Lorenzo M Polvani (2021). "Arctic amplification of climate change: a review of underlying mechanisms". In: *Environmental Research Letters* 16.9, p. 093003.

Riehl, H. (1988). "General circulation studies in Chicago from the 1940's into the 1950's". In: *"Palmén Mem. Symo. on Extratropical Cyclones" Helsinki, Finnland, 29 Aug.-2 Sep.*, pp. 4–5.

Rossby, C. G. (1939). "Relation between Variations in the Intensity of the Zonal Circulation of the Atmosphere and the Displacements of the Semi-Permanent Centers of Action". In: *Journal of Marine Research* 2, pp. 38–55.

– (1941). "The Scientific Basis of Modern Meteoroogy". In: *Yearbook of Agriculture, Climate and Man, Department of Agriculture, Washington DC*, pp. 599–655.

– (1947). "On the Distribution of Angular Velocity in Gaseous Envelopes Under the Influence of Large-Scale Horizontal Mixing Processes*". In: *Bulletin of the American Meteorological Society* 28.2, pp. 53–68.

Sawford, B. L. and J. S. Frederiksen (1983). "Mountain torque and angular momentum in barotropic planetary flows: Equilibrium solutions". In: *Quarterly Journal of the Royal Meteorological Society* 109.460, pp. 309–324.

Schneider, Stephen H. and Robert E. Dickinson (1974). "Climate modeling". In: *Reviews of Geophysics* 12.3, p. 447.

Schneider, Tapio (2006). "The General Circulation of the Atmosphere". In: *Annual Review of Earth and Planetary Sciences* 34.1, pp. 655–688.

Shepherd, Theodore G. (2014). "Atmospheric circulation as a source of uncertainty in climate change projections". In: *Nature Geoscience* 7.10, pp. 703–708.

Speranza, A. and P. Malguzzi (1988). "The Statistical Properties of a Zonal Jet in a Baroclinic Atmosphere: A Semilinear Approach. Part I: Quasi-geostrophic, Two-Layer Model Atmosphere". In: *Journal of the Atmospheric Sciences* 45.21, pp. 3046–3062.

Staff Members, of the Department of Meteorology of the University of Chicago (1947). "On the General Circulation of the Atmosphere in Middle Latitudes: A Preliminary Summary Report on Certain Investigations Conducted at the University of Chicago during the Academic Year 1946–1947". In: *Bulletin of the American Meteorological Society* 28.6, pp. 255–280.

Starr, Victor P. (1948). "An essay on the general circulation of the earths atmosphere". In: *Journal of Meteorology* 5.2, pp. 39–43.

Stone, Peter H. (1978). "Baroclinic adjustment". In: *Journal of Atmospheric Sciences* 35.4, pp. 561–571.

Straub, David N. (1993). "On the transport and angular momentum balance of channel models of the Antarctic Circumpolar Current". In: *Journal of Physical Oceanography* 23.4, pp. 776–782.

Thompson, Philip D. (1987). "Large-scale dynamical response to differential heating: Statistical equilibrium states and amplitude vacillation". In: *Journal of the Atmospheric Sciences* 44.8, pp. 1237–1248.

Thomson, James (1892). "Bakerian Lecture: On the Grand Currents of Atmospheric Circulation". In: *Philosophical Transactions of the Royal Society of London* 183, pp. 653–684.

Woollings, Tim, Abdel Hannachi, and Brian Hoskins (2010). "Variability of the North Atlantic eddy-driven jet stream". In: *Quarterly Journal of the Royal Meteorological Society* 136.649, pp. 856–868.

Wuebbles, Donald J. et al. (2017). "Climate Science Special Report: Fourth National Climate Assessment". In: *U.S. Global Change Research Program, Washington, DC, USA* 1, 470 pp.

Yin, Jeffrey H. (2005). "A consistent poleward shift of the storm tracks in simulations of 21st century climate". In: *Geophysical Research Letters* 32.18.

Zurita-Gotor, Pablo (2007). "The Relation between Baroclinic Adjustment and Turbulent Diffusion in the Two-Layer Model". In: *Journal of the Atmospheric Sciences* 64.4, pp. 1284–1300.